NASA CR-145068

ADVANCED COMPOSITE RUDDERS FOR DC-10 AIRCRAFT — DESIGN, MANUFACTURING, AND GROUND TESTS

By George M. Lehman, et al

Prepared Under Contract No. NAS1-12954

McDonnell Douglas Corporation
Douglas Aircraft Company
Long Beach, California 90846

for

NASA

PREFACE

This report was prepared by the Douglas Aircraft Company, McDonnell Douglas Corporation, Long Beach, California under contract NAS1-12954. It is the final technical report covering design, manufacture, and ground test activities during development of an advanced composite rudder for flight-service on the DC-10 transport aircraft. The work was conducted between 18 January 1974 and 30 April 1976.

The following Douglas personnel were the principal contributors to the program: G. M. Lehman, Technical Director; Dr. D. M. Purdy, Deputy Technical Director; A. Cominsky, Structural Design Criteria and Analysis; A. V. Hawley, Structural Design; M. P. Amason and J. T. Kung, Lightning Protection System Design; R. J. Palmer, Material and Process Engineering; N. B. Purves and P. J. Marra, Tooling and Manufacturing Development; G. R. Hancock, Industrial Engineering; E. G. Willoughby and R. G. Wolfe, Instrumentation and Static Testing; G. G. Stuart and G. E. Hinote, Modal Vibration Testing; and C. A. Felton, Flutter Analysis.

The project was sponsored by the National Aeronautics and Space Administration (NASA), Langley Research Center. Mr. Marvin B. Dow was the Project Engineer for NASA.

TABLE OF CONTENTS

LIST OF FIGURES

LIST OF FIGURES
(Continued)

LIST OF FIGURES
(Continued)

LIST OF TABLES

LIST OF TABLES
(Continued)

ADVANCED COMPOSITE RUDDERS FOR DC-10 AIRCRAFT - DESIGN, MANUFACTURING, AND GROUND TESTS

by George M. Lehman, et al.

S U M M A R Y

Design synthesis, tooling and process development, manufacturing, and ground testing of a graphite epoxy rudder for the DC-10 commercial transport are discussed. An objective of the program was to develop a structure with significant weight saving and potentially competitive cost in comparison with the existing metal design. The composite structure was fabricated using a unique processing method in which the thermal expansion characteristics of rubber tooling mandrels were used to generate curing pressures during an oven cure cycle. This method eliminated the need for autoclave curing and secondary assembly bonding of the rudder structure. Development of the rudder is traced through construction and testing of a group of fabrication feasibility specimens and structural development components representing salient details of the structure. The ground test program was fully coordinated with the FAA and resulted in certification of the rudder for passenger-carrying flights. Results of the structural and environmental tests are interpreted and detailed development of the rudder tooling and manufacturing process is described. Processing, tooling, and manufacturing problems encountered during fabrication of four development rudders and ten flight-service rudders are discussed and the results of corrective actions are described. Non-recurring and recurring manufacturing labor man-hours are tabulated at the detailed operation level. Production progress (learning) curve slopes of 87.4 and 89.4 percent, respectively, were attained for the graphite-epoxy box structure fabrication and completed composite rudder assemblies during construction of the ten flight-service rudders. A weight reduction of 13.58 kg (33 percent) was attained in the composite rudder.

INTRODUCTION

The excellent potential of advanced composite materials to reduce airframe weight, and therefore enhance the economic performance of aircraft systems, has been conclusively demonstrated by numerous structural research and development programs. However, the application of these materials to commercial transport aircraft has been inhibited by the lack of adequate manufacturing cost data and demonstrated resistance to long-term environmental exposures. Before these new material systems gain wide acceptance in commercial aircraft, a firm base of manufacturing and maintenance cost data, based on multi-unit production, is needed for a true assessment of airframe and aircraft system costs relative to competing materials. Flight-service evaluation of complete structural units is also required to determine the long-term behavior of composite material under actual service loads and environments.

This program is intended to develop experience and confidence in composite structures through the design, fabrication, certification, and flight-service evaluation of a graphite-epoxy structural component for a commercial transport. Specific program objectives are: (1) to develop the technology to design and fabricate composite structural components for transport aircraft, (2) to obtain production and maintenance cost data for composite structure, (3) to develop confidence and experience in the utilization of composite materials in commercial aircraft, and (4) to provide data for correlating flight-service behavior with ground-based tests.

The program objectives are being met through design, development, ground testing, and commercial flight service of graphite-epoxy upper-aft rudders for the DC-10 transport aircraft. The composite rudder was extensively ground tested for verification of strength and integrity of all critical details of the structural design concept. Ten rudders were produced in a pre-production manufacturing mode to obtain manufacturing cost data and production progress curve trends.

A significant advancement to the state-of-the-art in composite structure manufacturing was achieved through development of the thermal expansion molding technique for production of the graphite rudder box-structures. The thermal expansion molding technique is a unique method of consolidating laminated composite elements into a monolithic assembly in a single cure cycle, reducing the need for precision dimensional control of detail parts and eliminating the need for autoclave bagging preparations, autoclave curing and cleanup operations, and secondary bonding operations.

The thermal expansion molding technique exploited the thermal expansion characteristics of silicone rubber tools to supply curing and bonding pressures and to eliminate manufacturing tolerance accumulations during a single oven cure cycle. The individual parts of the molding assembly were laid-up using uncured laminates, densified, and trimmed to size on simple ancillary tools. The individual parts were then assembled in a curing tool which consisted of various metal and silicone rubber elements. The assembled tool was heated so that the thermal expansions of the rubber elements furnished the pressure required to consolidate the individual parts into a cured laminate assembly. The heating cycle was controlled to provide the temperature and pressure phasing required to cure and bond the laminates.

This report summarizes the design, manufacturing development, and ground test aspects of the program. The culmination of the program will be a monitored five-year exposure of the graphite rudders in actual airline service. The rudders are fully certified for commercial aircraft in regular passenger-carrying operations, meeting the requirements of the Federal Aviation Regulations, Part 25, in which the Federal Aviation Agency specifies the airworthiness standards for transport category aircraft. Flight service experience will be reported at annual intervals during the five-year flight-service period.

The measurement values in this report are expressed in the International System of Units (SI) and also U.S. Customary Units. The U.S. Customary Units were used for the principle measurements and calculations.

ANALYSIS AND DESIGN STUDIES

Preliminary design of the graphite-epoxy rudder was initiated using mechanical property data representative of the Thornel 300/Narmco 5208 (T300/5208) material prepreg system. This material system was selected for development of the graphite rudder because of prior contractor research and development experience with this product, excellent mechanical properties, demonstrated shop-readiness, and ready availability in the required quantities. Preliminary and detail designs of the rudder were consumated based on T300/5208 properties, existing DC-10 design criteria, and adaptability of the configuration to the manufacturing approach. Final design and analysis of the rudder was based on experimentally determined allowable stresses and finite element analysis of the selected rudder configuration.

Rudder Configuration and Manufacturing Concept

The general arrangement of the DC-10 rudder system is shown in Figure 1. The rudder is divided into upper and lower rudder assemblies, each consisting of a forward and aft rudder. The upper aft rudder has a span of four meters (158 inches) and a planform area of approximately 3.16 square meters (34 square feet). Each of the aft rudders is driven by a mechanical linkage connected to the forward rudder assembly. When the forward rudder is deflected, the mechanical linkage causes the desired differential motion between forward and aft rudder assemblies.

In preliminary design studies, seven candidate structural design concepts were evaluated. These concepts are shown in Figure 2.

Interest was initially centered on the honeycomb sandwich skin panel and full-depth honeycomb configurations because of the fully stabilized skin panels and relative simplicity in terms of part numbers and conventional assembly techniques. Rib and hat-stiffened concepts were later added because a unique fabrication approach, the thermal expansion molding technique, was developed which eliminated the need for autoclave curing and secondary bonding of laminated details.

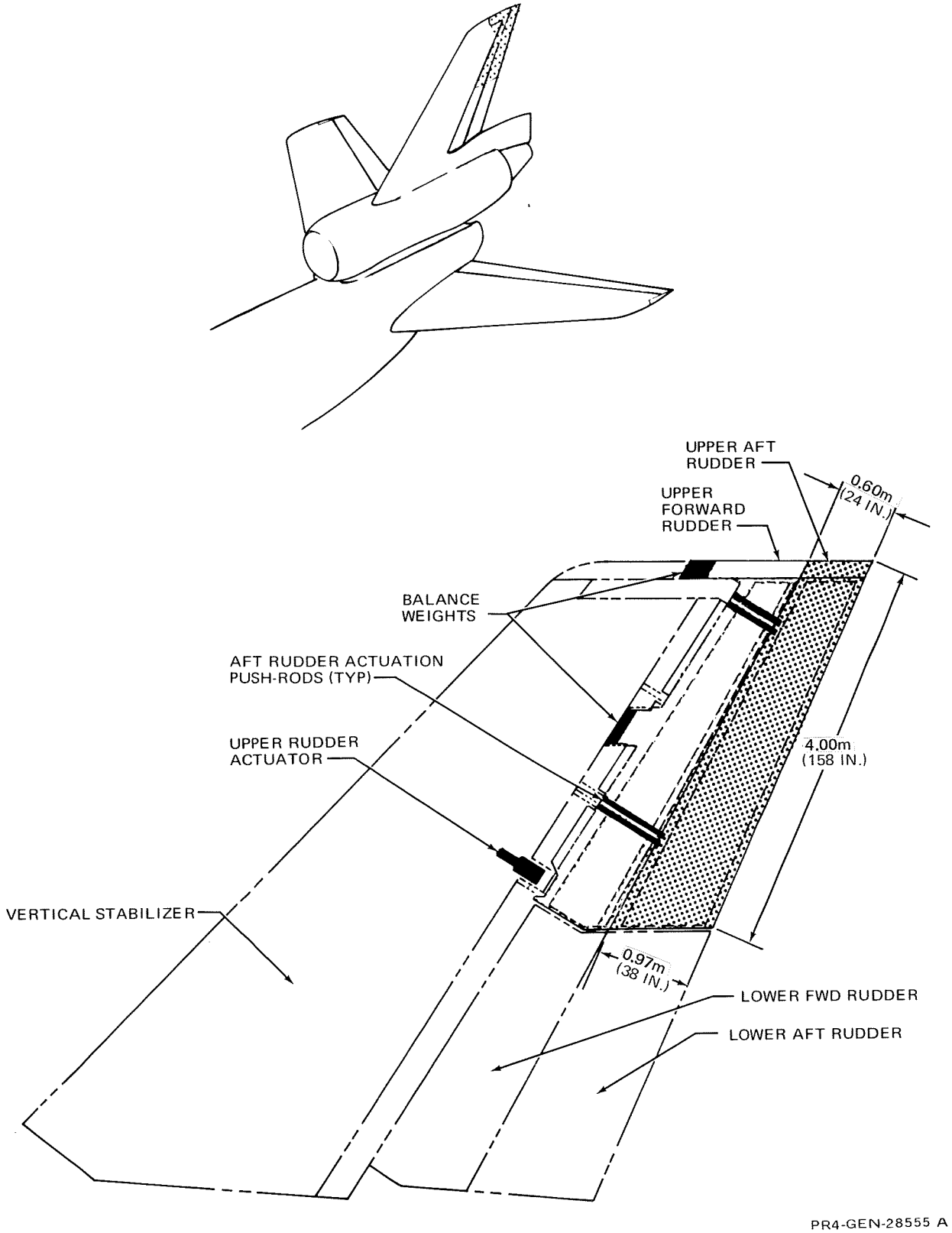

FIGURE 1. GENERAL ARRANGEMENT OF RUDDER SYSTEM

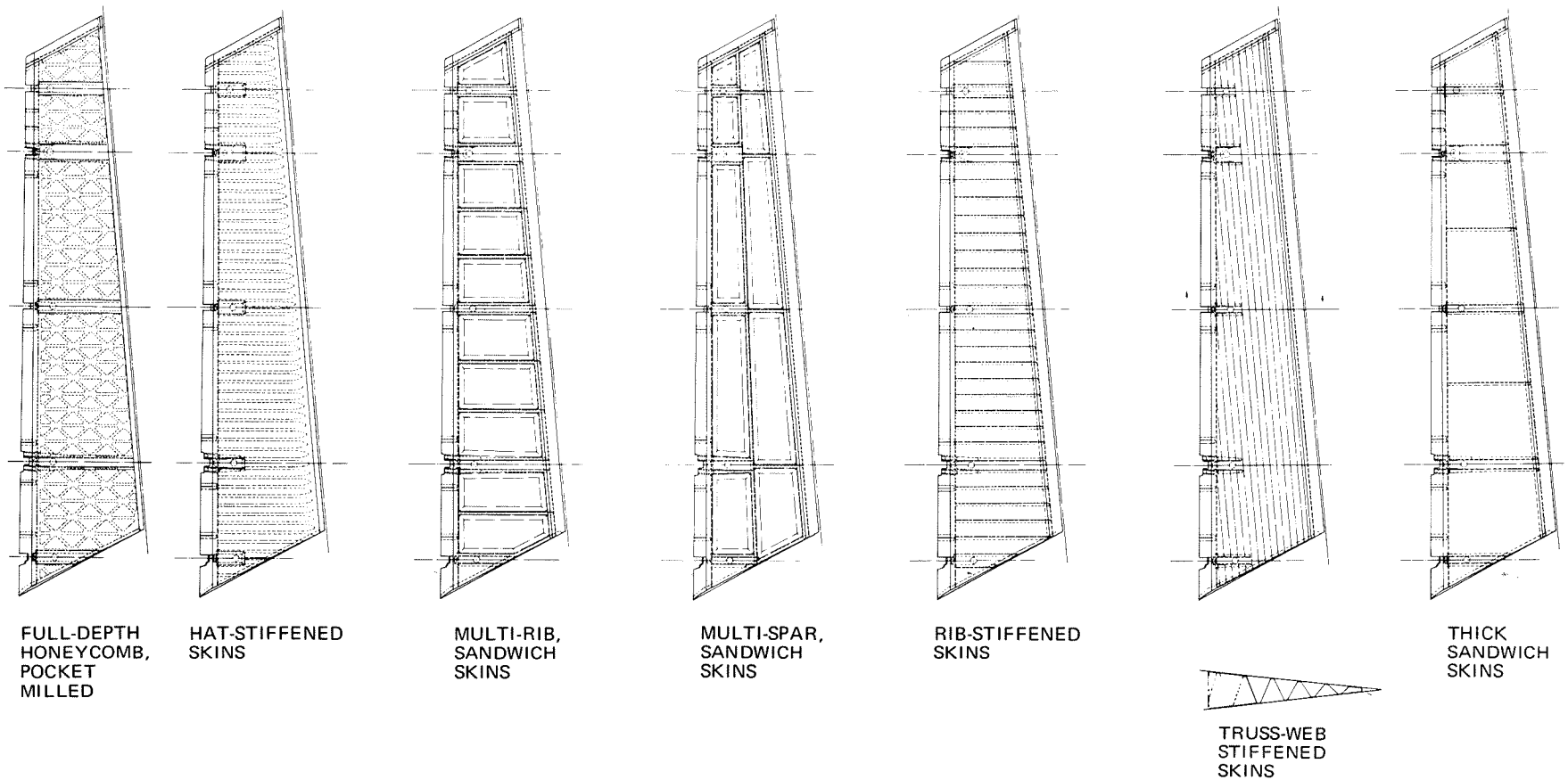

FIGURE 2. CANDIDATE STRUCTURAL CONFIGURATIONS

The fundamental elements of the thermal expansion molding technique are illustrated in Figure 3. The individual parts of the molding assembly were laid up in the "B" stage, densified, and trimmed to size on simple ancillary tools. The individual parts were then assembled in a curing tool which consisted of various metal and silicone rubber elements. The assembled tool was heated so that the thermal expansions of the rubber elements furnished the pressure required to consolidate the "B" stage parts into a cured laminate assembly. The heating cycle was controlled to provide the temperature and pressure phasing required to cure the laminate assembly.

Cost and weight tradeoff studies were conducted on the seven basic design configurations. The rib-stiffened configuration, Figure 4, was finally selected because it indicated significant advantages in weight, structural integrity, and adaptability to the thermal expansion molding technique.

The thermal expansion molding technique was used to fabricate the stiffened panel shown in Figure 5. The overall size of the panel was 34.3 x 59.7 centimeters (13.5 by 23.5 inches). The skin was a 6-ply layup (0°, 45°, -45°)S with a thickness of 0.86 millimeter (0.034 inch). The panel stiffeners were spaced 10.16 centimeters (4 inches) on center to represent anticipated spacings in the rudder. The panel was first tested in fatigue to 4000 cycles of limit shear stress in a critical rudder design condition and then under static loads to failure. Shear loads were introduced to the panel through the pin-ended "picture frame" jig shown in Figure 5. The static load was applied in 8.9 kilonewton (2000-pound) increments and visual observations for buckling deformations were made after each load application. Skin buckling was first observed at 78 megapascal (11,300-psi) shear stress in the skin panel. The buckle pattern became more fully developed with increasing loads, developing an ultimate shear stress of 183 megapascal (26,550 psi) at failure. These test results established the feasibility of permitting elastic buckling of skin panels in the graphite rudder design.

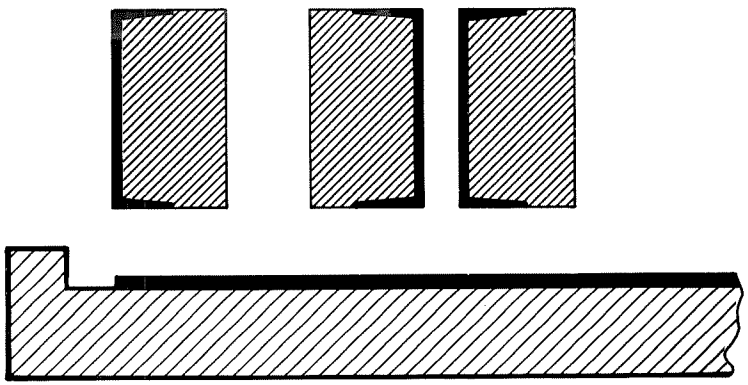

- LAYUP INDIVIDUAL PIECES ON ANCILLARY TOOLS
- DENSIFY
- TRIM TO SIZE
- STORE IN FREEZER

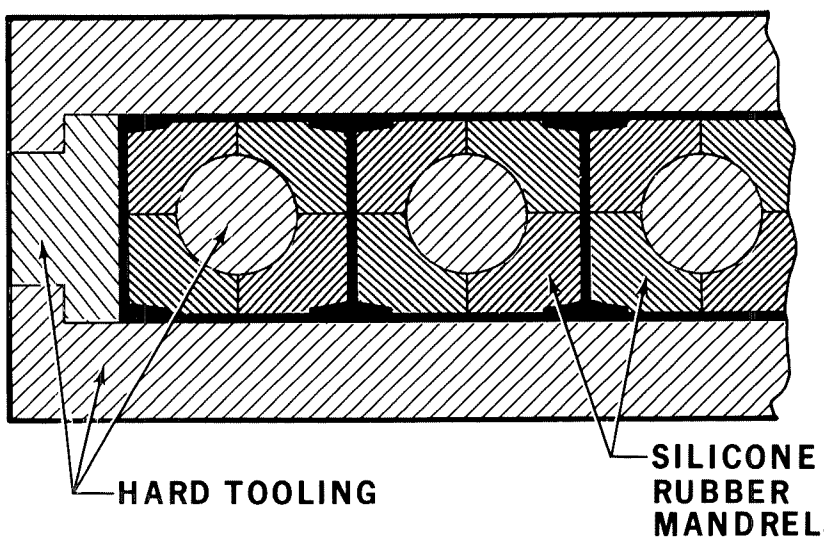

- ASSEMBLE PIECES IN CURE TOOL
- APPLY HEAT
- PRESSURE SUPPLIED BY EXPANSION OF SILICONE RUBBER WITHIN TOOL CAVITY
- NO BAGGING, BLEED-OFF, OR ADHESIVE REQUIRED

PR3-STOL-1989A

FIGURE 3. SCHEMATIC DRAWING OF THERMAL EXPANSION MOLDING TECHNIQUES

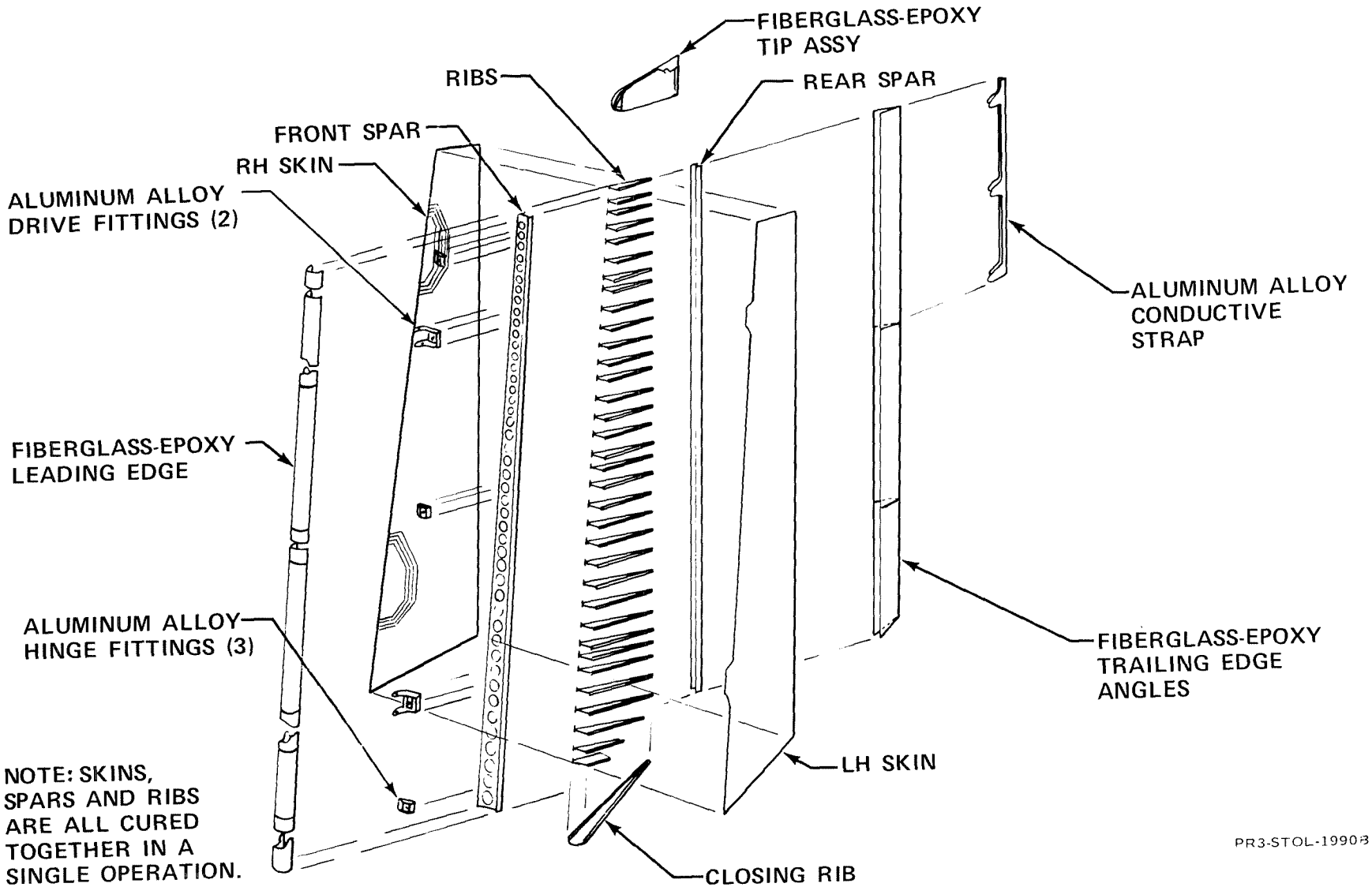

FIGURE 4. STRUCTURAL ARRANGEMENT FOR THE ADVANCED COMPOSITE RUDDER

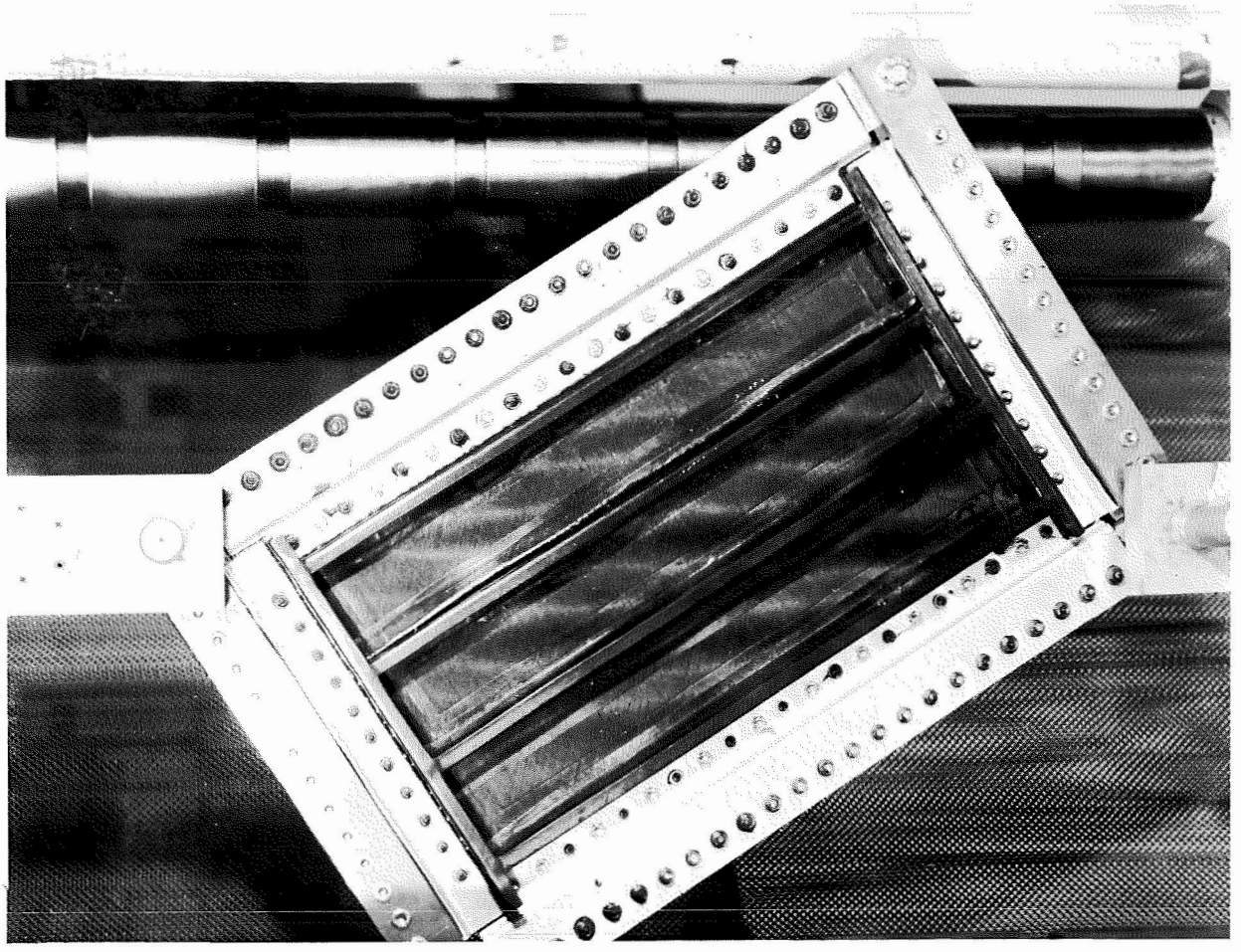

FIGURE 5. TENSION – FIELD TEST PANEL

Design Criteria

Critical loads and conditions for the graphite-epoxy rudder, including failsafe considerations, were determined from existing DC-10 design criteria documents. Allowable stresses in tension, compression, and shear were determined experimentally for unidirectional laminates and for each laminate pattern used in the rudder design.

Loads and Conditions. - Critical loads occur on the rudder (1) during yawing and rolling maneuvers (induced by full rudder throw and/or engine flame-out), (2) during dynamic overswing conditions which result from these maneuvers, and (3) from lateral gust and inertia conditions. The rudder must withstand design ultimate loads (150 percent design limit loads) during these conditions without failure. The Federal Aviation Regulations, Part 25, also require that the structure must withstand design limit loads after the failure of any single structural element (e.g., hinge bolt, fitting, skin panel, etc.).

The conventional aluminum alloy rudder system for the DC-10 was analyzed for four basic flight conditions with failsafe variations (i.e., analysis cases involving the failure of various hinges) from which 18 separate analysis cases were required. Eleven of these cases (Table 1) which produced maximum internal loads were selected for analysis of the graphite rudder.

Allowable Stresses. - Allowable stresses and elastic properties were derived from accumulated test data for both unidirectional and patterned laminates. Average values, "A" and "B" basis allowable stresses, elastic properties, and critical strains are summarized in this section.

Lamina (unidirectional) strength allowables and elastic properties at 219°, 294°, and 394°K (-65°, 70°, and 250°F) were developed from 132 individual specimen tests summarized in Table 2. This data base was supplemented by additional room temperature specimens tested periodically during incoming material quality control checks.* The 132 specimens in the lamina test program were supplemented by an additional 95 sandwich-beam tension tests and 90 sandwich-beam compression tests.

*Incoming material quality control test data (resin and volatile contents, flexural strengths and moduli, interlaminar shear strengths, and ply thicknesses) are tabulated in Appendix A.

TABLE 1

SUMMARY OF CRITICAL DESIGN CONDITIONS FOR ADVANCED COMPOSITE RUDDER

DESIGN CONDITION	GROSS WEIGHT		VELOCITY		ALTITUDE		δ_r	β	HINGES ASSUMED FAILED	CRITICALLY LOADED HINGE NO.
	kg	LB	m/SEC	KNOTS	m	FT	(DEG)	(DEG)		
DYNAMIC OVERSWING	167,830	370,000	167.8	326	7315	24,000	9.62	10.11	NONE	14
RUDDER KICK	217,160	478,750	182.7	250	0	0	9.65	0	NONE 15 7 AND 12 14	13 AND 14 16 NONE 13, 15 AND 16
ENGINE FLAME-OUT HINGELINE LOAD FACTOR	215,910	476,000	216.2	420	0	0	−15.40	2.74	NONE 15 16 7 AND 12 14	16 NONE 17 NONE 13 AND 15
±36G ULTIMATE	—	—	—	—	—	—	—	—	NONE	15

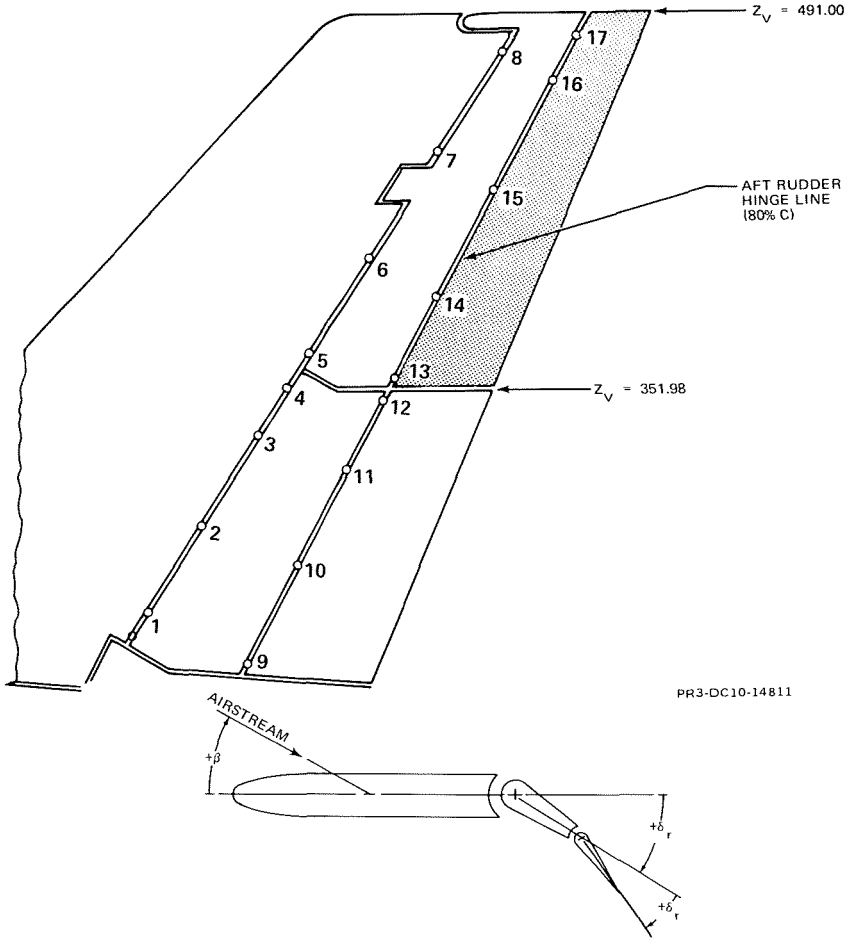

TABLE 2

LAMINA DESIGN ALLOWABLE STRESS FOR THORNEL 300/5208 MATERIAL

PROPERTY	TEMP °K	TEMP °F	ALLOWABLE STRESSES: STANDARD DEVIATION MPa	STANDARD DEVIATION KSI	AVERAGE MPa	AVERAGE KSI	"A" VALUE MPa	"A" VALUE KSI	"B" VALUE MPa	"B" VALUE KSI
F_L (TENSION)	294	70	158.80	23.03	1539.39	223.27	913.86	132.54	1170.76	169.81
F_L (COMPRESSION)	294	70	162.48	23.57	1392.74	202.00	726.80	105.41	999.90	145.02
F_T (TENSION)	294	70	3.31	0.48	42.31	6.14	29.26	4.24	34.62	5.02
F_T (COMPRESSION)	294	70	19.98	2.90	147.55	21.40	68.81	9.98	101.15	14.67
F_{LT} (SHEAR)	294	70	3.72	0.54	95.35	13.83	80.70	11.70	86.72	12.58
SHEAR (SHORT BEAM)	294	70	–	–	130.31	18.90	–	–	–	–
F_L (TENSION)	219	−65	–	–	1404.57	203.72	834.27	121.00	1068.69	155.00
F_L (COMPRESSION)	219	−65	–	–	1565.68	227.08	813.58	118.00	1123.84	163.00
F_T (TENSION)	219	−65	–	–	33.16	4.81	22.89	3.32	27.10	3.93
F_T (COMPRESSION)	219	−65	–	–	168.23	24.40	78.60	11.40	115.14	16.70
F_{LT} (SHEAR)	219	−65	–	–	94.94	13.77	79.98	11.60	86.18	12.50
SHEAR (SHORT BEAM)			–	–	156.51	22.70	–	–	–	–
F_L (TENSION)	394	250	–	–	1522.94	220.88	903.21	131.00	1158.32	168.00
F_L (COMPRESSION)	394	250	–	–	1086.84	157.63	566.75	82.20	779.11	113.00
F_T (TENSION)	394	250	–	–	24.99	3.63	17.24	2.50	20.41	2.96
F_T (COMPRESSION)	394	250	–	–	143.34	20.78	66.81	9.69	97.91	14.20
F_{LT} (SHEAR)	394	250	–	–	63.09	9.15	53.37	7.74	57.36	8.32
SHEAR (SHORT BEAM)	394	250	–	–	79.98	11.60	–	–	–	–

The allowable stress data (Table 2) were normalized to a constant ply thickness of 0.14 millimeter (5.5 mils). The reduction factors used in the derivation of "A" and "B" basis allowables at room temperature were assumed to apply at 219° and 394°K also. The lamina stiffness data (Table 3) were obtained from strain-gaged specimens. Average strains to failure and Poisson's ratios are summarized in Table 4.

Allowable stresses for patterned laminates were determined from the 264 specimen tests summarized in Table 5. These data were also normalized to a ply thickness of 0.14 millimeter and reduced at 219° and 394°K in the same manner as the lamina allowables. The elastic properties and allowable stresses are presented in Tables 6 and 7, respectively.

A group of bolt-bearing specimens was tested to confirm bearing stress allowables used in analysis of the hinge and crank fitting attachments of the graphite rudder. The joint specimen configurations were designed to simulate the geometry and load-path eccentricities of the hinge and crank fitting details selected for the rudder.

TABLE 3

AVERAGE VALUES OF LAMINA YOUNG'S MODULI FOR THORNEL 300/5208 MATERIAL

TEMP		YOUNG'S MODULI									
		TENSION E_L		COMPRESSION E_L		TENSION E_T		COMPRESSION E_T		SHEAR G_{LT}	
^oK	^oF	GPa	MSI	GPa	MSI	GPa	MSI	GPa	MSI	GPa	MSI
294	70	146.86	21.30	131.00	19.00	10.89	1.58	13.03	1.89	6.41	0.93
219	−65	148.93	21.60	142.72	20.70	12.13	1.76	12.20	1.77	8.07	1.17
394	250	150.31	21.80	128.24	18.60	7.52	1.09	7.93	1.15	5.79	0.84

TABLE 4
AVERAGE VALUES OF LAMINA FAILURE STRAINS AND POISSON'S RATIOS FOR THORNAL 300/5208 MATERIAL

TEMP		FAILURE STRAINS (PERCENT)			POISSON'S RATIO μ_{LT}	
		0-DEG DIRECTION		90-DEG DIRECTION		
^oK	^oF	TENSION	COMPRESSION	TENSION	TENSION	COMPRESSION
294	70	1.10	0.86	0.36	0.377	0.380
219	−65	0.93	0.78	0.21	0.386	0.373
394	250	0.99	0.97	0.32	0.379	0.400

TABLE 5
LAMINATE DESIGN ALLOWABLE TEST PROGRAM FOR THORNEL 300/5208 MATERIAL

SPECIMEN CONFIGURATION	BASIC LAMINATE PATTERN	SPECIMENS REQUIRED[1] PER TEST TEMP ^oK (^oF)		
		219 (−65)	294 (70)	394 (250)
a) IITRI TENSION	(45/−45)S	6	12	6
	(0/45/−45)S	6	12	6
	(0/45/90/−45)S	6	12	6
	(90/45/−45)S	6	12	6
b) SANDWICH BEAM COMPRESSION	(45/−45)S	6	12	6
	(0/45/−45)S	6	12	6
	(0/45/90/−45)S	6	12	6
	(90/45/−45)S	6	12	6
c) RAIL SHEAR	(45/−45)S	6	12	6
	(0/45/90/−45)S	6	12	6
	(90/45/−45)S	6	12	6

[1] ONE OF EACH THREE SPECIMENS WAS STRAIN-GAGED.

TABLE 6
AVERAGE VALUES FOR LAMINATE YOUNG'S MODULI
FOR THORNEL 300/5208 MATERIAL

PATTERN	TEMP °K	TEMP °F	YOUNG'S MODULI TENSION (E_T) GPa	TENSION (E_T) KSI	COMPRESSION (E_L) GPa	COMPRESSION (E_L) KSI	SHEAR (G_{LT}) GPa	SHEAR (G_{LT}) KSI
(45/−45)S	294	70	26.1 (4)	3.78	24.9 (4)	3.61	31.5 (3)	4.57
	219	−65	26.9 (2)	3.90	30.6 (2)	4.44	33.1 (1)	4.80
	394	250	16.4 (2)	2.37	21.3 (1)	3.08	32.2 (1)	4.66
(0/45/−45)S	294	70	64.9 (4)	9.40	64.3 (4)	9.32	SEE	
	219	−65	65.8 (2)	9.53	70.9 (2)	10.27	(90/45/45)S	
	394	250	60.6 (2)	8.78	54.3 (2)	7.87	DATA	
(0/45/90/−45)S	294	70	56.0 (4)	8.11	53.9 (4)	7.81	17.4 (1)	2.52
	219	−65	61.3 (2)	8.89	58.6 (2)	8.50	19.9 (2)	2.89
	394	250	53.1 (2)	7.70	53.7 (2)	7.78	18.2 (2)	2.64
(90/45/−45)S	294	RT	31.0 (4)	4.50	32.1 (4)	4.65	22.6 (4)	3.28
	219	−65	26.0 (2)	3.77	37.0 (2)	5.36	30.6 (1)	4.44
	394	250	30.7 (2)	4.45	28.1 (2)	4.07	22.0 (2)	3.19

NUMBERS IN PARENTHESES INDICATE NUMBER OF TESTS FROM WHICH AVERAGE WAS COMPUTED.

Two test results were obtained from each of the 22 specimens. Four tests were run with a 0.5 millimeter (0.02 inch) spacer at the faying surface of the laminate. This spacer represented the nominal tolerance take-up shims anticipated at the rudder hinge fittings. An additional four tests were run with a 4.8 millimeter (0.19 inch) spacer at the faying surface to represent the thickness of the hinge fitting flange to which the crank fitting attached. The spacers accurately represented the load path eccentricities of the rudder fitting installations.

Both the rudder and the joint specimens were designed to preclude tension-through-the-hole failures in the laminates. The specimens failed either in bearing or in combined bearing and shear modes as shown in Figures 6 and 7.

The tests were conducted at 219°, 294°, and 394°K and selected specimens were tested after a 30-day exposure to 100 percent relative humidity. Joint configurations, test conditions, and test results are summarized in Table 8.

TABLE 7

LAMINATE DESIGN ALLOWABLE STRESSES FOR THORNEL 300/5208 MATERIAL

PATTERN	TEMP °K	TEMP °F	BASIS	ALLOWABLE STRESS: TENSION[1] MPa	TENSION[1] KSI	IN-PLANE COMPRESSION[1] MPa	IN-PLANE COMPRESSION[1] KSI	SHEAR MPa	SHEAR KSI
(45/−45)S	294	70	AVERAGE	139.71	20.26	180.43	26.16	391.94	56.84
			A	106.56	15.45	152.95	22.18	123.97	17.98
			B	120.21	17.43	164.27	23.82	234.19	33.96
	219	−65	AVERAGE	169.27	24.55	268.29	38.91	328.31	47.61
			A	129.10	18.72	227.42	32.98	103.85	15.06
			B	145.64	21.12	244.26	35.42	196.17	28.45
	394	250	AVERAGE	92.30	13.38	155.80	22.59	336.46	48.80
			A	70.40	10.21	132.07	19.15	106.42	15.43
			B	79.42	11.51	141.84	20.57	201.04	29.15
(0/45/−45)S	294	70	AVERAGE	503.02	72.95	504.52	73.17	SEE (90/45/−45)S DATA	
			A	208.03	30.17	307.87	44.65		
			B	329.53	47.79	388.87	56.40		
	219	−65	AVERAGE	480.36	69.67	588.64	85.37		
			A	198.66	28.81	359.20	52.09		
			B	314.68	45.64	453.71	65.80		
	394	250	AVERAGE	342.69	49.70	412.15	59.77		
			A	141.72	20.55	251.50	36.47		
			B	224.49	32.56	317.67	46.07		
(0/45/90/−45)S	294	70	AVERAGE	413.91	60.03	454.96	65.98	309.31	44.86
			A	238.27	34.55	272.55	39.53	142.51	20.66
			B	310.62	45.05	347.68	50.42	211.21	30.63
	219	−65	AVERAGE	388.06	56.28	517.46	75.05	226.56	32.86
			A	223.38	32.39	309.99	44.96	104.38	15.13
			B	291.21	42.23	395.44	57.35	154.70	22.43
	394	250	AVERAGE	305.93	44.37	355.85	51.61	223.06	32.35
			A	176.11	25.54	213.17	30.91	102.77	14.90
			B	229.58	33.29	271.94	39.44	152.31	22.09
(90/45/−45)S	294	70	AVERAGE	167.54	24.30	185.34	26.88	428.16	62.09
			A	108.68	15.76	131.13	19.01	299.99	43.51
			B	132.92	19.27	153.46	22.25	352.78	51.16
	219	−65	AVERAGE	177.63	25.76	204.74	29.69	122.83	39.09
			A	115.23	16.71	144.86	21.01	188.87	27.39
			B	140.93	20.44	169.52	24.58	222.11	32.21
	394	250	AVERAGE	129.09	18.72	169.24	24.54	365.13	52.95
			A	83.74	12.14	119.75	17.36	255.82	37.10
			B	102.41	14.85	140.13	20.32	300.84	43.63

[1] LOAD DIRECTION ALONG 0-DEG FIBER AXIS.

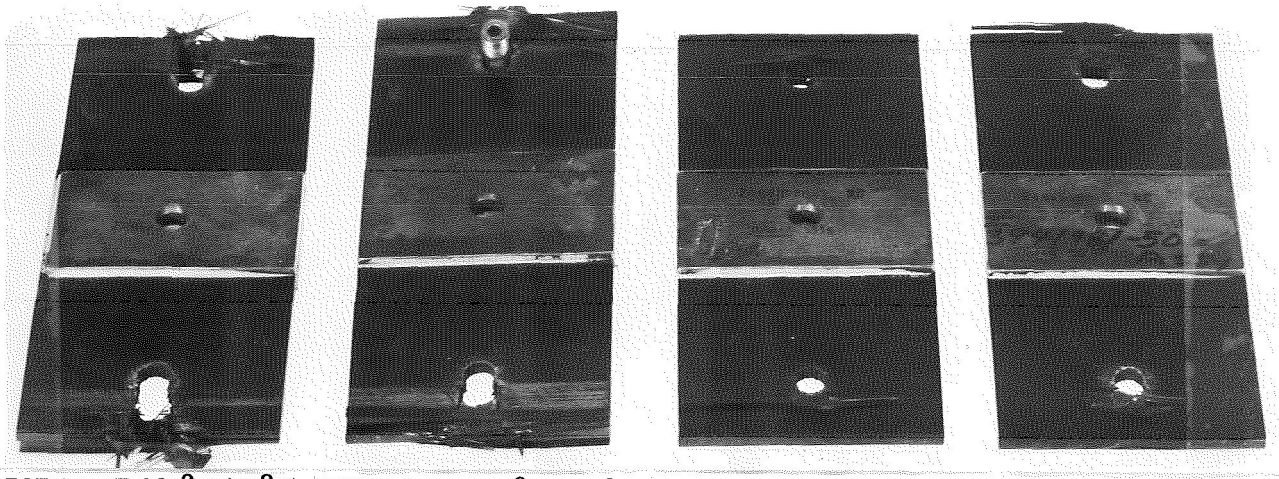

TESTED AT 294°K (70°F) | TESTED AT 394°K (250°F) | TESTED AT 219°K (–65°F) | TESTED AT 294°K (70°F) WITH 4.8 mm SPACER

FIGURE 6. BOLT BEARING SPECIMEN FAILURES

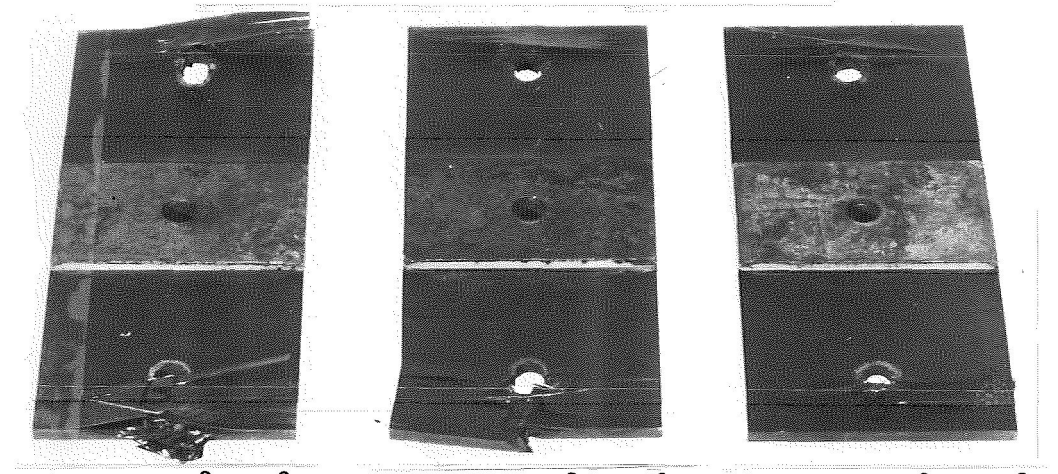

TESTED AT 294°K (70°F) | TESTED AT 394°K (250°F) | TESTED AT 219°K (–65°F)

AFTER 30 DAYS EXPOSURE TO 100-PERCENT RELATIVE HUMIDITY

FIGURE 7. BOLT BEARING SPECIMEN FAILURES AFTER HUMIDITY EXPOSURE

TABLE 8

BOLT BEARING TEST RESULTS

THORNEL 300/5208 LAMINATE
(0, 45, 90, –45) 4S NOMINAL THICKNESS = 4.47 mm (0.176 INCH)
7.94-mm (5/16-INCH) DIAMETER TITANIUM BOLT

SPECIMEN GROUP NO.	PRE-TEST ENVIRONEMENT EXPOSURE	TEST TEMP		SPACER THICKNESS		NO. OF TESTS	AVERAGE FAILURE LOAD		STANDARD DEVIATION		ALLOWABLE ULTIMATE BEARING STRESS (PSI)			
											"A" BASIS		"B" BASIS	
		°K	°F	mm	IN.		N	LB	N	LB	MPa	KSI	MPa	KSI
1	NONE	294	70	NONE	NONE	8	27,174	6109	1944.0	437.0	524.76	76.11	621.29	90.11
2	NONE	394	240	NONE	NONE	4	24,327	5469	1740.1	391.2	469.74	68.13	556.20	80.67
3	NONE	219	–65	NONE	NONE	6	28,171	6333	2015.0	453.0	543.93	78.89	643.97	93.40
4	NONE	294	70	0.51	0.02	4	25,635	5763	1833.6	412.2	495.04	71.80	586.12	85.01
5	NONE	294	70	4.83	0.19	4	25,088	5640	1794.9	403.5	484.43	70.26	573.51	83.18
6	100-PERCENT	294	70	NONE	NONE	8	28,135	6325	2344.2	527.0	502.77	72.92	514.62	74.64
7	RELATIVE	394	250	NONE	NONE	4	24,269	5456	2022.2	454.6	433.68	62.90	443.88	64.38
8	HUMIDITY 30 DAYS	219	–65	NONE	NONE	6	27,948	6283	2328.6	523.5	499.39	72.43	511.18	74.14

The test results indicated that adequate safety margins were attained at all hinge and crank fitting attachments throughout the service temperature and humidity environment of the rudder.

Design Details

The rib-stiffened rudder configuration consisted of the graphite-epoxy box-structure, conventional machined aluminum alloy fittings at the five hinge or actuator stations, the fiberglass-epoxy leading and trailing edge installations, and the fiberglass-epoxy tip installation. A lightning protection system was incorporated to preclude structural damage due to lightning strikes. A modification to the metal forward rudder was required to accommodate differential thermal expansions between the forward and aft rudders in the operating temperature range. Salient design details of these structures are described in this section.

Graphite-Epoxy Box-Structure. - The graphite-epoxy box-structure was conceived as a single molded assembly consisting of the two skin panels, the front and rear spars and 31 ribs. The skin panels consisted primarily of a basic 6-ply pattern (0°, +45°, -45°)S with the 0° ply oriented spanwise. The fore and aft boundaries and the upper edges of the skin panels were reinforced as shown in Figure 8 to provide for attachment of the leading and trailing edge assemblies, the tip assembly, and hinge and actuator fittings.

Five access holes were required in the right-hand skin panel to provide wrench access for the hinge-bearing nut installations. These regions were reinforced locally to 16 plies. Similarly, both skin panels were built-up locally at the four attach points for the rudder crank fittings (up to 28 plies) for increased bearing strength. The reinforced regions consisted of multiple layers of a quasi-isotropic four-ply pattern (0°, 45°, 90°, -45°)S to enhance bearing properties for the mechanical fasteners in these regions.

The rib elements, Figure 9, consisted of the eight-ply quasi-isotropic (0°, 45°, 90°, -45°)S pattern at the five hinge locations (10 ribs) and the six-ply (0°, 45°, -45°)S pattern otherwise. A single chordwise ply was added to each rib-cap at the skin interface to increase bending strength and rigidity.

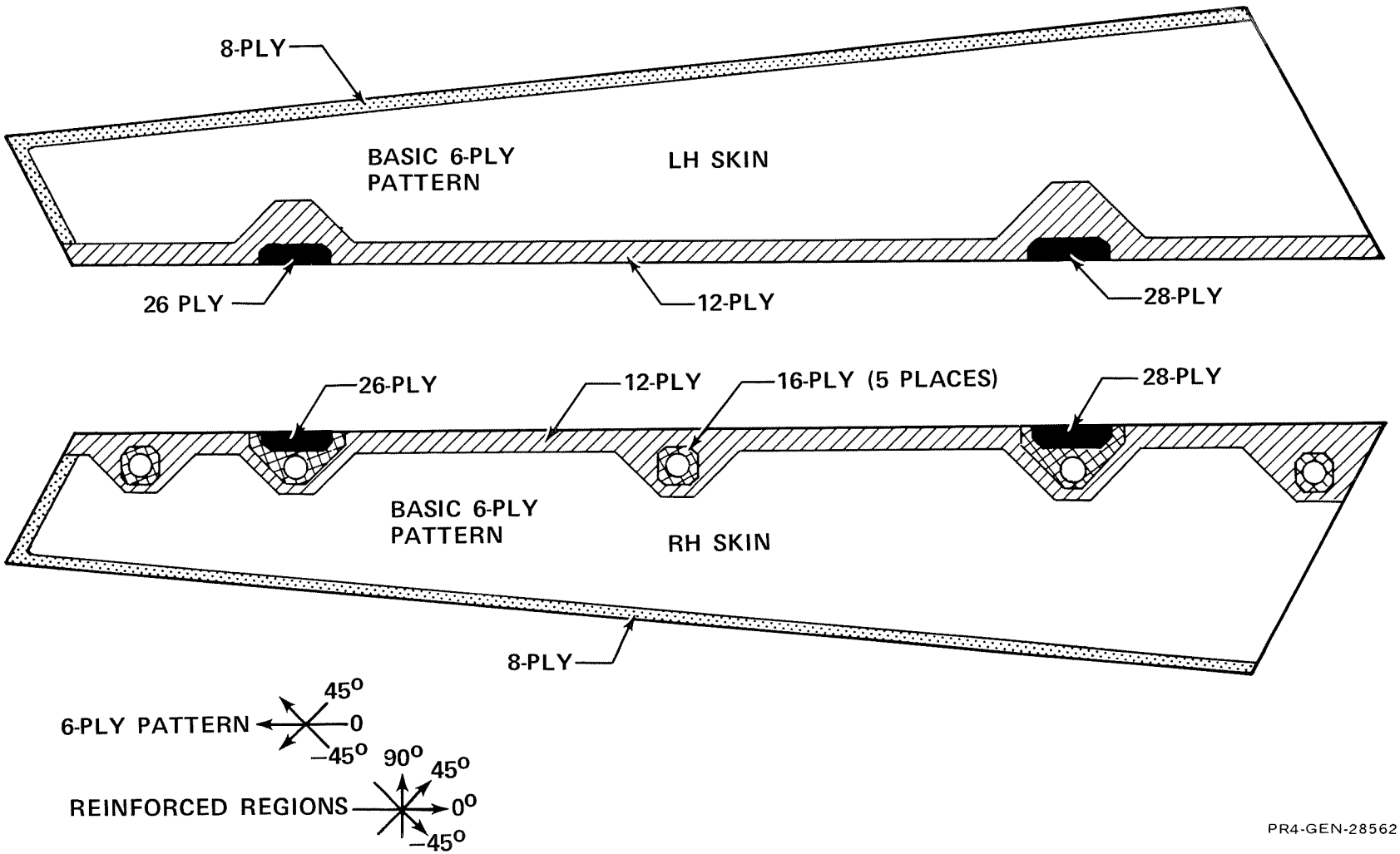

FIGURE 8. LAMINATED SKIN PANEL DESIGN

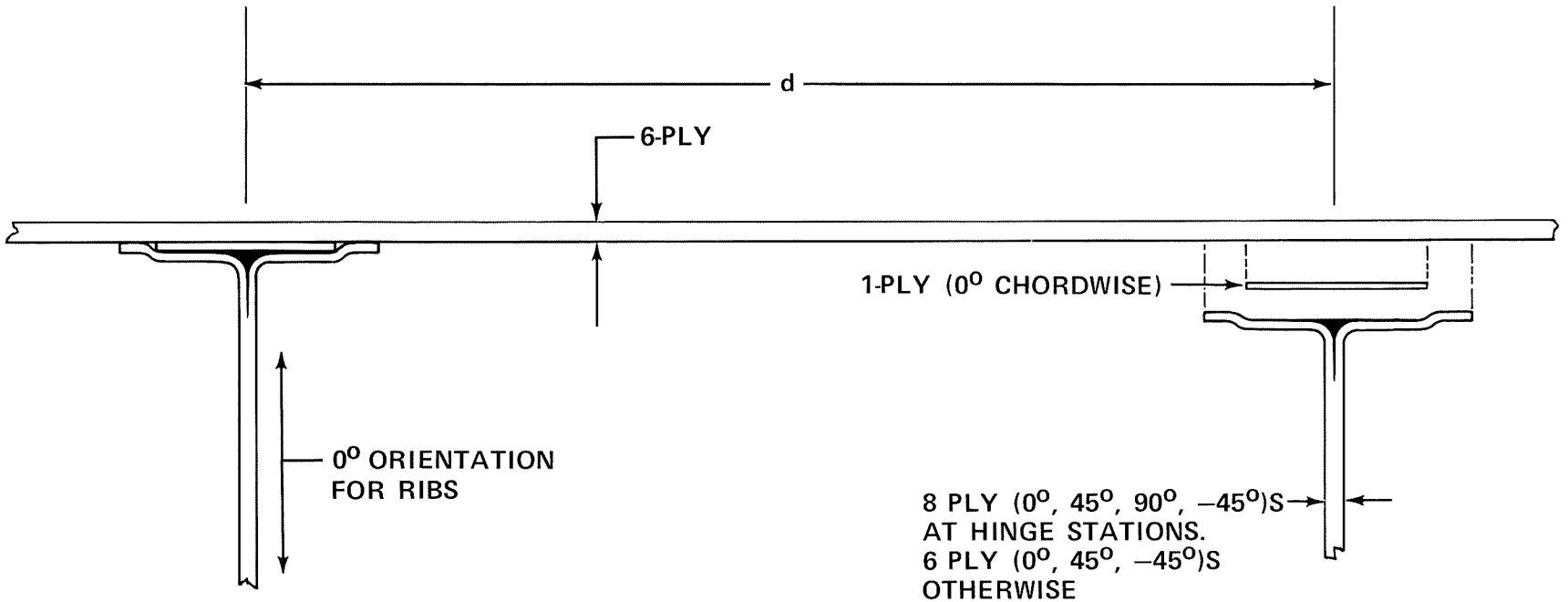

RUDDER SECTOR	RIB SPACING d		ULTIMATE LOAD INTENSITIES			
			COMPRESSION IN RIB-CAP		SHEAR-IN SKIN	
	(cm)	(IN.)	(N)	(LB)	(N/m)	(LB/IN.)
UPPER	11.7	4.6	6,636	1492	194	111
CENTRAL	13.0	5.1	3,456	777	182	104
LOWER	14.5	5.7	11,436	2571	193	110

PR4-GEN-28561B

FIGURE 9. DETAILS OF SKIN-RIB INTERFACE

Details of the aluminum alloy crank and hinge fitting attachments are shown in Figures 10 and 11. The indicated laminate thicknesses included the contribution of the front-spar flange (eight-ply) in addition to the reinforced skin regions. Pan-head Hi-Lok pins were specified at the external skin attach points. These pins provided increased bearing strengths in comparison to countersunk bolts and a low head profile for reduced drag in comparison to equivalent hex-head bolts. Hex-head bolts were specified at skin attach points covered by aerodynamic fairings. Titanium alloy pins and bolts were used in all cases for improved corrosion resistance.

Leading Edge Installation. - The fiberglass-epoxy leading edge structure, Figure 12, consisted of 12 segments to provide maintenance access to the hinge fittings equivalent to the conventional metal rudder. Each segment of the leading edge was attached with flush titanium alloy screws and nutstrips or nutplates using steel nuts. The basic laminate thickness consisted of five plies of 181 style glass fabric with a nominal cured thickness of 1.27 millimeter (0.050 inch). The basic laminate thickness was increased at points of attachment and in splice regions as shown in Figure 12.

Trailing Edge Installation. - The fiberglass-epoxy trailing edge structure, Figure 13, was an adaptation of the existing DC-10 design to the graphite rudder box geometry. It was divided into three segments similar to the production installation. The basic four-ply laminate was increased to five plies at the points of attachment to the graphite rudder box. The trailing edge segments were attached to the box structure with a cold-set adhesive in addition to the attach rivets in keeping with design policy established through development of several previous transport aircraft. The aluminum alloy rivets were anodized and coated to inhibit galvanic corrosion at the graphite interface.

Tip Installation. - The tip installation, Figure 14, was also a fiberglass-epoxy construction with thicknesses similar to the trailing edge. The tip assembly was riveted to the fiberglass-epoxy closing rib of the rudder box. No special corrosion protection was required for these rivets since they interfaced only with fiberglass.

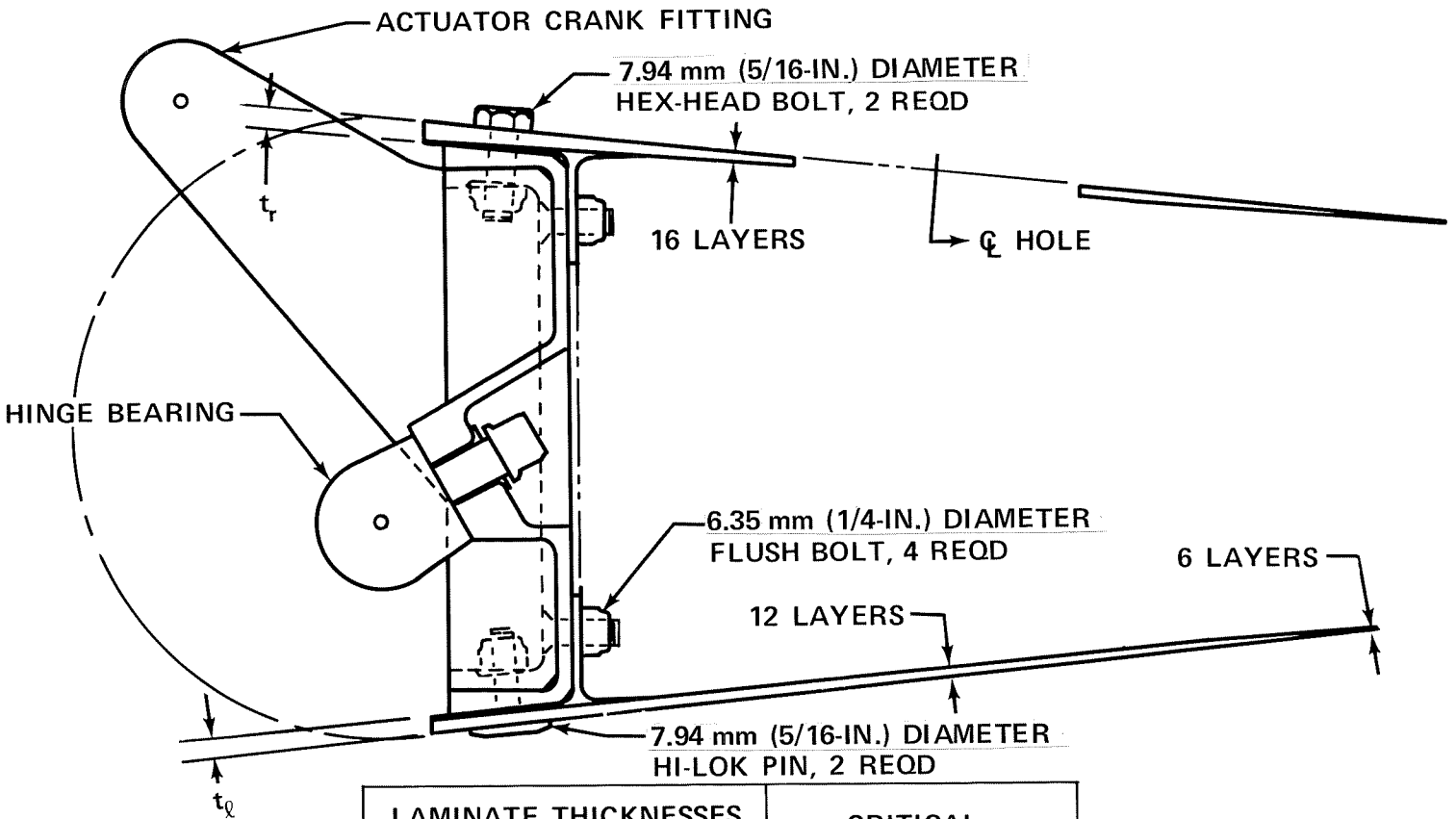

	LAMINATE THICKNESSES		CRITICAL MODE
	t_r	t_ℓ	
UPPER STATION	34-PLY	34-PLY	BEARING STRESS IN LAMINATE
LOWER STATION	36-PLY	36-PLY	ROD LUG SHEAR
			BEARING STRESS IN LAMINATE

PR4-GEN-28576A

FIGURE 10. ACTUATOR FITTING ATTACHMENT DETAILS

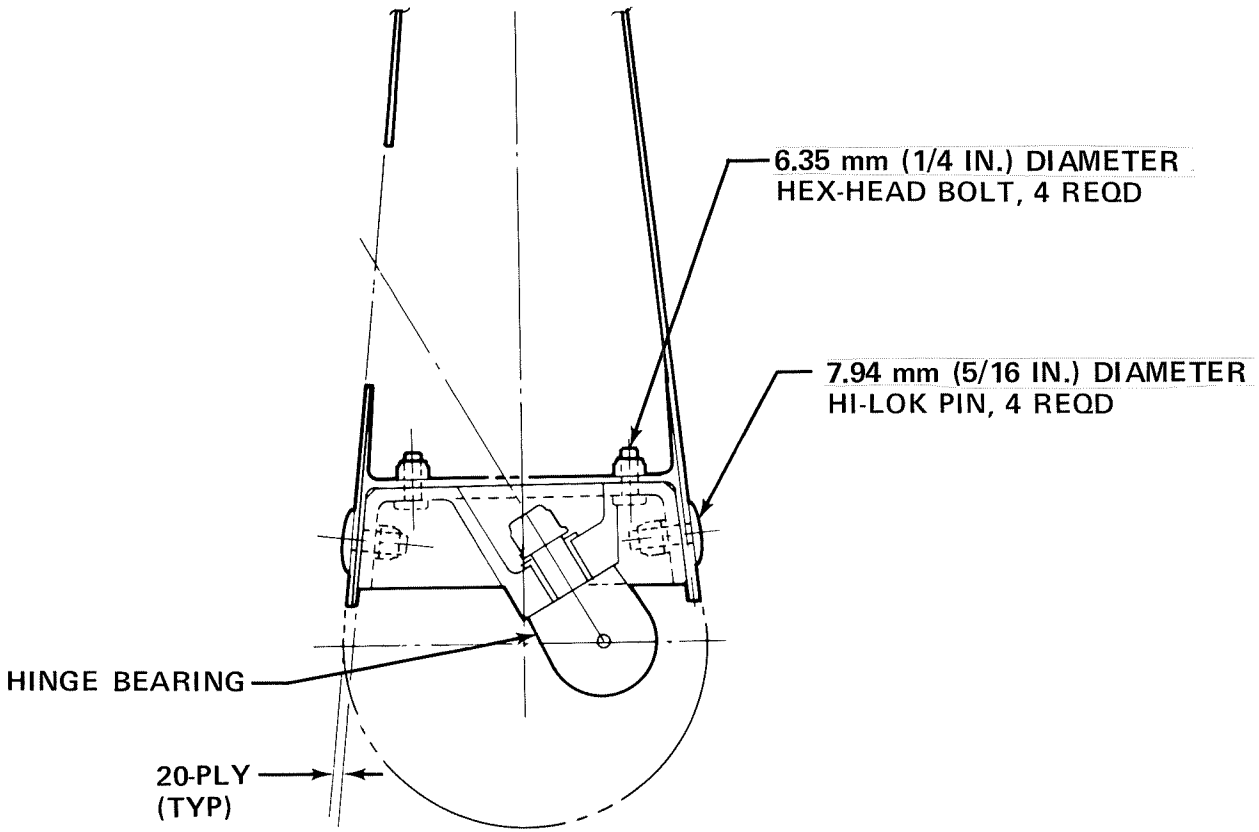

STATION	CRITICAL MODE
UPPER	BEARING STRESS IN LAMINATE
CENTER	FITTING FLANGE CRIPPLING
LOWER	BEARING STRESS IN LAMINATE

PR4-MA-4474 B

FIGURE 11. HINGE FITTING ATTACHMENT DETAILS

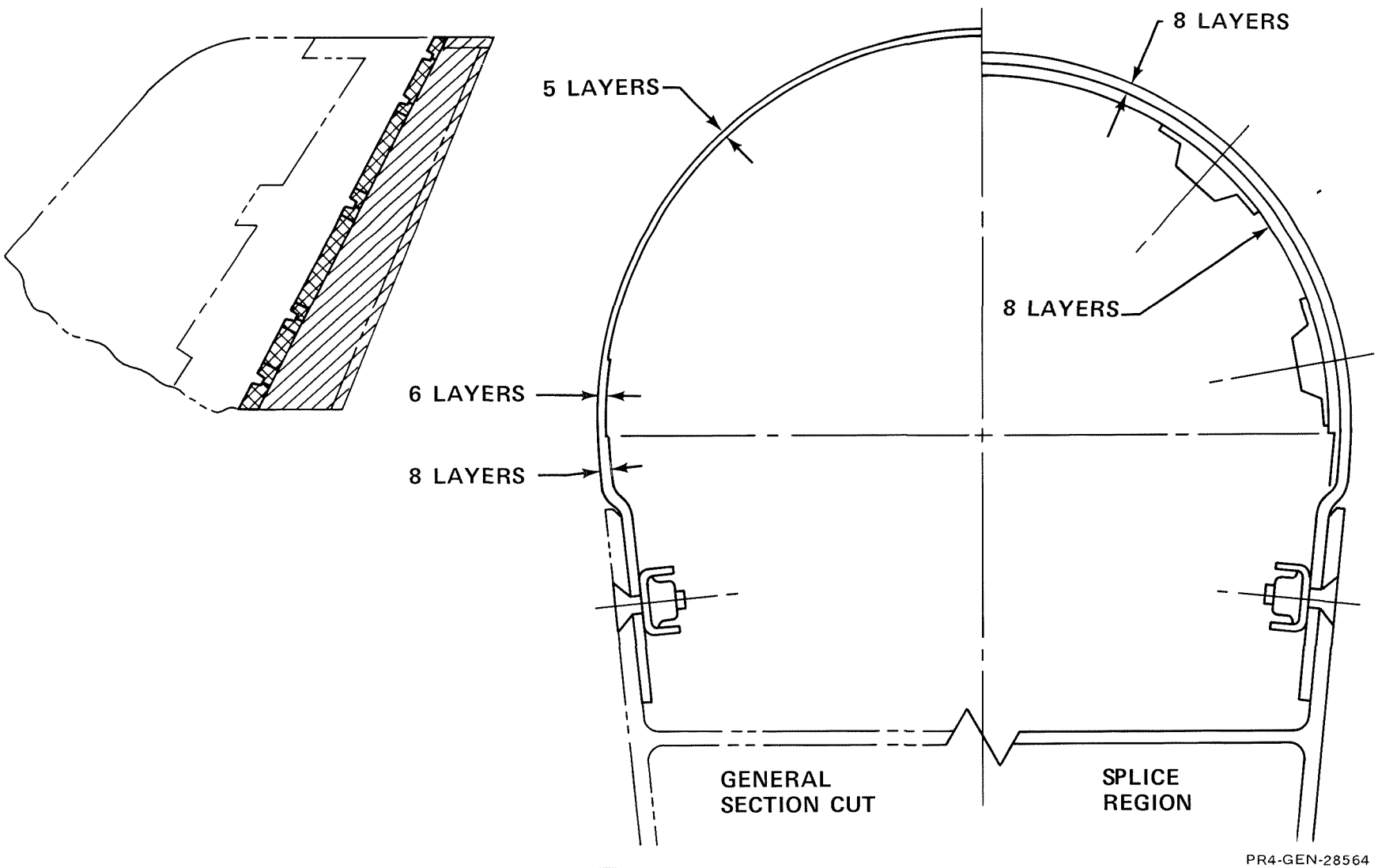

FIGURE 12. LEADING EDGE INSTALLATION

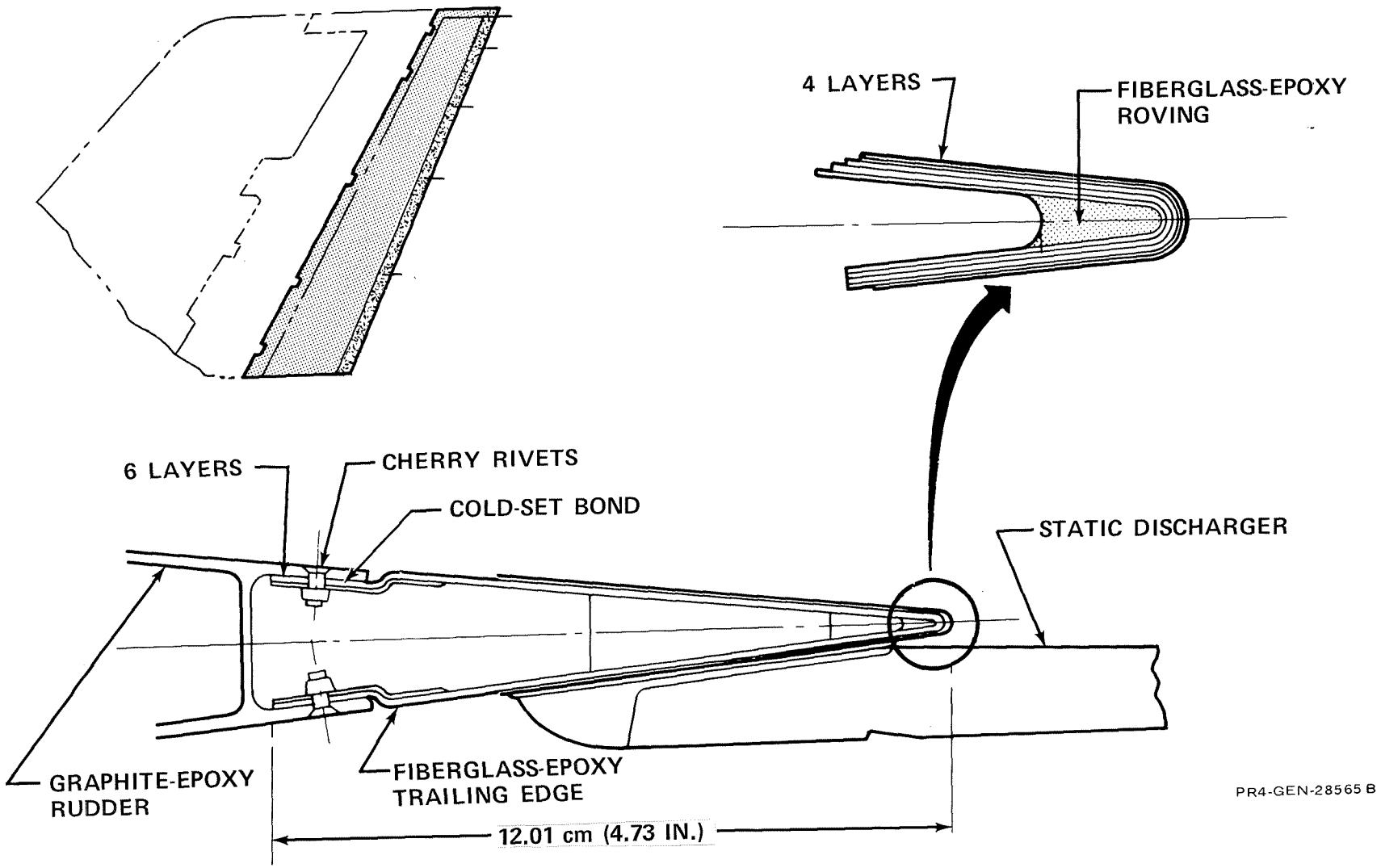

FIGURE 13. TRAILING EDGE INSTALLATION

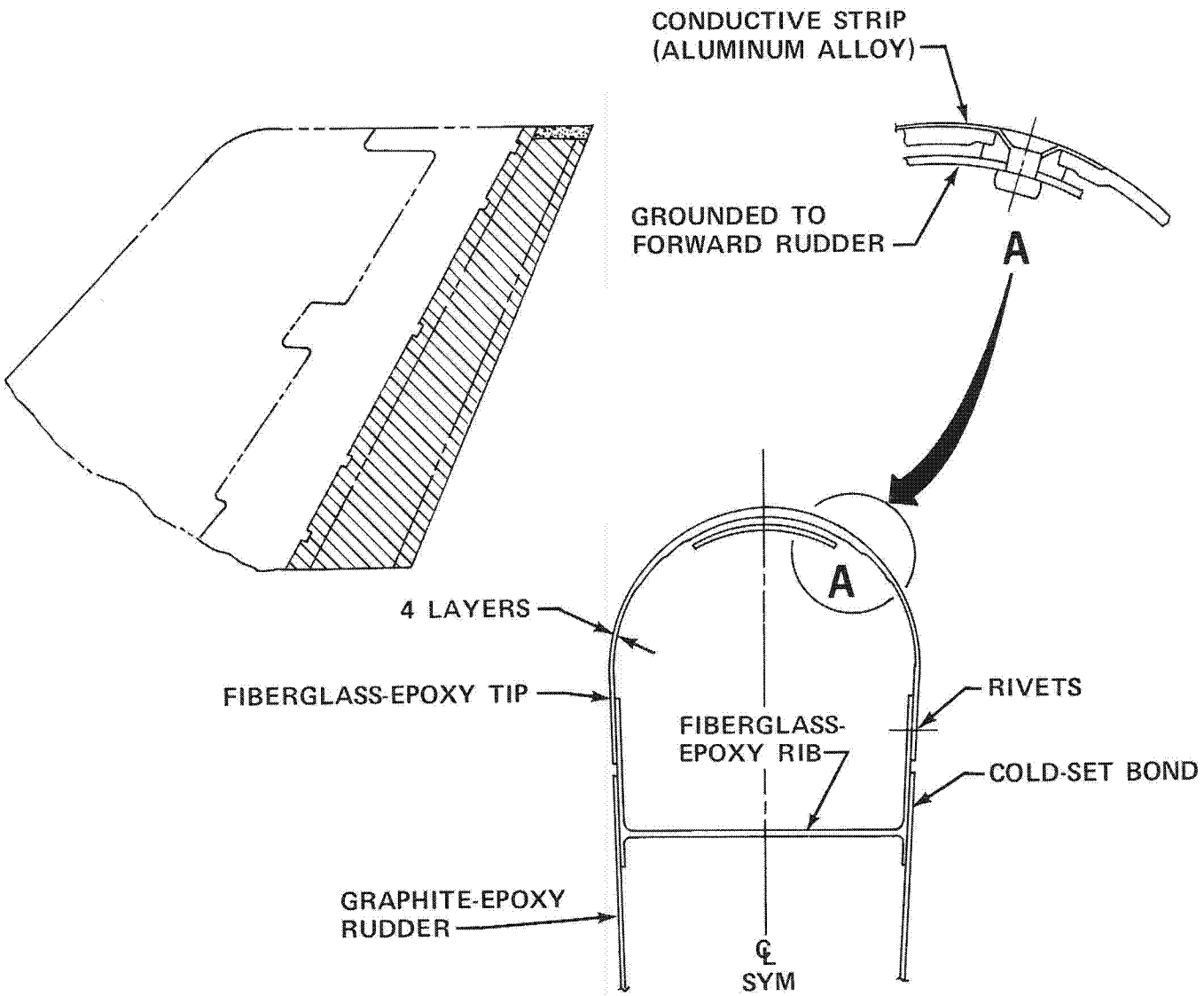

FIGURE 14. TIP INSTALLATION

Lightning Protection System. - The composite rudder is located at the upper-aft extremity of the aircraft and is vulnerable to both direct and swept-stroke lightning attachments. A design study was conducted to evaluate lightning protection and related system requirements for the composite rudder. The following conclusions were reached:

- Electromagnetic shielding was not required because the rudder did not contain electrical or avionics components.

- The composite rudder design did not adversely affect operation of the VOR/Localizer and HF antenna system located in the vertical stabilizer.

- Four precipitation static (p-static) dischargers were required at the rudder trailing edge. These dischargers required an electrical connection to the metal structure of the aircraft.

An isolation design concept, illustrated in Figure 15, was therefore selected for the composite rudder. Two thin aluminum alloy conductive straps were installed around the fiberglass tip and upper trailing edge to divert and guide direct lightning stroke currents to the forward metal structure through a bonding jumper installation. The four p-static dischargers were electrically connected to these aluminum straps. A dielectric coating, 0.15 to 0.25 millimeter (6-10 mil) thick, of epoxy and polyurethane paint was applied over the graphite skin surface for swept-stroke and restrike protection. This design assured complete isolation between the graphite composite structure and lightning current paths and thus protected the composite structure from lightning damage.

Forward Rudder Modification. - A design modification to the forward rudder "A" frame hinge brackets was required to accommodate the thermal expansion and contraction differentials between the forward and aft rudders throughout the operating temperature range (219°K to 344°K) without inducing large thermal stresses. The thermal contraction differential between 294°K (70°F) and 219°K (-65°F) was a nominal 6.1 millimeters (0.24 inch) between the lower and upper hinge stations.

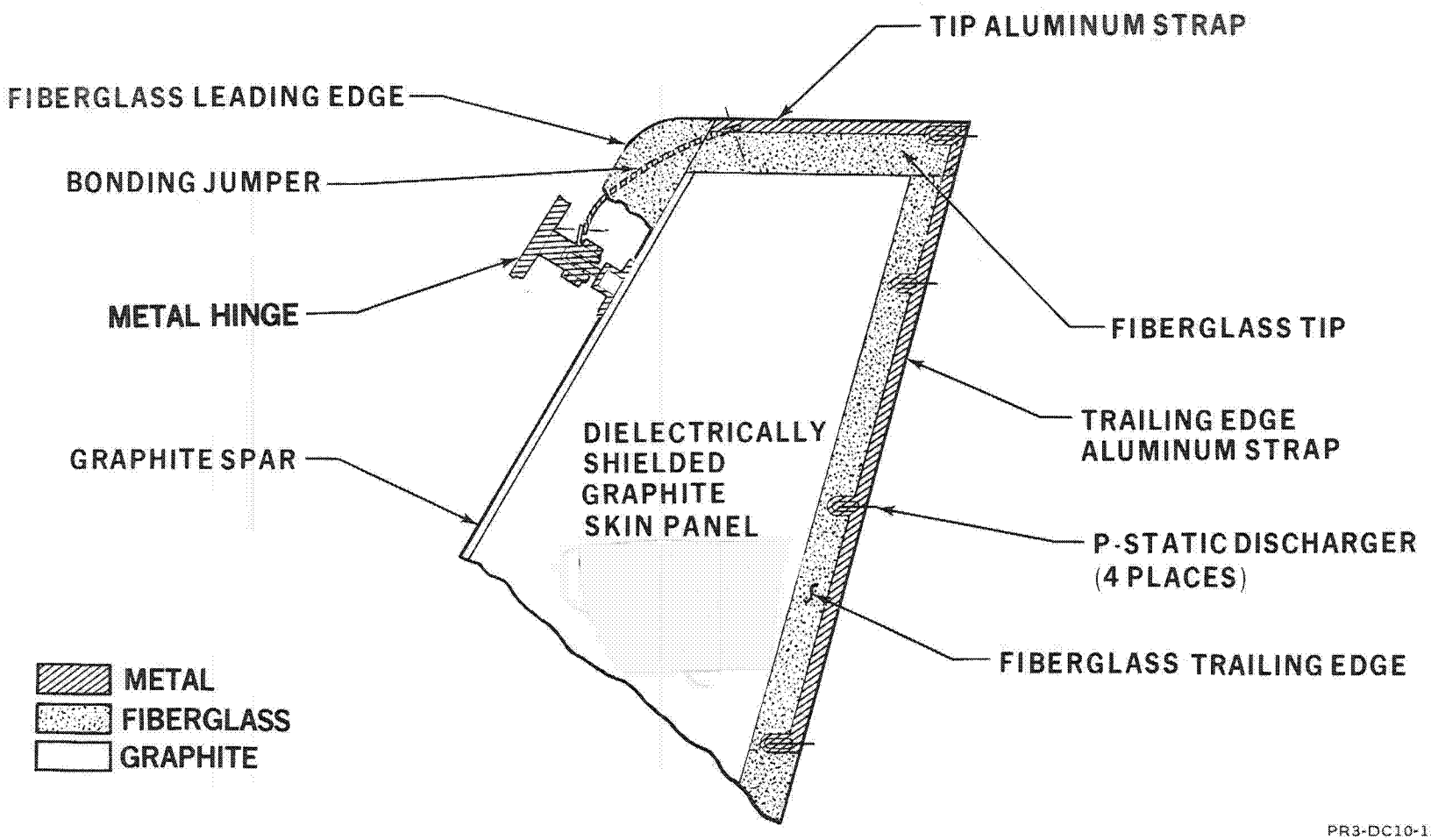

FIGURE 15. LIGHTNING PROTECTION SYSTEM

The forward rudder hinge bracket modification is shown schematically in Figure 16. The thermal problem was resolved by providing the required vertical load reaction at a rigid center hinge bracket (rather than at the lower bracket as was done on the aluminum rudder) and by providing brackets which were flexible under loads parallel to the aft rudder hingeline at the other four hinge stations. All five brackets had rigidities equivalent to the production design in planes normal to the aft rudder hingeline to retain adequate flutter margins. Dimensional free-play levels equivalent to the production installation were also maintained for the same reason.

The force-deflection characteristics of the lower four "A" frame hinge brackets were carefully designed to accommodate the necessary deflections at nominal working stress levels well within the endurance limit stress of the material to preclude fatigue problems due to the thermal flexing. Because of geometry restraints at the upper hinge station, a pivoting rather than a flexing hinge bracket was used to avoid excessive bending stresses. The modified forward rudder retained complete interchangeability with the existing metal aft rudders.

Stress Analysis

A finite element analysis model was formulated to determine internal load distributions for the graphite-epoxy rudder considering the revised stiffness characteristics and orthotropy of the selected laminate patterns. The analysis model, illustrated in Figure 17, consisted of 237 node points, 498 bar elements, and 259 shear panel elements. The aft rudder skins, front-spar, rear-spar, and all ribs were included in the model. The shear panel elements were assumed to admit shear forces only.

A coarse idealization of the forward rudder was also included together with idealizations of the five "A" frame hinge brackets. The latter elements of the model represented the fitting support normal and parallel to the hinge centerline for analysis of loads induced by the differing coefficients of thermal expansion between the forward and aft rudders.

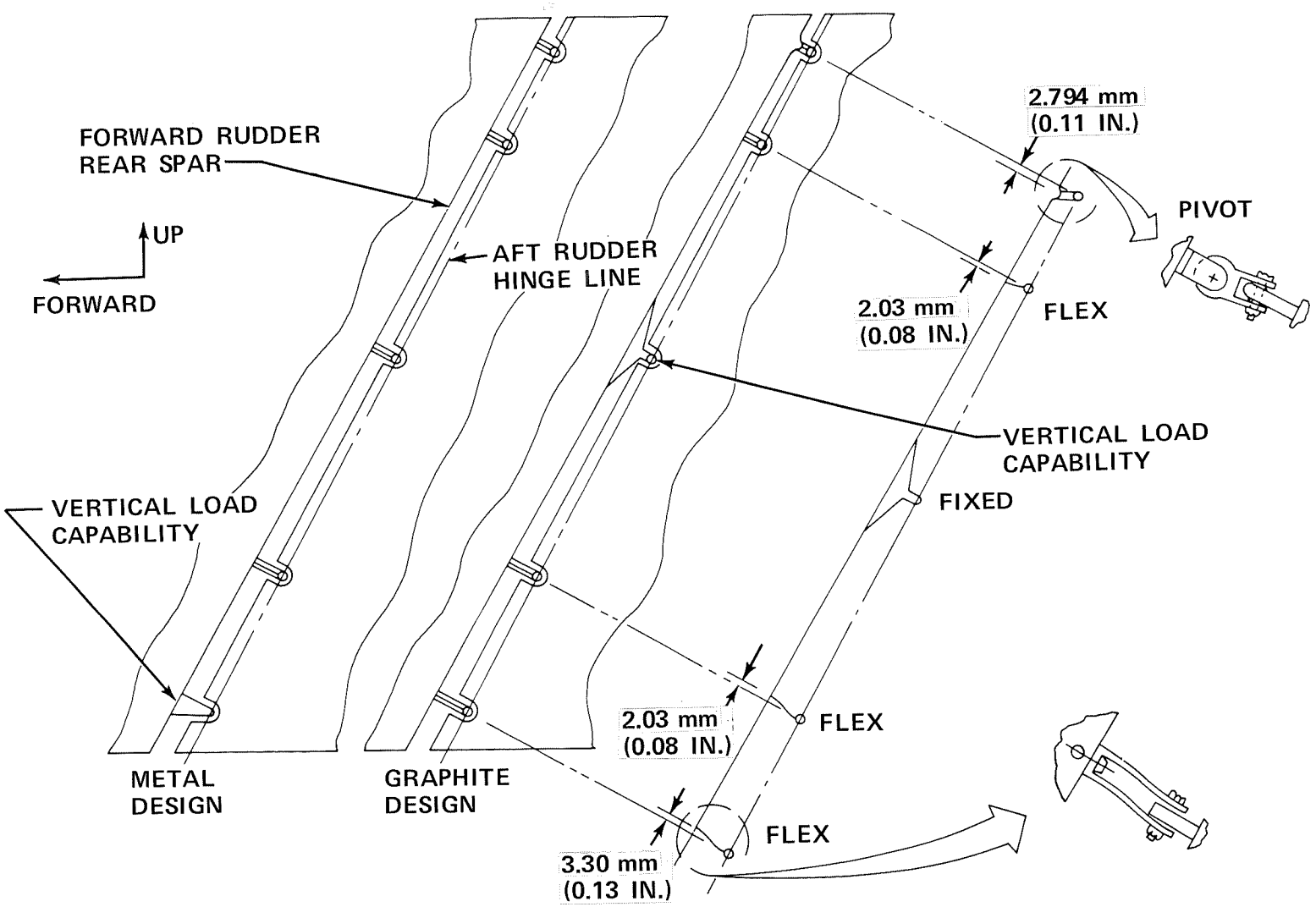

FIGURE 16. SCHEMATIC DRAWING OF FORWARD RUDDER MODIFICATION

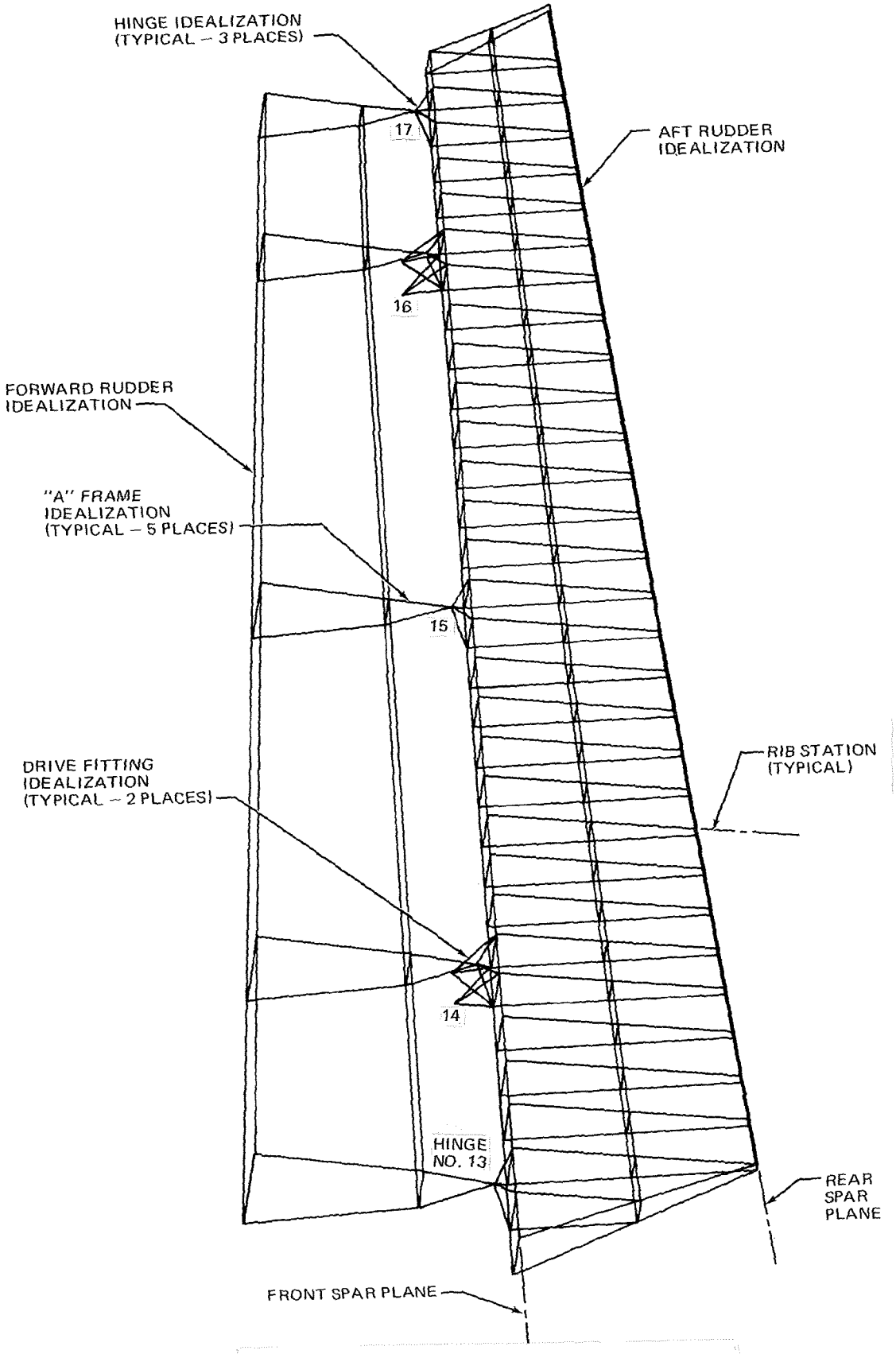

FIGURE 17. FINITE ELEMENT ANALYSIS MODEL

The normal and chordal airloads for the critical conditions were arranged into point loads which acted at the node points of the analysis model. Hinge point deflections induced by vertical fin and forward rudder bending deformations were obtained from the original aluminum alloy rudder analysis and were used as boundary restraints in the finite element analysis. There were 1126 equilibrium equations in the mathematical formulation and 1275 unknown element forces were determined in the solution.

Ten critical flight conditions were investigated in the finite element analysis. Three of the conditions were all-well conditions for which the ultimate factor of safety (1.5) was used. The remaining seven conditions resulted from the failsafe requirement that the structure sustain limit load after failure of any single structural element. Each of the critical failsafe conditions involved failed hinges.

The ten critical conditions required 40 analysis cases because the rudder hingeline was offset (i.e., the structure was not symmetric about the midplane) and two temperature conditions were significant. Internal loads varied with positive and negative rudder angles and with the temperature at which the loads were applied. The 40 analysis cases are summarized in Table 9.

The analysis results indicated that the critical hinge loads for the graphite rudder had changed significantly from the metal design, see Table 10. Analysis of the forward rudder indicated that the increased loads at hinges 13, 15, and 17 were acceptable and strength increases were not required in the forward rudder.

Critical stresses in the basic graphite box-structure are shown in Figures 18 through 20. The plots indicated the maximum-minimum stress envelopes which resulted from all 40 conditions analyzed. The influence of the driverod loads was clearly indicated in the rudder stress distributions.

TABLE 9

SUMMARY OF ANALYSIS CASES FOR THE GRAPHITE RUDDER

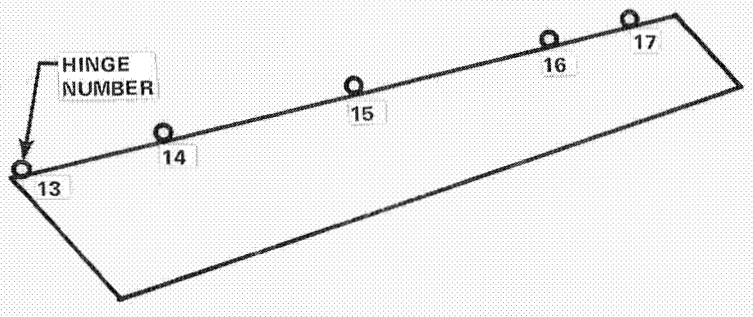

CONDITION NO.				CONDITION DESCRIPTION	δ_r (DEG)	TEMPERATURE DIFFERENTIAL, ΔT ^{o}K (^{o}F)		HINGES ASSUMED FAILED	ULTIMATE SAFETY FACTOR
1	11	21	31	A11Y (DYNAMIC OVERSWING)	±9.62	0	−75 (−135)	NONE	1.5
2	12	22	32	M11Y (RUDDER KICK)	±9.65	0	−75 (−135)	NONE	1.5
3	13	23	33					7 AND 12*	1.0
4	14	24	34					14	
5	15	25	35					15	
6	16	26	36	8A (ENGINE FLAMEOUT)	±15.4	0	−75 (−135)	NONE	1.5
7	17	27	37					7 AND 12*	1.0
8	18	28	38					14	
9	19	29	39					15	
10	20	30	40					16	

*HINGES 7 AND 12 ARE ON FORWARD RUDDER

TABLE 10

CRITICAL HINGE LOAD SURVEY

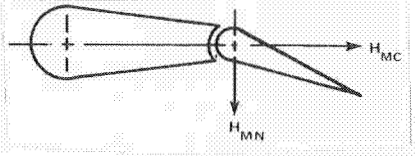

HINGE NUMBER	METAL RUDDER HINGE LOADS					GRAPHITE RUDDER HINGE LOADS					R_G/R_M
	H_{MN}		H_{MC}		CONDITION	H_{MN}		H_{MC}		CONDITION	
	N	LB	N	LB		N	LB	N	LB		
13	2,722	612	752	169	RUDDER KICK (NO. 14 OUT)	5,378	1,209	−6,294	−1,415	RUDDER KICK (NO. 14 OUT)	2.93
14*	10,898	2,450	−26,645	−5,990	ENGINE OUT	−4,724	−1,062	24,287	5,460	ENGINE OUT	0.86
15	5,556	1,249	271	61	RUDDER KICK (NO. 14 OUT)	8,496	1,910	−2,366	−532	RUDDER KICK (NO. 14 OUT)	1.59
16*	−7,211	1,621	19,915	4,477	ENGINE OUT (NO. 14 OUT)	9,328	2,097	−11,588	−2,605	ENGINE OUT (NO. 14 OUT)	0.70
17	1,303	293	489	110	ENGINE OUT (NO. 16 OUT)	3,879	872	−3,790	−852	ENGINE OUT (NO. 16 OUT)	3.89

*ROD LOCATION

$$R_G/R_M = \frac{\text{RESULTANT LOAD ON HINGE WITH GRAPHITE RUDDER}}{\text{RESULTANT LOAD ON HINGE WITH METAL RUDDER}}$$

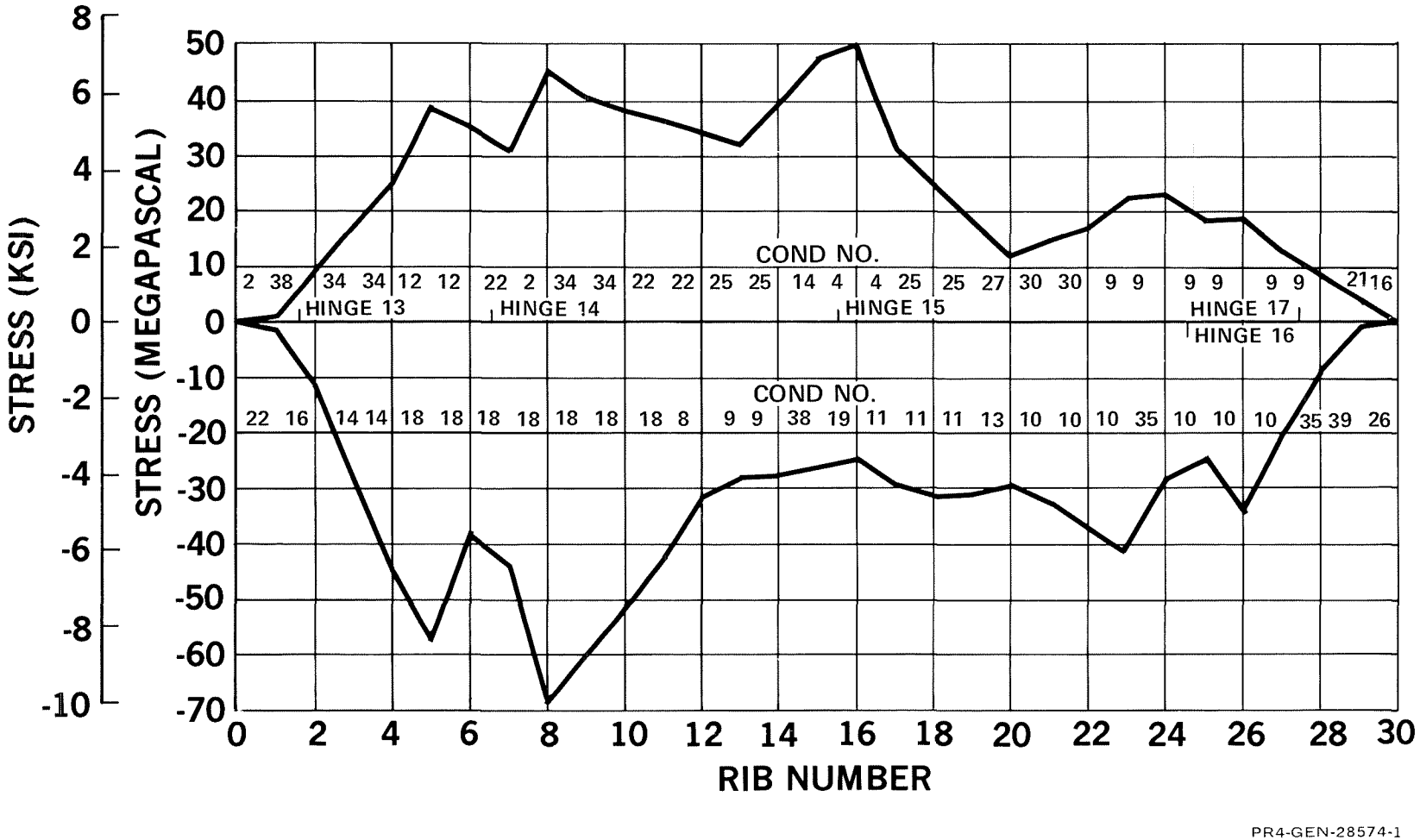

FIGURE 18. ENVELOPE OF MAXIMUM AND MINIMUM STRESSES FOR FRONT-SPAR CAP – L.H. SIDE

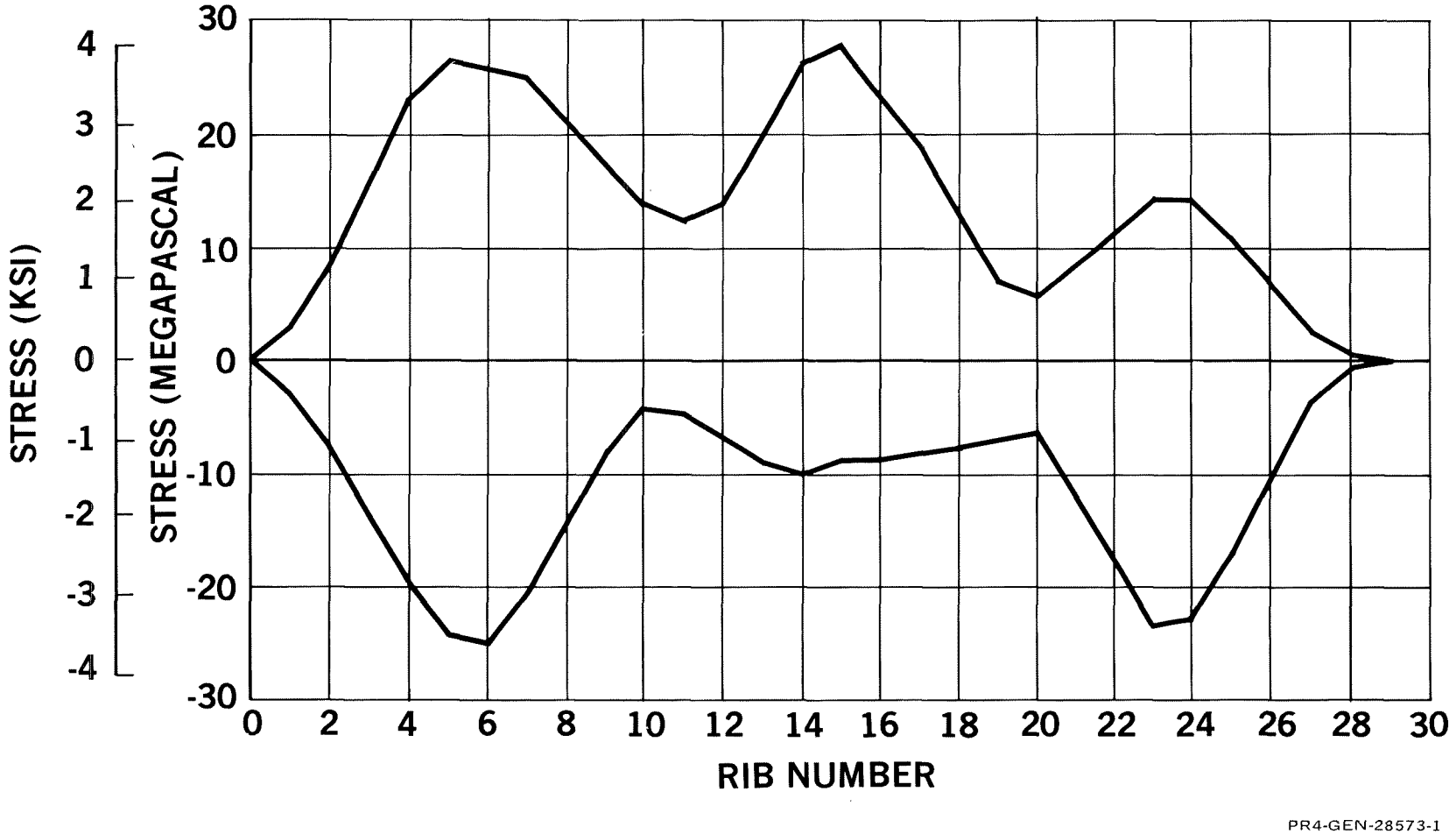

FIGURE 19. ENVELOPE OF MAXIMUM AND MINIMUM STRESSES FOR RIB CAPS – L.H. SIDE

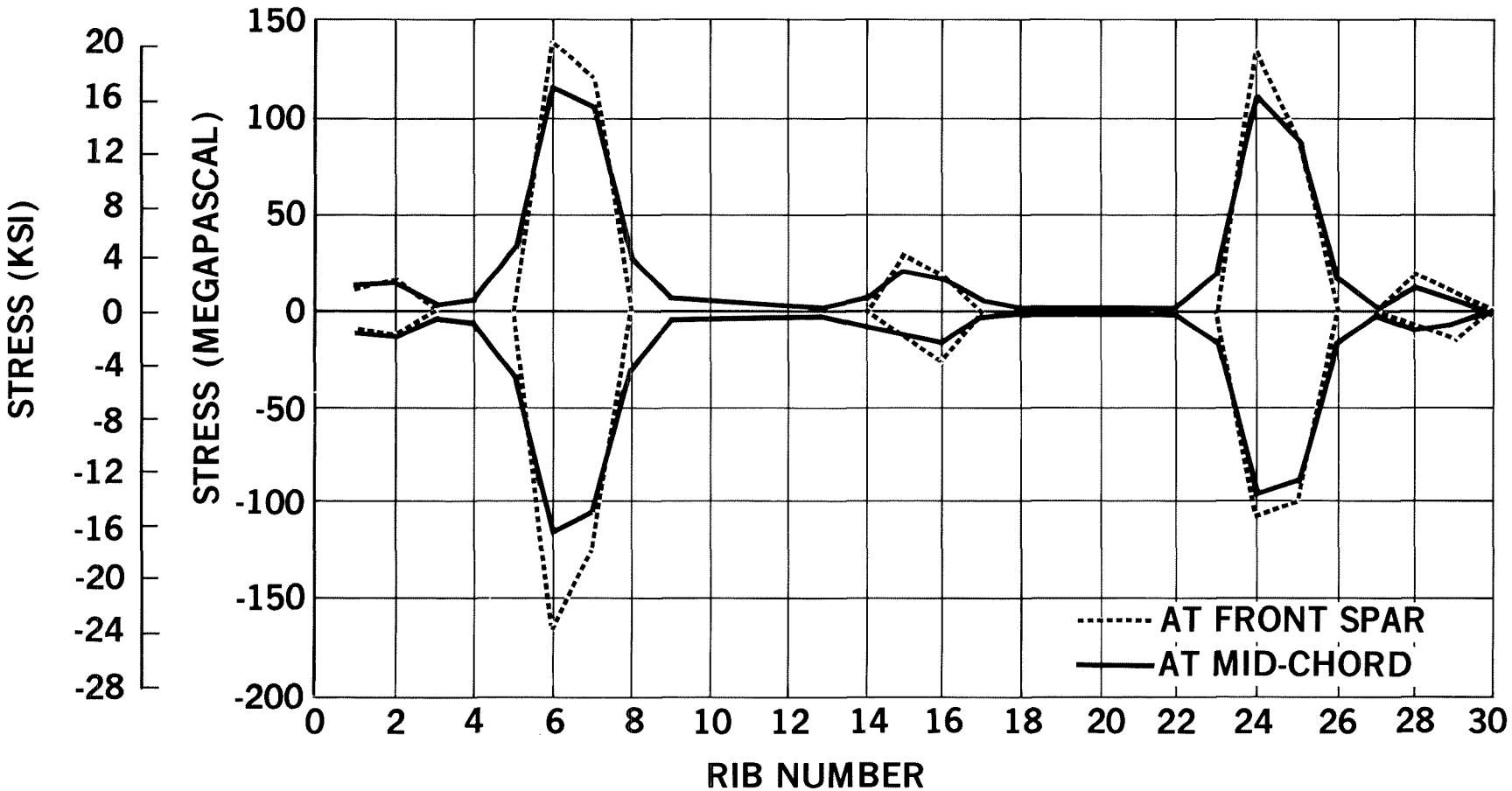

FIGURE 20. ENVELOPE OF MAXIMUM AND MINIMUM STRESSES FOR RIB CAPS – R.H. SIDE

Weight Summary

A weight summary for the conventional and graphite composite upper aft rudders is given in Table 11. The actual weight of the first composite rudder was 27.83 kilograms (61.34 pounds), a weight reduction of 33 percent in comparison with the conventional metal rudder. The actual weights of the composite rudder components were in close agreement with predicted weights. The actual weight of the paint finish (2.67 kg) exceeded the predicted weight (1.36 kg) because of the added thickness for swept-stroke lightning protection.

Rudder units 1, 6, 7, and 8 were heavier than average because of repair doublers added during construction of the graphite-epoxy mold assemblies. Unit 1 was inadvertantly cured with the wrong fiber orientation in the six-ply ribs. The rib strength was restored by secondarily bonding three ply (0°, 90°, 0°) graphite-epoxy doublers to each side of the affected ribs. Approximately 1.4 kg (3 pounds) of doublers and adhesive were required. In units 6, 7, and 8, graphite-epoxy doublers and adhesive ranging in weight from about 0.6 to 0.9 kg (1.3 to 2.0 pounds) were installed to repair minor cracks and "oilcan" regions (see Rudder Manufacturing).

Weight variations of the ten composite rudders were analogous to metal rudder variations. For the ten composite rudders, including the repair doublers discussed previously, finished weights varied 2.76 percent from the mean value. For a sampling of 25 metal rudders, finished weights varied 2.85 percent from the mean value.

TABLE 11

WEIGHT DATA FOR CONVENTIONAL AND ADVANCED COMPOSITE UPPER-AFT RUDDER

(A) DETAILED WEIGHT DISTRIBUTION FOR COMPOSITE RUDDER SERIAL NO. 4

ITEM	METAL RUDDER WEIGHTS		ACTUAL COMPOSITE RUDDER WEIGHTS						PREDICTED COMPOSITE RUDDER WEIGHTS					
			GRAPHITE		FIBERGLASS		OTHER		GRAPHITE		FIBERGLASS		OTHER	
	kg	LB	kg	LB	kg	LB	kg	LB	kg	LB	kg	LB	kg	LB
SKIN	14.58	32.14	7.20	15.87					7.03	15.50				
RIBS	6.84	15.09	3.55	7.85					3.90	8.60				
FRONT SPAR	4.64	10.22	1.46	3.21					1.59	3.50				
REAR SPAR	3.00*	6.62*	0.23	0.50					0.25	0.55				
TRAILING EDGE					2.19	4.83	0.10	0.22			2.18	4.80	0.11	0.25
TIP ASSEMBLY	0.49	1.09			0.43	0.95	0.05	0.10			0.45	1.00	0.05	0.10
LEADING EDGE	6.30	13.89			4.36	9.60	0.14	0.31			4.36	9.60	0.14	0.30
FAIRINGS	0.83	1.83			0.54	1.19					0.54	1.20		
FITTINGS	3.36	7.41					3.10	6.83					3.27	7.20
ACCESS DOORS	0.17	0.37					0.13	0.29					0.14	0.30
PAINT	0.68	1.50					2.67	5.90					1.36	3.00
SEAL	0.48	1.05					0.48	1.05					0.70	1.55
ADDITIONAL ITEMS	0.04	0.89					1.20	2.64					0.48	1.05
			12.44	27.43	7.52	16.57	7.87	17.34	12.77	28.15	7.53	16.60	6.25	13.75
TOTAL	41.41	91.30	27.83 kg (61.34 LB)						26.55 kg (58.50 LB)					

*INCLUDES TRAILING EDGE WEIGHT

(B) UNIT WEIGHTS FOR COMPOSITE RUDDERS PRIOR TO PAINTING

RUDDER SERIAL NO.	1	2	3	4	5	6	7	8	9	10
UNIT WEIGHT (kg)	26.57	25.19	25.48	25.15	25.18	26.09	25.92	25.77	25.40	25.26
(LB)	58.59	55.53	56.17	55.44	55.52	57.52	57.15	56.82	56.01	55.70

SPECIMEN AND SUBCOMPONENT DEVELOPMENT

The design, tooling concepts, and test results for a series of structural specimens and subcomponents are discussed in this section. The previously discussed design allowable tests were supplemented with selected fatigue and fracture toughness tests to indicate acceptable structural durability and fracture characteristics for the rudder design. Manufacture of the subcomponents substantiated tooling and processing techniques, and testing of the subcomponents verified the structural integrity of critical design details of the rudder.

Fatigue Tests

A group of 24 sandwich-beam fatigue specimens was tested to failure to determine acceptable working stress levels for the rudder design. The graphite-epoxy laminate facing of the sandwich-beam specimens incorporated a laminate pattern representative of the front-spar caps of the rudder (0°, 45°, 90°, -45°)S. Twelve of the specimens had continuous laminates (K_t = 1.0) and 12 contained centrally located 6.35 millimeter (1/4 inch) diameter holes (K_t = 3.0) representative of the bolt holes in the front-spar cap at the hinge and crank fitting attach points. Three beams of each specimen configuration were tested statically, and nine each were tested under reversing stress conditions (R = -1.0) at load levels ranging from 35 to 67 percent of the average static ultimate loads. Test results are shown in Table 12 and Figure 21. The failures all occurred in the test sections and the scatter of data was very good. On a net stress basis, the specimens containing the holes indicated slightly improved fatigue performance.

Fracture Toughness Tests

Five fracture toughness test panels, Figure 22, were fabricated and four of these were intentionally damaged in a Gardner Impact Test apparatus using a 12.7 millimeter (1/2 inch) diameter penetrator and impact energies ranging from 1.13 to 4.52 joules (10 to 40 inch-pounds). The fifth panel, undamaged, was used as a control specimen. A six-ply laminate pattern representative of the rudder skins, (0°, 45°, -45°)S, was used in the specimens.

TABLE 12

SANDWICH-BEAM FATIGUE TEST RESULTS FOR THORNEL 300/5208 MATERIAL
(0, 45, 90, -45^{o})S LAMINATE AT STRESS RATIO, R = −1.0

SPECIMEN CONFIGURATION	SPECIMEN NUMBER	TEST LOAD			NET STRESS		CYCLES TO FAILURE	REMARKS
		N	LB	PERCENT AVERAGE STATIC LOAD	MPa	KSI		
Z3941117-1 (NO HOLE)	1	7900	1776	–	534.34	77.5	–	STATIC TESTS – AVERAGE STATIC LOAD IS 8007N (1800 LB)
	2	7509	1688	–	AVG	AVG	–	
	3	8674	1950	–			–	
	4	5338	1200	66.7	356.46	51.7	1,000	FAILED IN TEST SECTION
	5	4003	900	50.0	266.83	38.7	5,000	FAILED IN TEST SECTION
	6	3559	800	44.4	237.18	34.4	55,000	FAILED IN TEST SECTION
	7	3203	720	40.0	213.74	31.0	306,000	FAILED IN TEST SECTION
	8	3203	720	40.0	213.74	31.0	113,000	FAILED IN TEST SECTION
	9	3203	720	40.0	213.74	31.0	577,000	FAILED IN TEST SECTION
	10	2802	630	35.0	186.85	27.1	2,471,000	FAILED IN TEST SECTION
	11	2802	630	35.0	186.85	27.1	4,680,000	FAILED IN TEST SECTION
	12	2802	630	35.0	186.85	27.1	1,006,000	FAILED IN TEST SECTION
Z3941117-501 [6.35 mm (1/4-INCH) DIAMETER OPEN HOLE]	1	4946	1112	–	393.0	57.0	–	STATIC TESTS – AVERAGE STATIC LOAD IS 4982N (1120 LB)
	2	4706	1058	–	AVG	AVG	–	
	3	5276	1186	–			–	
	4	3336	750	67.0	263.38	38.2	11,000	FAILED IN TEST SECTION
	5	3336	750	67.0	263.38	38.2	23,000	FAILED IN TEST SECTION
	6	3336	750	67.0	263.38	38.2	42,000	FAILED IN TEST SECTION
	7	3069	690	61.7	242.70	35.2	10,000	FAILED IN TEST SECTION
	8	3069	690	61.7	242.70	35.2	59,000	FAILED IN TEST SECTION
	9	3069	690	61.7	242.70	35.2	132,000	FAILED IN TEST SECTION
	10	2669	600	53.5	210.29	30.5	1,281,000	FAILED IN TEST SECTION
	11	2669	600	53.5	210.29	30.5	2,392,000	FAILED IN TEST SECTION
	12	2669	600	53.5	210.29	30.5	2,566,000	FAILED IN TEST SECTION

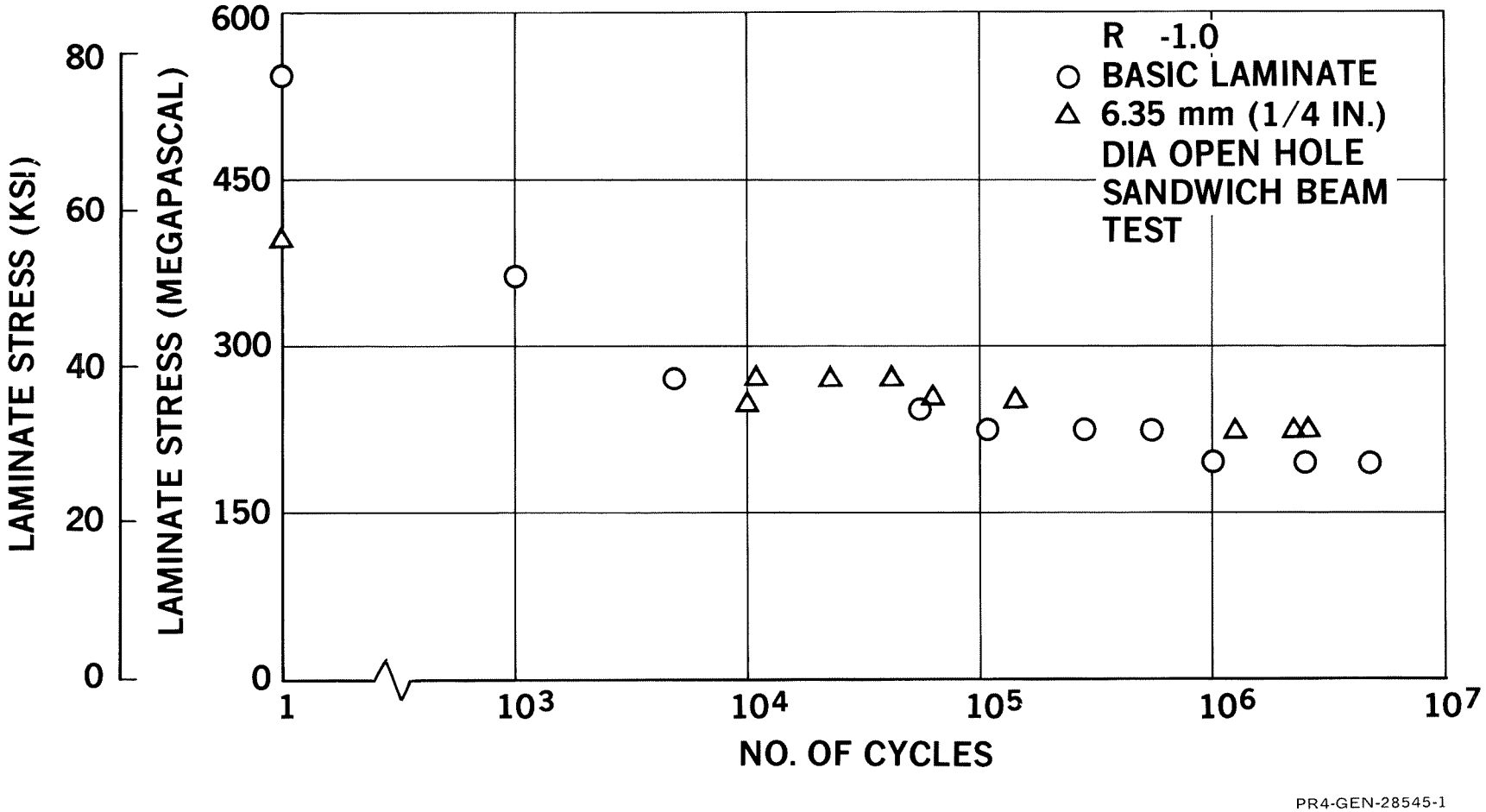

FIGURE 21. FATIGUE CHARACTERISTICS OF THORNEL 300/5208 (0^o, 45^o, 90^o, -45^o)S LAMINATE

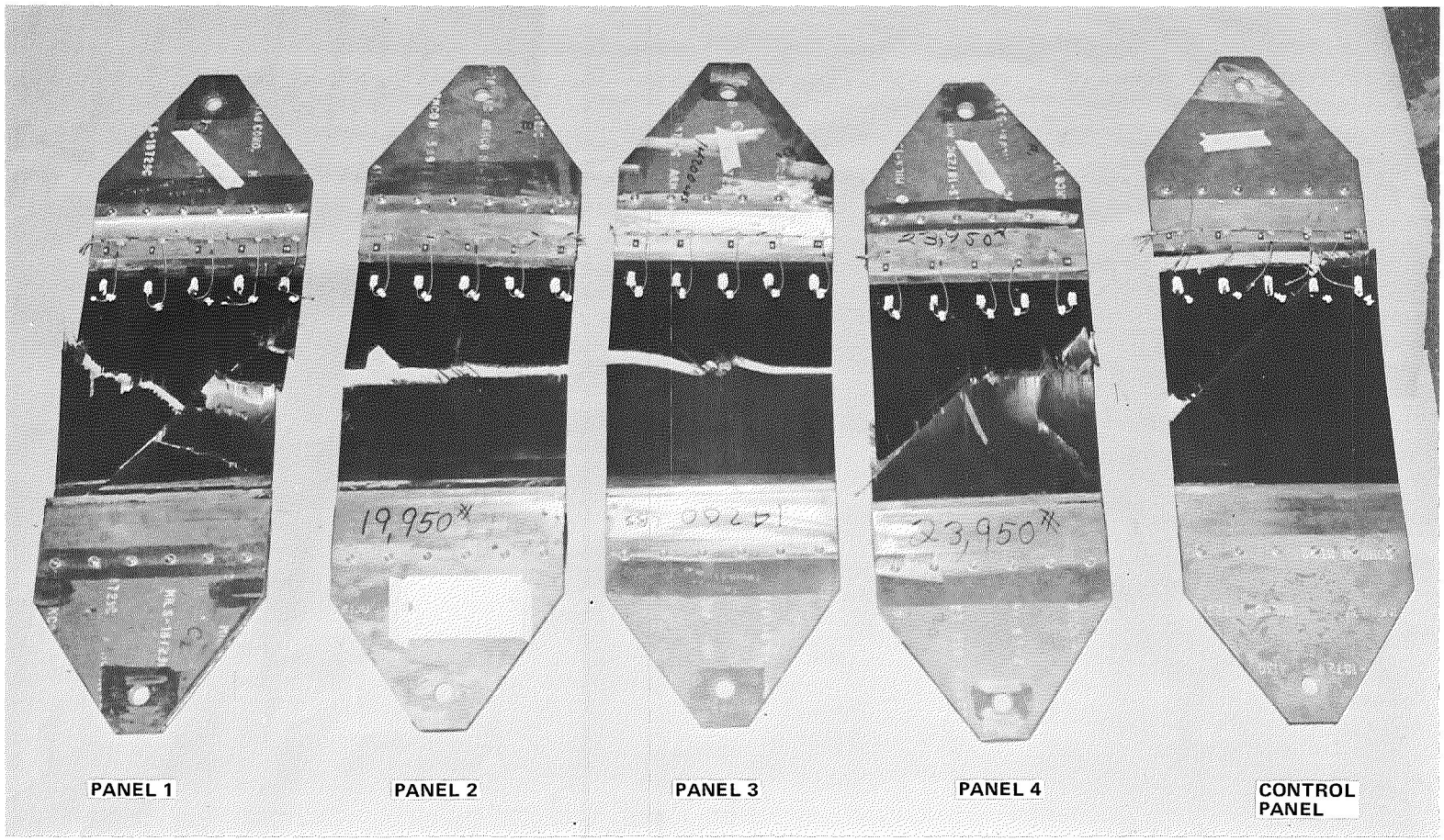

FIGURE 22. FRACTURE TOUGHNESS TEST PANEL FAILURES

The damage was centrally located in the 305 millimeter (12-inch) width of the test specimens. The extend of damage at 4.52 joules impact energy is illustrated in Figure 23. At 1.13 joules impact energy, the damage was barely visible. After the panels were instrumented with strain-gages, residual strength tests were conducted using a Riehle Test Machine. Test results are summarized in Table 13.

The control panel failed at the edge of the grip reinforcement at an ultimate stress level 25 percent below the nominal strength of the panel indicated by the design allowable tests. The balance of the panels failed in the test sections and, excepting Panel 1, through the damaged areas (see Figure 22). Panel 1 failed through the basic laminate approximately 25 millimeters from the damage center at an ultimate stress level of 520 megapascals (75,500 psi). Panels 1, 2, and 3 indicated the expected trend of reduced residual strength with increased damage. Panel 4 attained a greater ultimate stress level than expected. The edges of the impact areas of Panel 4 did not exhibit the sharp cleavage found on Panel 3 (see Figure 23) and it was concluded that the stress concentration factor was less severe in Panel 4. The results of the panel tests led to the conclusion that the rudder skins can sustain significant damage without danger of fast fracture.

Manufacturing Development Components

Feasibility of the thermal expansion molding concept was demonstrated through fabrication of eight development components on the form mold die (FMD) shown in Figure 24. The side plates of the FMD (50 millimeter thick steel plates) were removed for clarity. The internal metal mandrels and the cast room temperature vulcanizing (RTV) rubber mandrels are shown separately. The rubber mandrels were subsequently cut into segments for removal through the three holes in the front-spar of the development component provided for the internal metal mandrels.

Four significant problems were encountered during fabrication of the development components. These problems are summarized in Table 14. During the first cure cycle, excessive pressures were developed in the Silastic "J" rubber

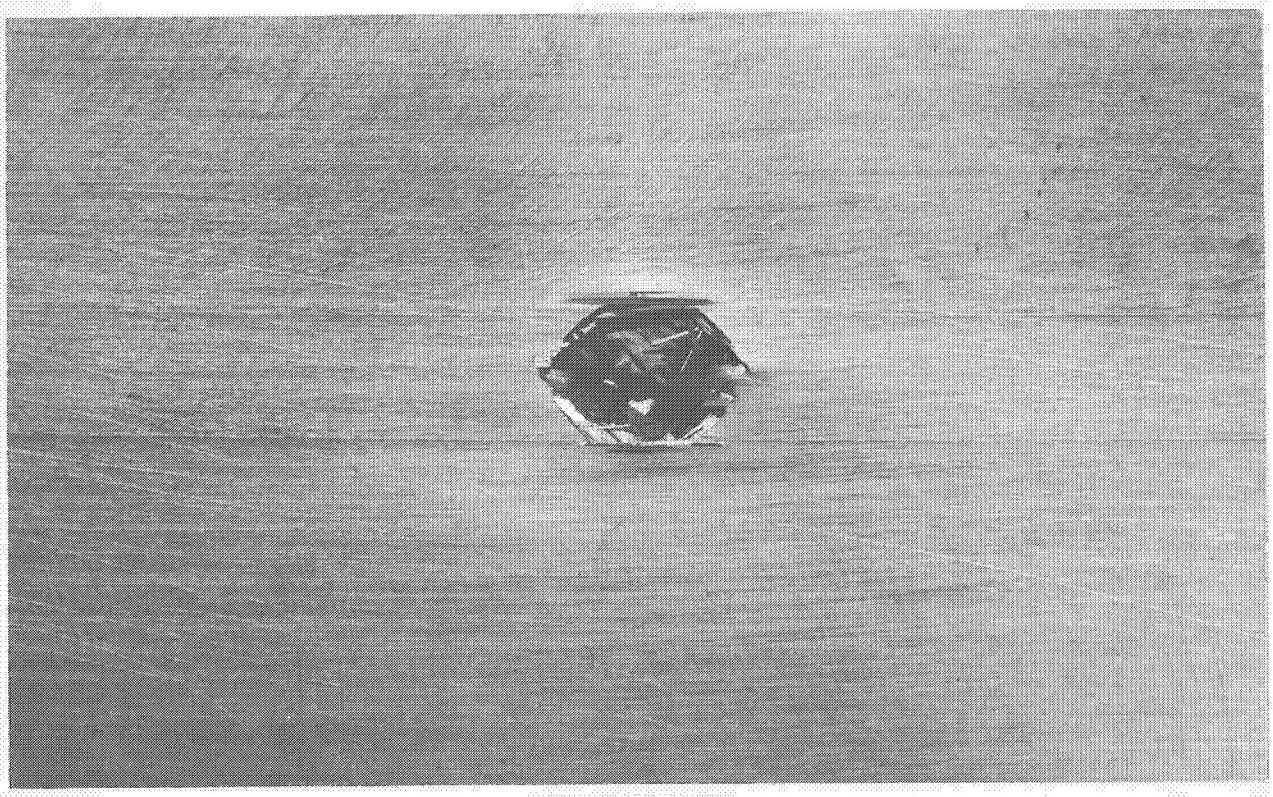

(A) PANEL NO. 3

(B) PANEL NO. 4

FIGURE 23. FRACTURE TOUGHNESS PANEL DAMAGE LEVELS

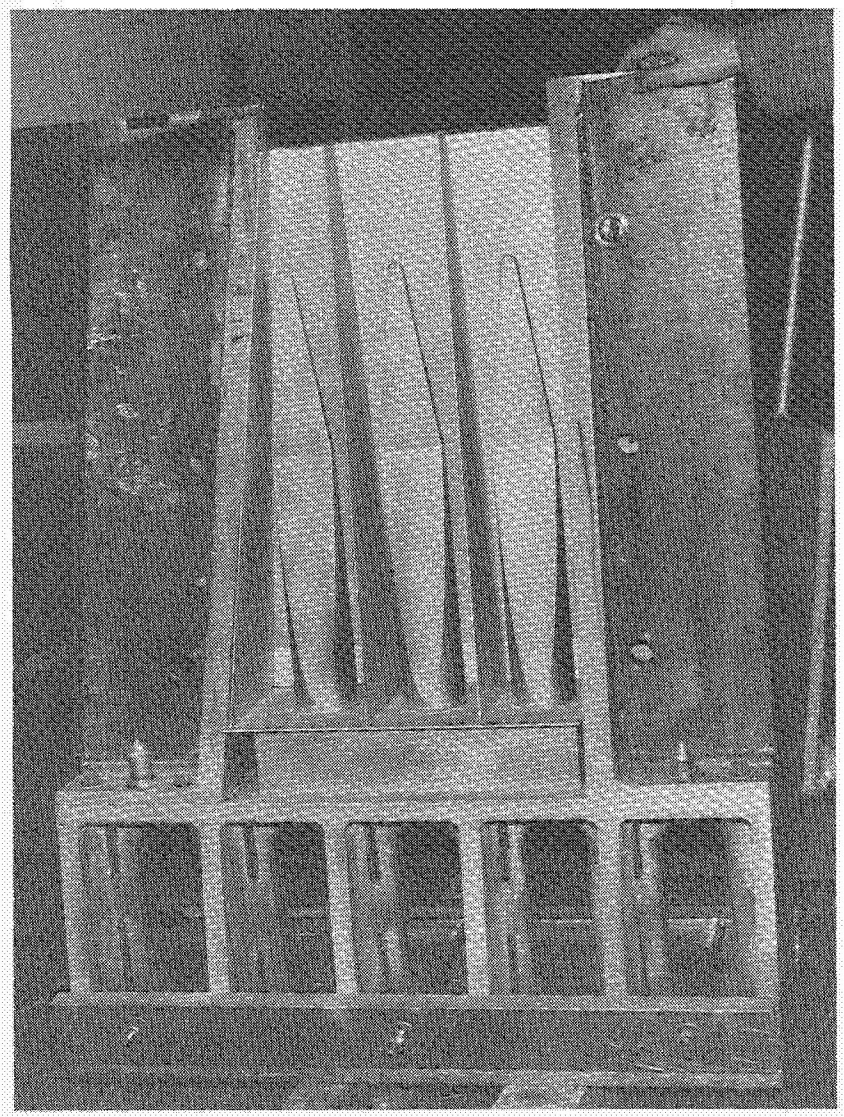

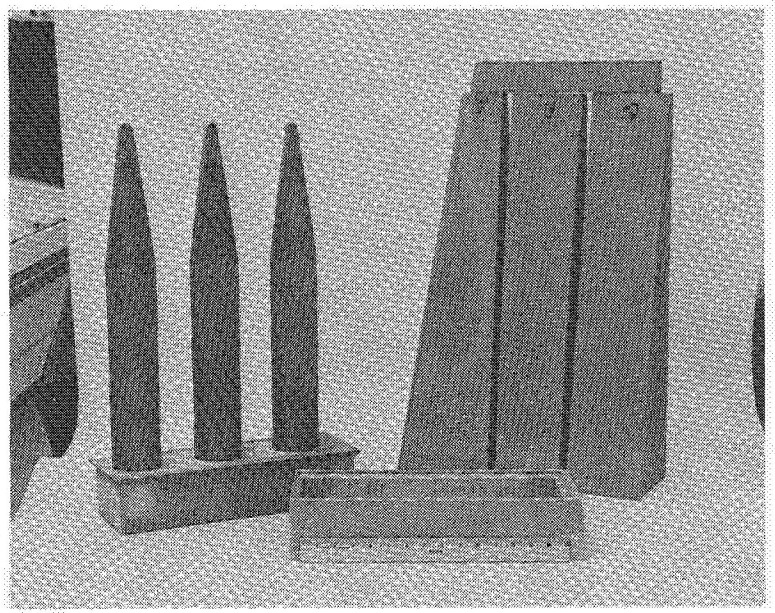

FIGURE 24. FORM MOLD DIE FOR VERIFICATION OF TOOLING CONCEPT

TABLE 13

FRACTURE TOUGHNESS PANEL TEST RESULTS

PANEL NO.	DAMAGE IMPACT ENERGY		ULTIMATE STRESS		REMARKS
	J	IN.-LB	MPa	KSI	
CONTROL	NONE	NONE	365.42	53.00	FAILED AT EDGE OF GRIP REINFORCEMENT
1	1.13	10	520.55	75.50	FAILED THROUGH LAMINATE PANEL 2.54 CM (1.00 IN.) FROM DAMAGE CENTER
2	2.26	20	348.19	50.50	FAILED THROUGH DAMAGE
3	4.52	40	248.21	36.00	FAILED THROUGH DAMAGE
4	(2) AT 4.52	(2) AT 40	417.13	60.50	FAILED THROUGH DAMAGE. THE EDGES OF THE IMPACT AREAS DID NOT HAVE THE SHARP CLEAVAGE FOUND IN PANEL NO. 3

TABLE 14

SUBCOMPONENT DEVELOPMENT PROBLEMS AND SOLUTIONS

CURE CYCLE	PROBLEMS	CAUSE	SOLUTION
1	25.4-MILLIMETER (1-INCH) DIAMETER TOOLING BOLTS FAILED.	EXCESSIVE PRESSURE	CHANGED RUBBER FORMULATION. REDUCED RUBBER VOLUME.
2	RUBBER MANDRELS SHRUNK.	CREEP BEHAVIOR UNDER CURING HEAT AND PRESSURE.	REMADE RUBBER MANDRELS WITH METAL INCLUSIONS TO STABILIZE DIMENSIONS.
3	POOR FIBER COLLIMATION AND LARGE ACCUMULATIONS OF RESIN.	LAMINATE CURED WITH INADEQUATE PRESSURE.	ADDED ELECTRICAL HEATERS WITH METAL MANDRELS FOR INSIDE-OUT HEATING.
4	RUBBER MANDRELS STUCK.	CURING HEAT AND PRESSURES.	ADDED TEFLON TAPE AT FAYING SURFACES.
5-8	NONE	—	—

mandrels (estimated at about 7 megapascal) and two of the 25.4 millimeter (1-inch) diameter tooling bolts retaining the side plates failed in tension. The heatup rate was also very slow due to the mass of the FMD.

The internal metal mandrels were redesigned and the rubber mandrels were recast (using Dapcocast 38-3) to reduce curing pressure for the second cure cycle. The redesigned metal mandrels reduced the volume of rubber and incorporated internal electrical heaters which increased the heatup rate and reduced thermal gradients through the assembled tool and laminate during the cure cycle. In addition, the metal mandrels were a multipiece aluminum alloy rather than the one-piece steel mandrel (Figure 24). The aluminum alloy promoted internal heat transfer and the multipiece construction facilitated mandrel removal.

A fiberglass subcomponent, shown in Figure 25, was successfully cured during the second cure cycle. However, considerable shrinkage of the rubber mandrels was discovered after their removal from the three rib-bays. The mandrels shrunk approximately 6 millimeters on the chordal dimension of about 0.6 meter.

The third cure cycle was attempted using the rubber mandrels which shrunk during the second cycle. Although the laminates were satisfactorily cured, there was poor fiber collimation and regions of large resin accumulation because the undersized mandrels expanded too late during the cure cycle. In subsequent cure cycles, the shrinkage problem was resolved by including a coarse wire-mesh screening within the pieces of cast rubber. The screening provided a mechanical restraint against shrinkage and the rubber mandrels were dimensionally stable thereafter.

During fabrication of the first three subcomponents, removal of the rubber mandrel segments was particularly difficult. Although the mandrels were liberally sprayed with a release agent prior to assembly, the temperatures and pressures sustained during the cure cycles effectively bonded the rubber segments to each other, to the metal mandrels, and to the laminates. This problem was finally resolved by coating the segments with a 0.08 millimeter thick Teflon tape at all appropriate faying surfaces.

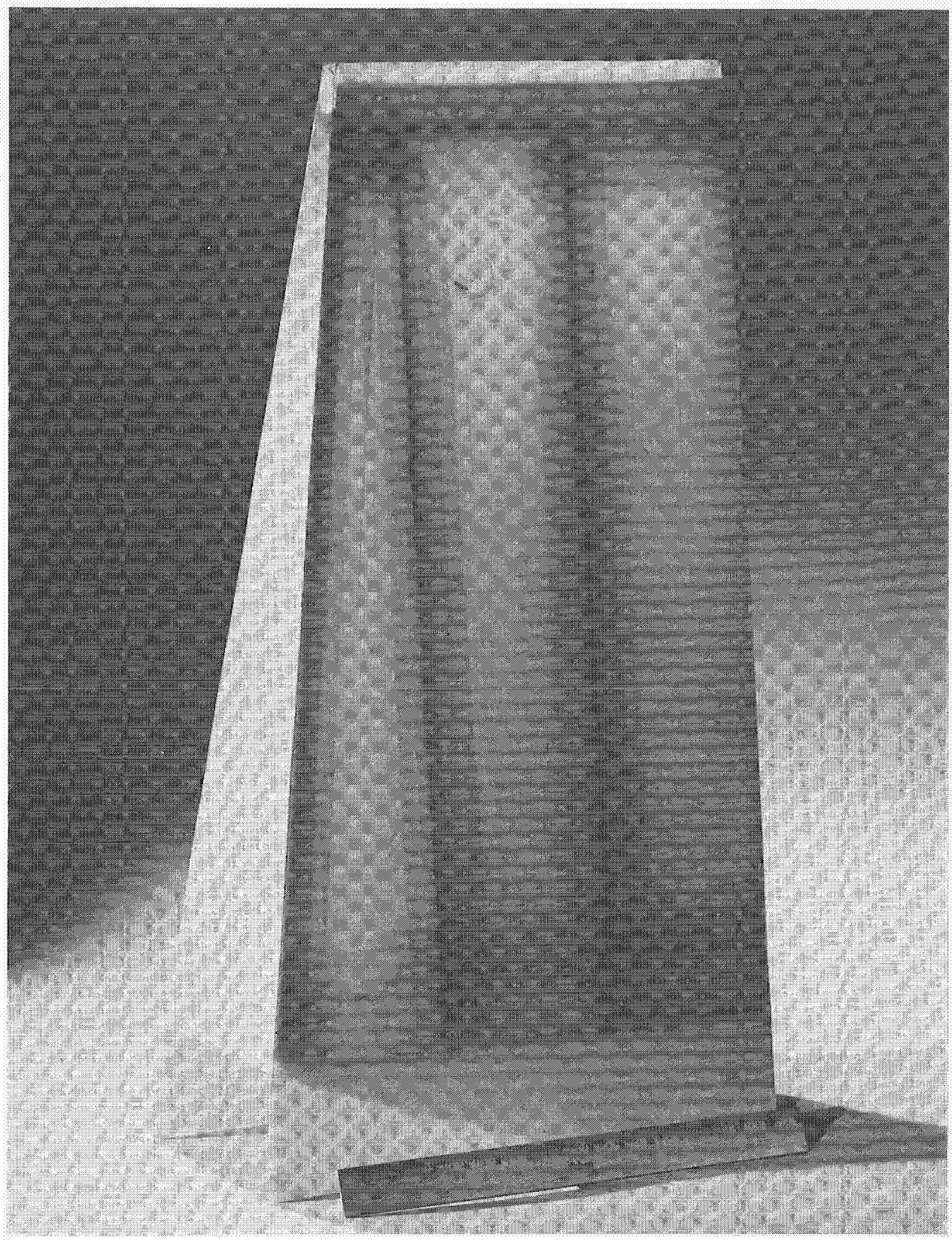

FIGURE 25. FIBERGLASS-EPOXY PROTOTYPE MOLDING ASSEMBLY

Four additional subcomponents were fabricated after the metal mandrels were modified to incorporate internal heaters and the rubber mandrels were stabilized with metal screening and coated with Teflon. No further problems were encountered and each of the four additional subcomponents was successfully completed.

Hinge Fitting Fastener Tests

A development component was fabricated and tested under a simplified fatigue load spectrum to verify the fatigue strength of the hinge fitting fasteners and laminates at the critical attach points of the rudder crank fittings. A simplified but conservative load spectrum was derived to permit testing on a Sonntag Machine. The completed test setup is shown in Figure 26.

During fatigue testing, fastener head failures were experienced with two types of 6.35 millimeter (0.25 inch) diameter screws because of spurious bending stresses in the screw heads in conjunction with the stress concentrations caused by the screwdriver slots. The 6.35 millimeter diameter screws were replaced with HLT336-10 pins (7.94 millimeter diameter) for increased bending strength at the head to shank interface. Some debonding and delaminating of the specimen was also experienced near the point of test load input, but the laminate was intact in the test section. After repair of the damage, the spectrum fatigue test was resumed and the specimen withstood three additional lifetimes of fatigue loads without difficulty. On completion of the spectrum loading, a residual static strength test indicated a positive margin of safety of 96 percent for the test loading mode (all fasteners installed). The fasteners failed in shear and the laminates were secondarily damaged at the bearing surfaces and under the bolt heads due to excessive deformation of the fasteners.

Spar Component Tests

Static tests were conducted on a spar component to verify design details in the vicinity of the hinge and actuator fittings as shown in Figure 27. Two separate test setups were used to simulate spar stresses, first at the lower

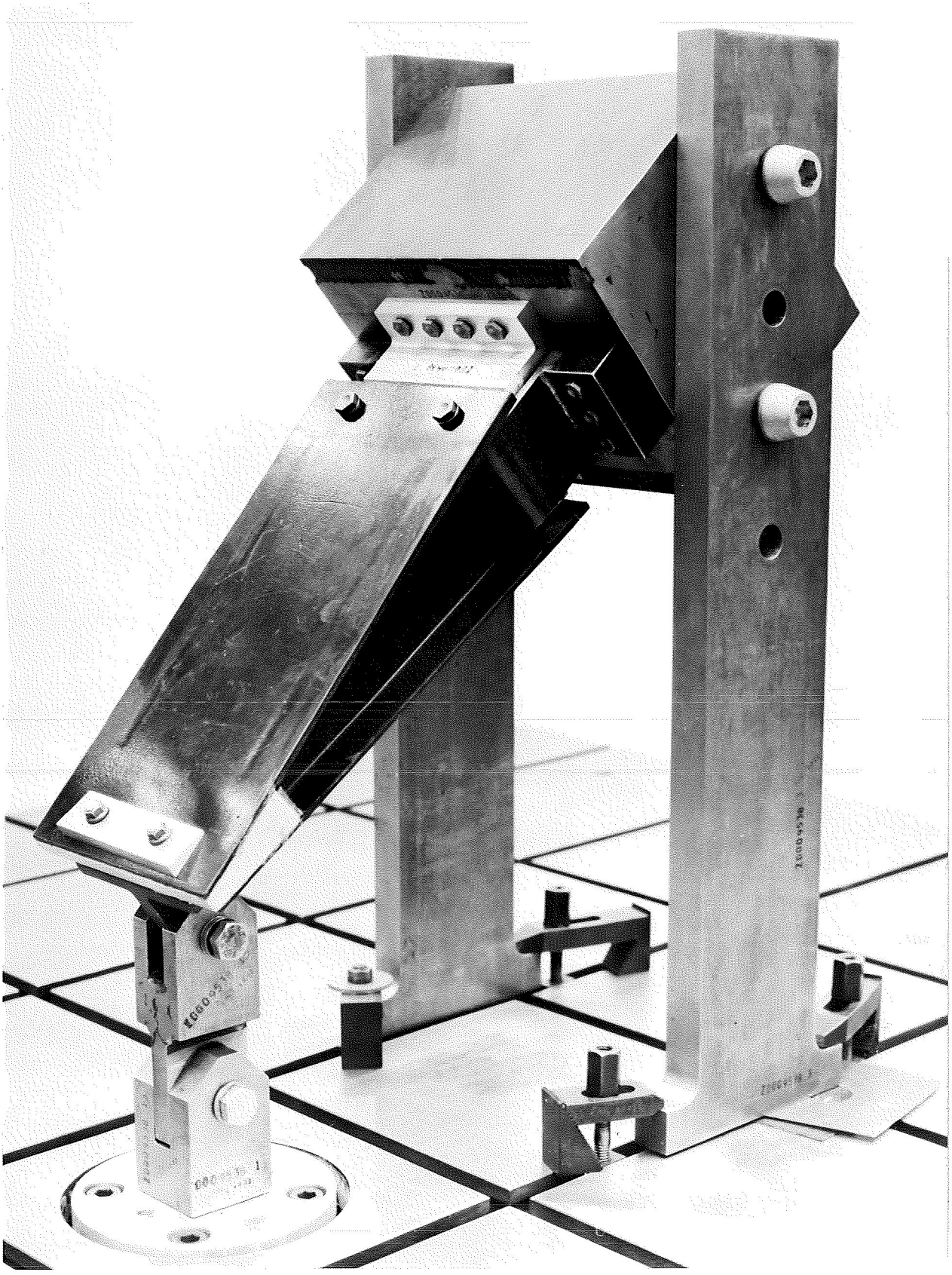

FIGURE 26. HINGE FITTING FASTENER TEST SETUP

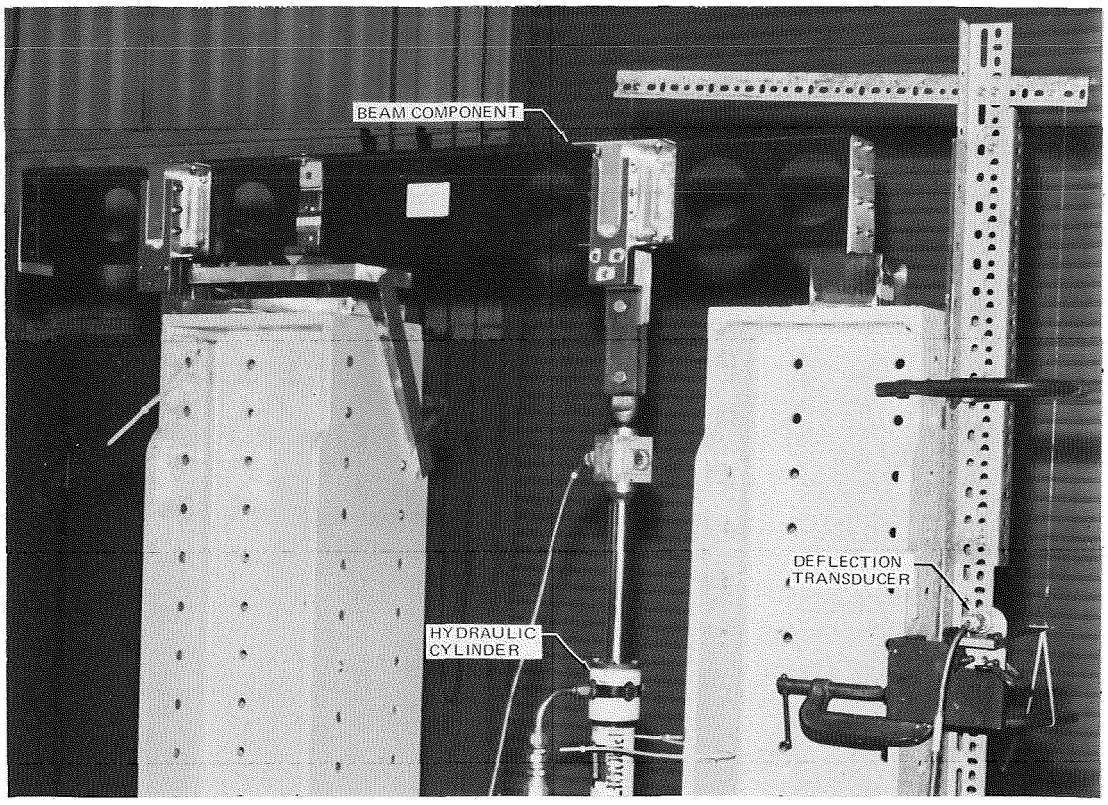

FIGURE 27. SPAR COMPONENT TEST SETUP

drive station and then at the center hinge station. Positive margins-of-safety of 78 and 140 percent, respectively, were indicated by the ultimate test loads. In each case, the specimen failed initially in a shear mode through a circular cutout in the shear web as shown in Figure 28.

Box Component Static Tests

A structural box component, Figure 29, was fabricated and tested to verify four critical aspects of the rudder design, namely (1) the drive hinge fitting attachment strength, (2) rear-spar flange strength, (3) skin panel stability, and (4) drive hinge fitting failsafe condition. The primary objective of the tests was to verify design concepts of the rudder in the vicinity of the critically loaded hinge and actuator fittings. Design details of the fitting attachments and supporting structures were substantiated under design load conditions and several failsafe variations.

The structural tests were conducted either in an "all well" configuration or in a "failed" configuration in which a single structural element (i.e., a

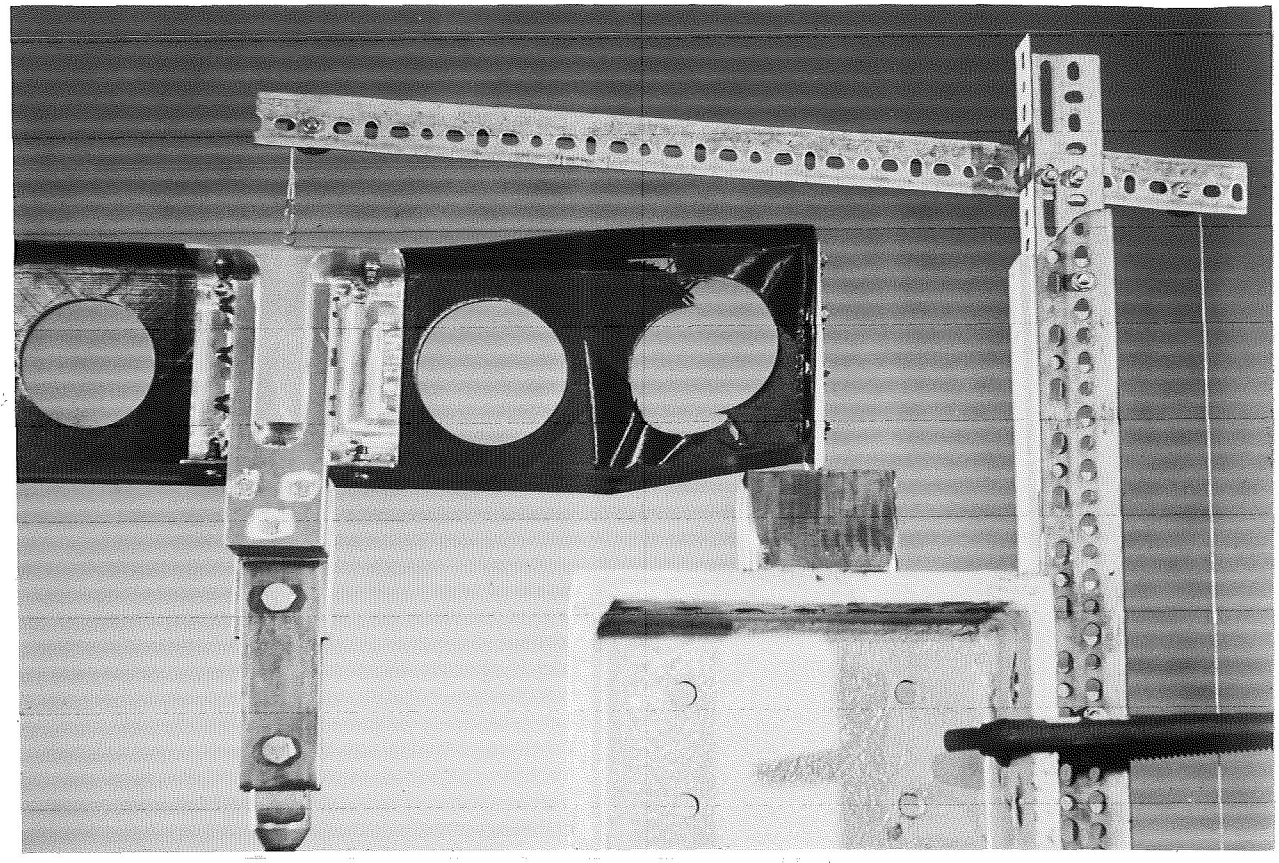

FIGURE 28. SPAR COMPONENT SHEAR WEB FAILURE

drive rod or attach bolt) was intentionally omitted from the structure. In the "all well" configurations, design ultimate loads (150 percent design limit loads) were applied. In the "failed" configurations, design limit loads were applied in accordance with design criteria requirements.

The test component consisted of the nine lower rib-bays of the graphite rudder and the lower hinge and actuator fittings. Bonded steel doublers at the upper end were provided for introduction of test loads into the component.

The basic test setup is shown in Figure 30. The external loads were applied by hydraulic cylinders and monitored through load-cells. The test loads were transmitted through the box structure and reacted in the test fixture. The box component static test conditions are summarized in Table 15. The test loads were successfully sustained in all cases. Test sequence numbers 1 through 6 represented the critical load conditions of primary interest. Test sequence number 7 was run to verify rib strength under whiffletree loads anticipated in the full-scale rudder static tests.

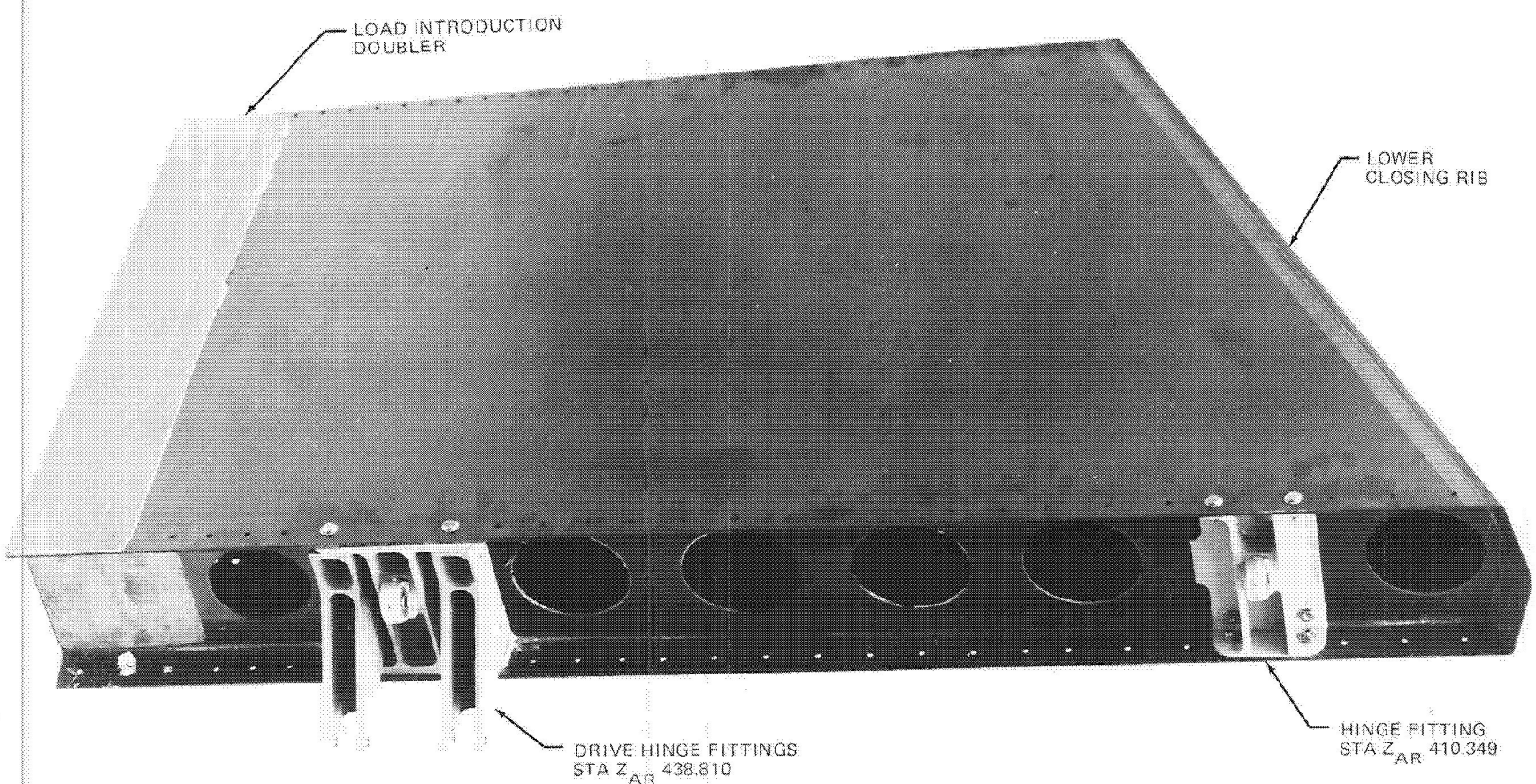

FIGURE 29. BOX STATIC – TEST COMPONENT

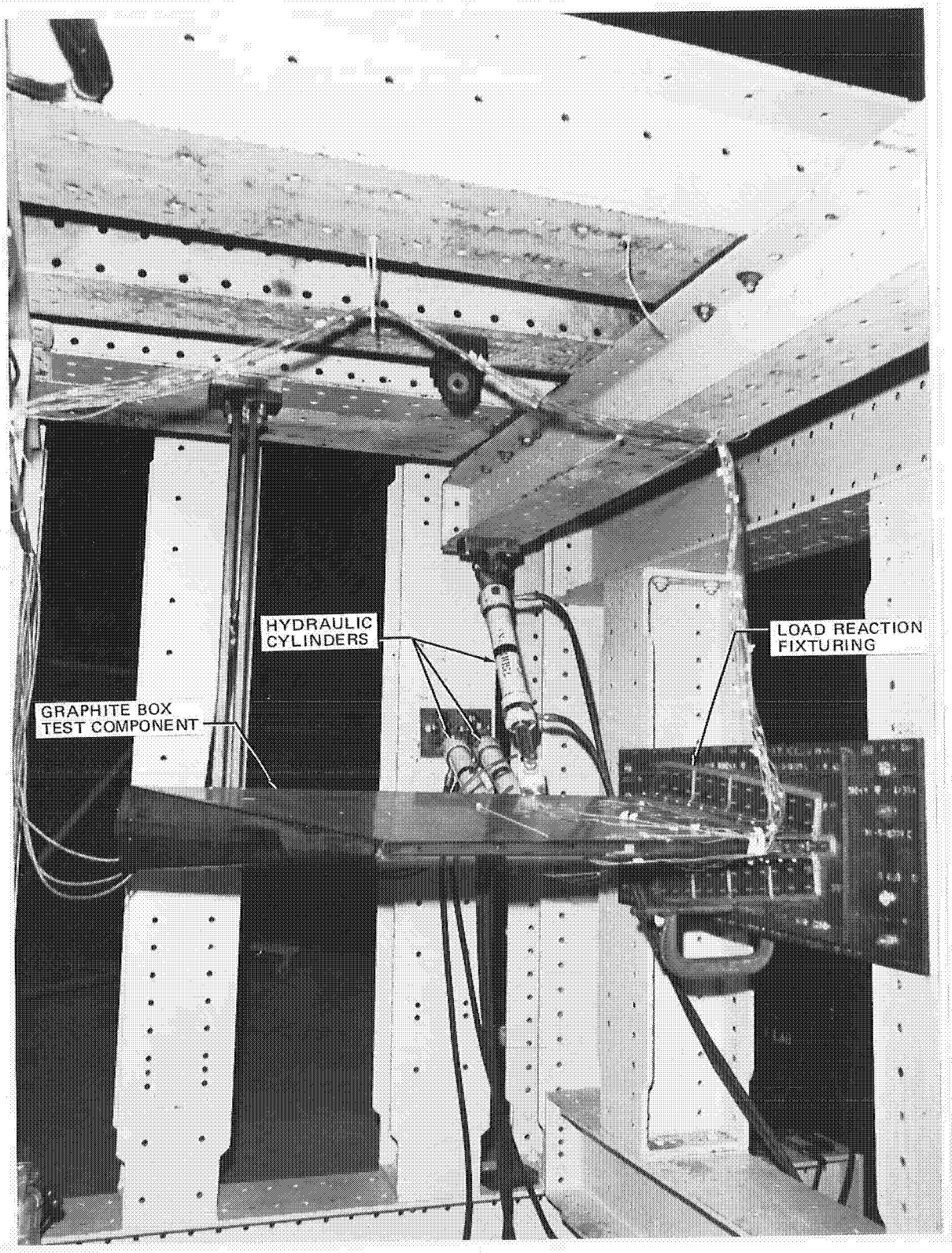

FIGURE 30. BOX COMPONENT STATIC-TEST SETUP

TABLE 15.

SUMMARY OF BOX COMPONENT STATIC TESTS

TEST SEQUENCE NUMBER	CRITICAL CONDITION			RUDDER CONFIGURATION			APPLIED LOAD (% DESIGN LIMIT LOAD)	CRITICAL STRUCTURE	REMARKS
	RUDDER KICK	ONE ENGINE OUT	DYNAMIC OVER-SWING	ALL WELL	FAIL-SAFE				
					ROD OUT	BOLT OUT			
1	X			X			150	LWR ACTUATOR HINGE FITTING ATTACH TO FRONT SPAR FLANGE; RIB STA 436.20 FLANGE	NO FAILURE
2		X		X			150		
3	X			X			150	SKIN PANEL JUST BELOW THE LWR ACTUATOR HINGE	
4	X				X		100	LWR ACTUATOR HINGE FITTING ATTACH TO FRONT SPAR FLANGE; RIB FLANGE	
5			X			X	100		
6		X				X	100		
7							150	RIB SHEAR-WEB	VERIFICATION OF RIB STRENGTH FOR FULL-SCALE STATIC-TEST RUDDER LOADING METHOD
8	X			X			184	RIB STA 436.20 FLANGE	COMPRESSION FLANGE FAILURE MS = +22%

The test procedure for test sequence number 8 was identical to number 1 except that number 8 was carried to ultimate strength (failure of the graphite specimen). The specimen failed in the expected mode (rib-cap compression) at an applied stress of 131 megapascals (19,000 psi). A positive margin-of-safety of 22 percent was indicated by this test.

Box Component Vibration Tests

Vibration tests were conducted on a box component, Figure 31, representing the upper end of the composite rudder. The component consisted of the upper eight rib-bays of the rudder, the upper hinge and actuator fitting installations, and appropriate sections of the leading edge, trailing edge, and tip installations. The aerodynamic fairing for the upper actuator fitting was also installed as shown in Figure 31. The component was mounted on a vibration test machine using production pushrods and attaching hardware as shown in Figure 32. The aerodynamic fairing was removed in Figure 32 for clarity.

A modal survey was first conducted and six channels of strain-gages were installed to monitor stresses in the component at selected locations on the skin panels. A random vibration environment, based on measured service conditions at the DC-10 fin tip and on acoustic levels at the upper rudder, was then applied to the specimen. The random vibration input, over a frequency bandwidth from 350-1800 Hz, was equivalent to 8.6 g root-mean-square lateral acceleration of the rudder.

The test was conducted for 46.5 hours, the time required to accumulate 100 million stress cycles in the critical skin panel. This input exceeded the maximum vibration levels encountered in service due to impinging noise and random vibration. At the conclusion of 46.5 hours of testing, the following two conditions were observed:

- a local partial disbond was indicated by nondestructive inspection at the left-hand skin flange of one rib, and
- the natural rotational frequency of the specimen had decreased to 59 Hz from a pre-test level of 65 Hz.

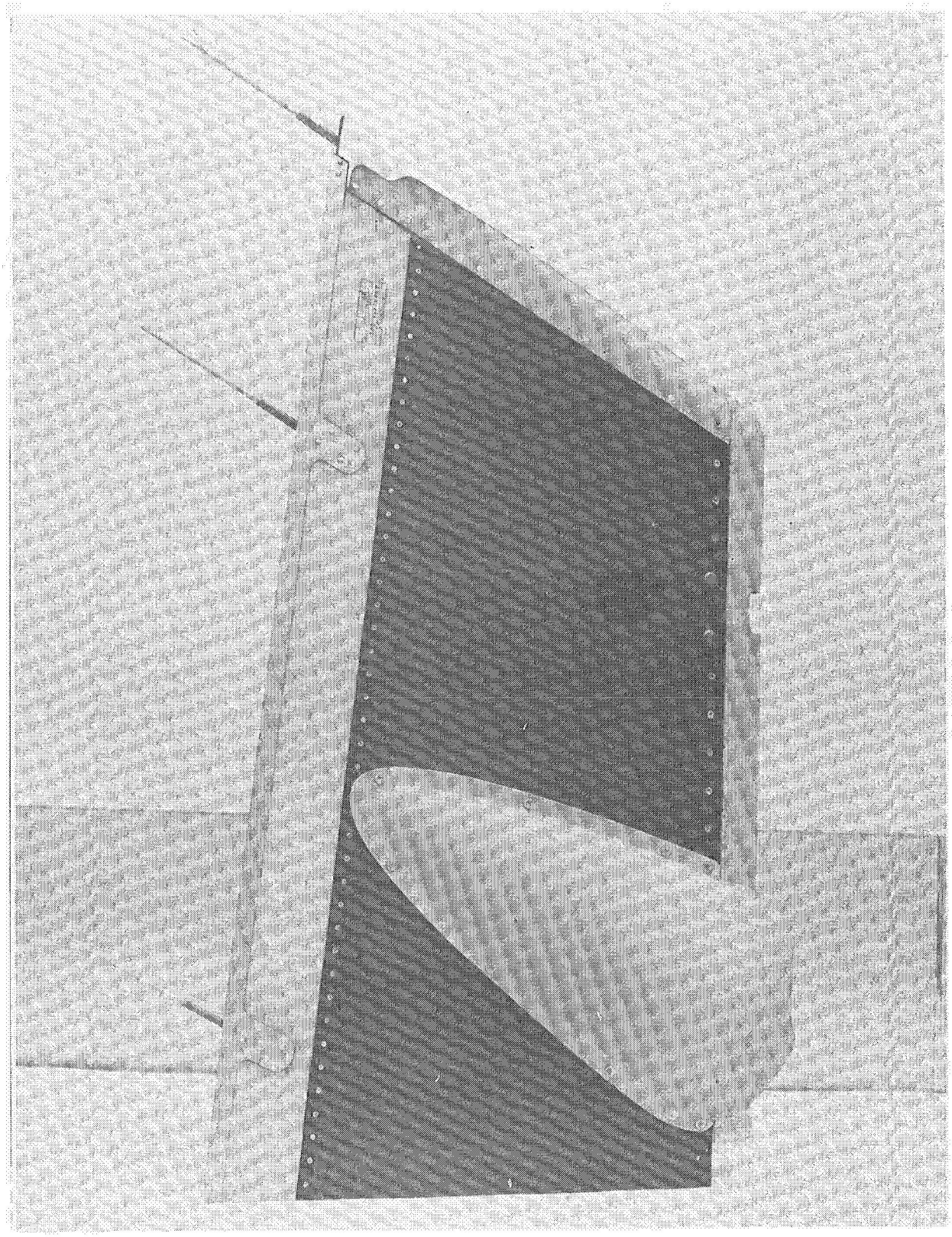

FIGURE 31. BOX VIBRATION TEST COMPONENT

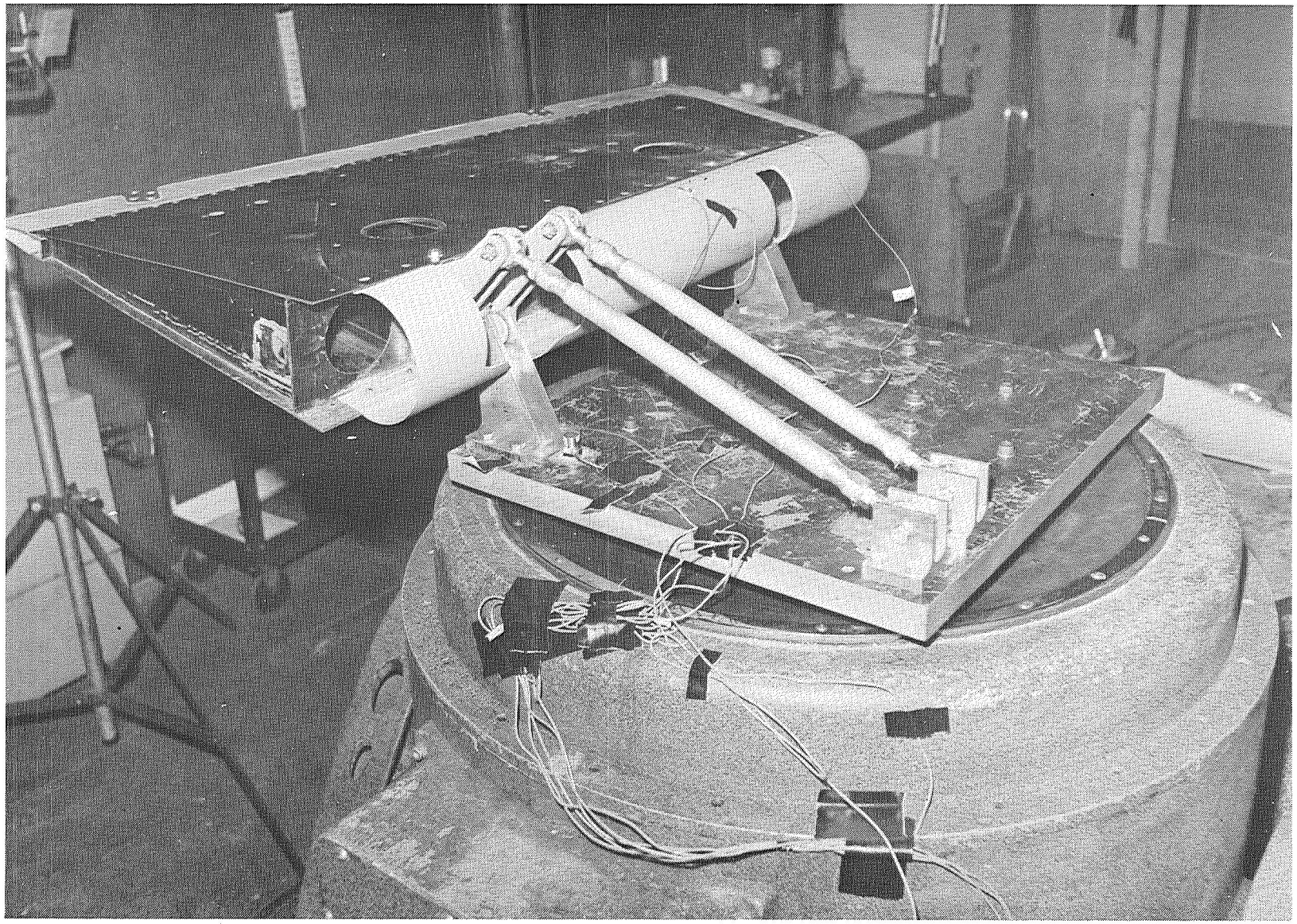

FIGURE 32. BOX VIBRATION TEST SETUP

To determine if the suspected disbond was propagating, an additional 8 hours (17 million cycles) of random vibration environment were applied to the specimen. A second nondestructive inspection indicated that the suspected disbond area remained stable (no propagation occurred) during the additional exposure.

During investigation of the drop in natural rotational frequency, the hinge brackets, rod bearings, and attach bolts were examined for wear or plastic deformation resulting from the vibration testing. All parts were found to be free of significant wear and well within manufacturing tolerances.

During disassembly of the component, it was noted that the aluminum alloy shims for tolerance take-up at the hinge bracket installation were disbonded. These parts were initially bonded to the graphite box with a cold-set adhesive to avoid loose parts during assembly. It was concluded that this bond detached during test, and though not structurally significant, this minor change in stiffness was sufficient to cause the observed change in natural frequency. At this point, the testing was suspended and the rudder was judged adequate to withstand service induced vibration environments.

Lightning Strike Tests

The graphite rudder lightning protection system consisted of a passive system (a dielectric coating on the graphite box to prevent swept-stroke and restrike attachments) and an active system (a conductive path electrically isolated from the graphite box and grounded to the metal aircraft structure to transfer direct strike currents). Lightning current transfer tests were conducted on two components incorporating design features of the passive and active systems, respectively.

Swept-Stroke and Restrike Tests. - A test panel was designed and fabricated to evaluate the effectiveness of the dielectric shielding protection in preventing swept-stroke and restrike lightning attachment to the graphite rudder skin panels. The tests were conducted aboard the Thunderbolt research vessel of the Lightning and Transient Research Institute (LTRI) of Miami Beach, Florida. The test panel was installed adjacent to a wind tunnel as shown in Figure 33.

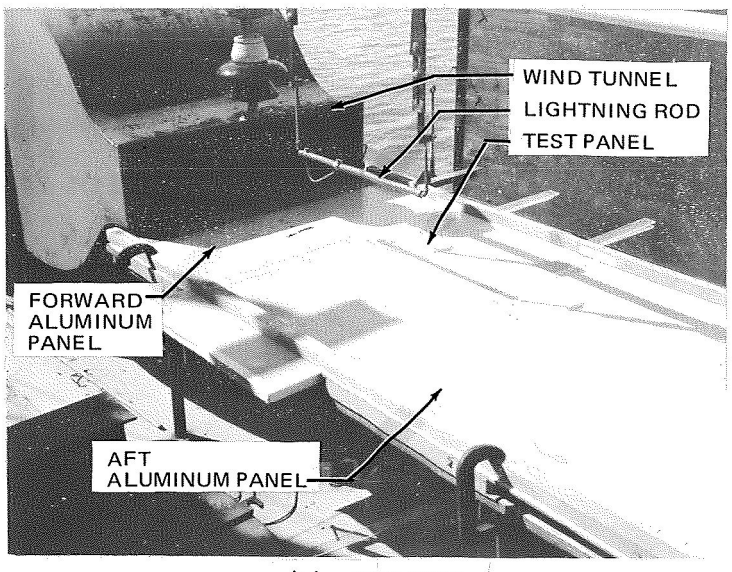

(A) SIDE-VIEW

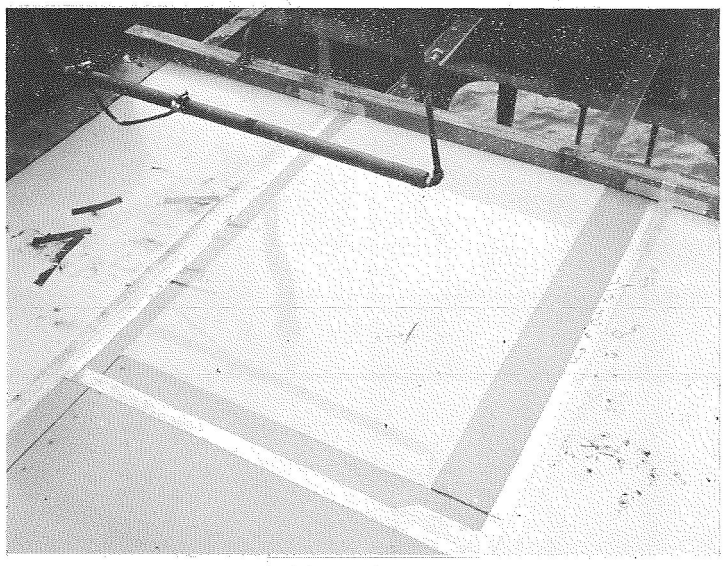

(B) TOP-VIEW

FIGURE 33. LIGHTNING SWEPT-STROKE TEST SETUP

The wind tunnel produced a wind velocity of 67 meters per second (150 miles per hour) during the tests.

A thin wire (not shown) inserted between the lightning rod and the forward aluminum panel was used to establish an ionized channel by vaporizing instantly at the beginning of each swept-stroke discharge. The wind then swept the arc-channel downstream across the test panel. The swept-stroke current generator provided an initial peak current of 400 amperes which decayed exponentially to zero in about 20 milliseconds. The restrike generator,

providing a 20 kiloampere peak current impulse, was controlled by a time-delay unit to discharge at a pre-selected time after the initiation of swept-stroke discharge. During each test, film records of the test events and current waveforms were obtained.

The test panel, Figure 34, simulated one side panel of the composite rudder. A 0.05 millimeter (2-mil) Kapton film and a 0.08 millimeter (3-mil) polyurethane paint coating were applied over the graphite composite skin to provide the dielectric shielding. The aluminum strip along the right-hand edge of the panel simulated the metal forward rudder. The aluminum strips across the

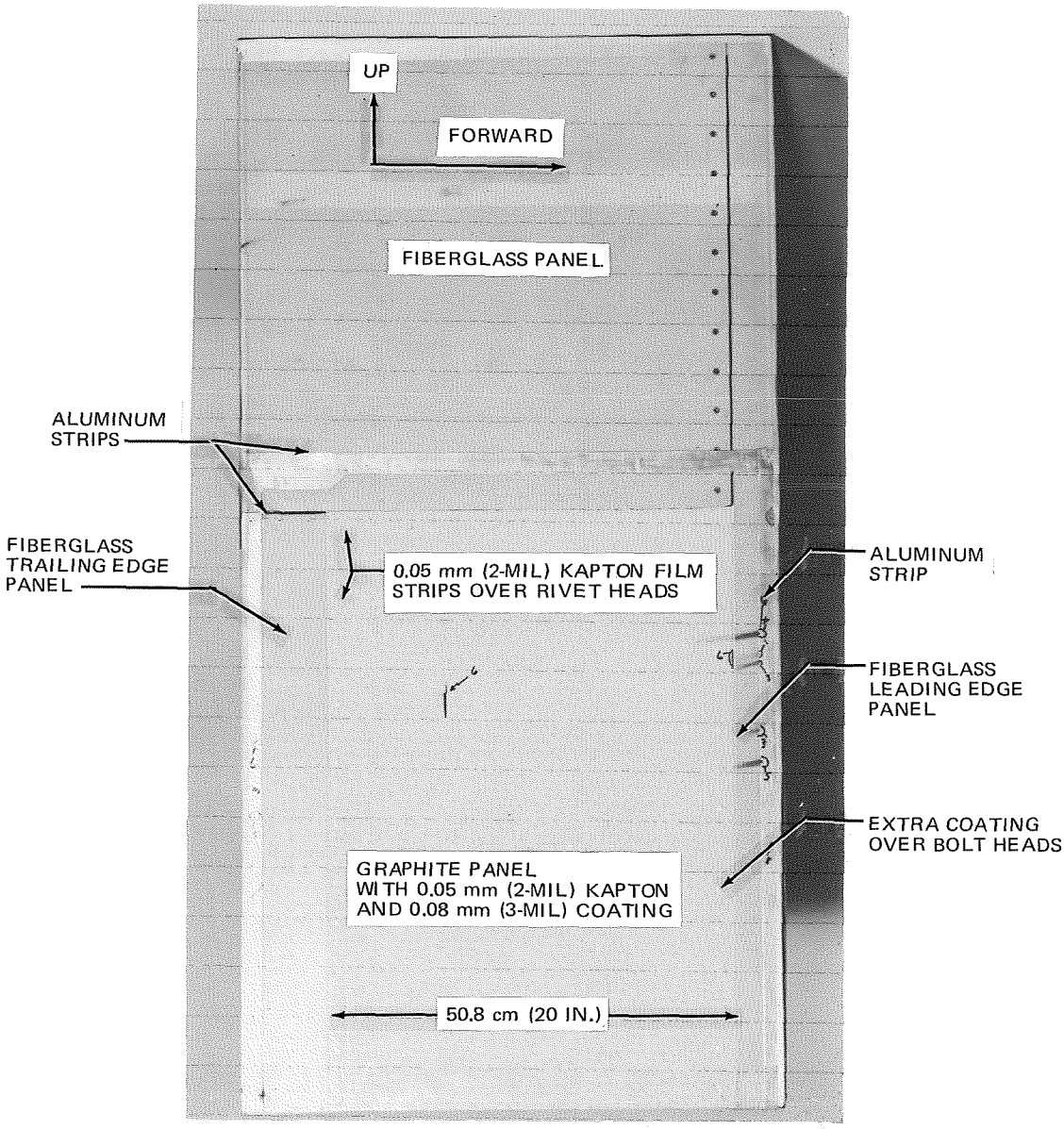

FIGURE 34. LIGHTNING SWEPT-STROKE PANEL AFTER TESTING

middle and along the left-hand edge simulated the active lightning protection strip installation. The panel surface bounded by these aluminum strips was the test area. The rivets along the panel edges simulated the leading and trailing edge structure attachments.

One swept-stroke and seven swept-stroke with restrike tests were made with the results shown in Table 16. Both negative and positive polarities of swept-stroke/restrike currents were used. The restrike time was increased from 10 to 15 milliseconds to achieve the most critical restrike test condition. The most critical test condition occurred when the longest arc-channel, laying over the composite panel while dwelling at the upstream side, conducted the restrike. This test condition applied the maximum voltage stress to the dielectric shielding system. The maximum voltage condition was achieved at 15 millisecond restrike time.

The film record showed that for tests 5 through 8, the arc-channel dwelled at the upstream side of the composite panel before restrike. In test 5, the restrike followed the existing arc-channel. In tests 6 through 8, the restrike reattached at the downstream side of the composite test panel.

Photographs of the arc-channels and the current waveforms for tests 4, 6, and 8 are shown in Figure 35. The restrike channels were clearly recorded in the photos because the high-intensity impulse current greatly increased the light

TABLE 16.
SUMMARY OF LIGHTNING PANEL TEST RESULTS

TEST SHOT NUMBER	SWEPT-STROKE RESTRIKE POLARITY	RESTRIKE TIME (MILLISECOND)	RESTRIKE RECORD FASTEX FILM FRAME NUMBER	TEST RESULT
1	SWEPT STROKE ONLY		—	SUCCESSFUL
2	NEGATIVE	10	12TH	SUCCESSFUL
3	NEGATIVE	10	12TH	SUCCESSFUL
4	NEGATIVE	12.5	15TH	SUCCESSFUL
5	NEGATIVE	15	18TH	SUCCESSFUL
6	POSITIVE	15	18TH	PARTIAL FAILURE
7	POSITIVE	15	17TH	SUCCESSFUL
8	POSITIVE	15	19TH	SUCCESSFUL

STILL PHOTO

CURRENT WAVEFORM
CALIBRATION: 200 AMP/DIV
2 MILLISECONDS/DIV

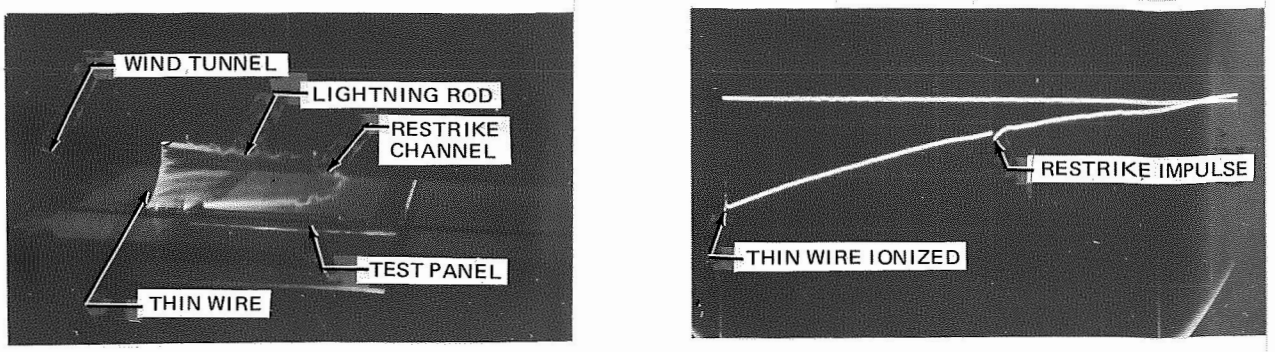

NEGATIVE RESTRIKE AT 10 MILLISECONDS – SUCCESSFUL

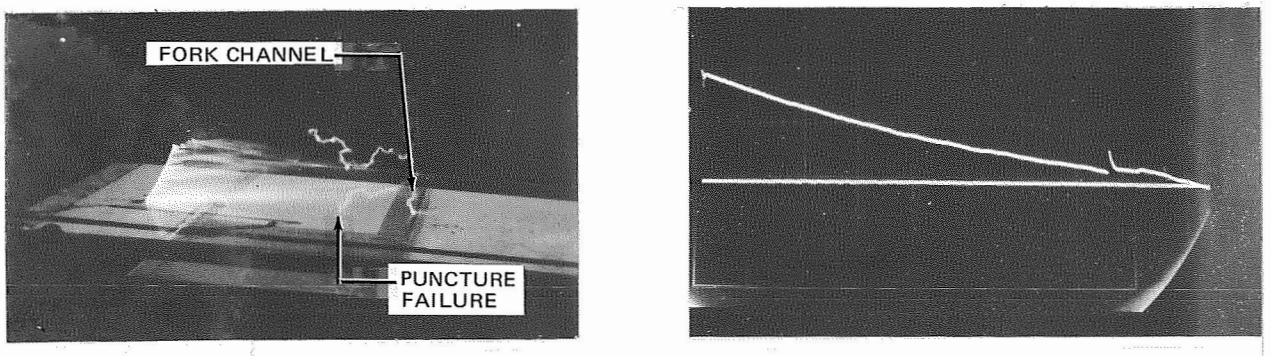

POSITIVE RESTRIKE AT 15 MILLISECONDS – MARGINAL FAILURE

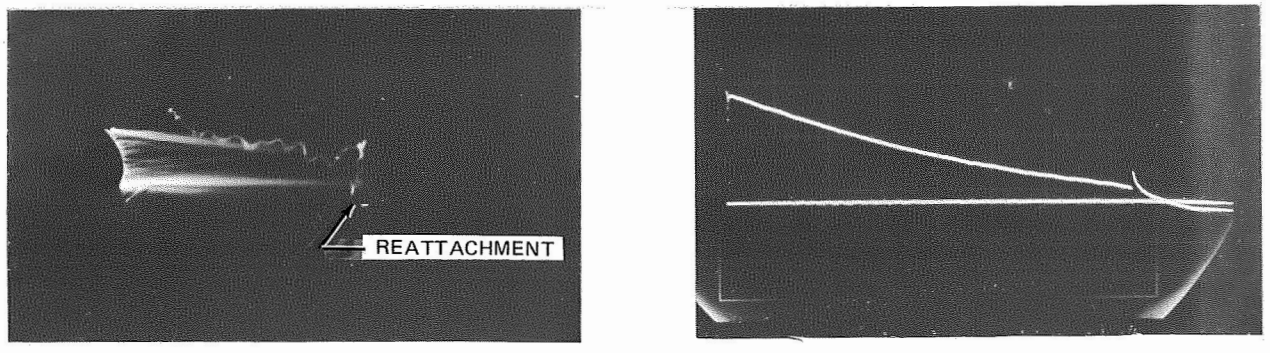

POSITIVE RESTRIKE AT 15 MILLISECONDS – SUCCESSFUL

FIGURE 35. LIGHTNING SWEPT-STROKE AND RESTRIKE TESTS

intensity of the arc-channel. Each restrike impulse and discharge time was recorded in the current waveform. The small dip in the current waveform at the beginning of the swept-stroke was caused by the vaporization of the thin wire which established the arc-channel. The photo of test 4 recorded the restrike channel attaching to the aluminum strip on the upstream side of the composite test panel. The photo of test 8 recorded the restrike attaching to the aluminum strip on the downstream side.

The dielectric shielding successfully protected the graphite panel in all tests except number 6. Test 6 was considered a marginal failure because the forked arc-channel attached to both the graphite panel and to the aluminum strip, rather than to the aluminum strip only. The arc-channel attach point to the graphite panel is shown in Figure 36(a). The damaged area was about 3 by 35 millimeters and was limited to the first ply of the graphite panel. The lightning current path from this area to ground was completed by an arc between the edge of the graphite panel as shown in Figure 36(b), and the leading edge aluminum strip. Figure 36(b) also shows several arc-channel dwell points at the leading edge aluminum strip during swept-stroke lightning tests. While dwelling at these points, the arc-channels left smoke trails on the adjacent fiberglass panel surface.

Four restrike tests at 15 milliseconds were conducted. Test 5 used negative polarity and there was no failure of the test panel. Test 6 used positive polarity and there was a marginal failure of the dielectric shielding protection system. The later test was repeated in tests 7 and 8 but the failure could not be reproduced.

In addition to the marginal dielectric strength of the 0.05 millimeter (2 mil) thickness Kapton film, peel tests indicated marginal bonding characteristics of the Kapton to the graphite-epoxy in the presence of high humidity environments. Because of the implications of poor paint adhesion in service, a decision was made to delete the Kapton film and replace it with equivalent epoxy and polyurethane paint coatings with dielectric strength equivalent to a 0.08 millimeter film of Kapton. The production rudder drawing therefore specified a finish paint thickness between 0.16 and 0.25 millimeters thickness.

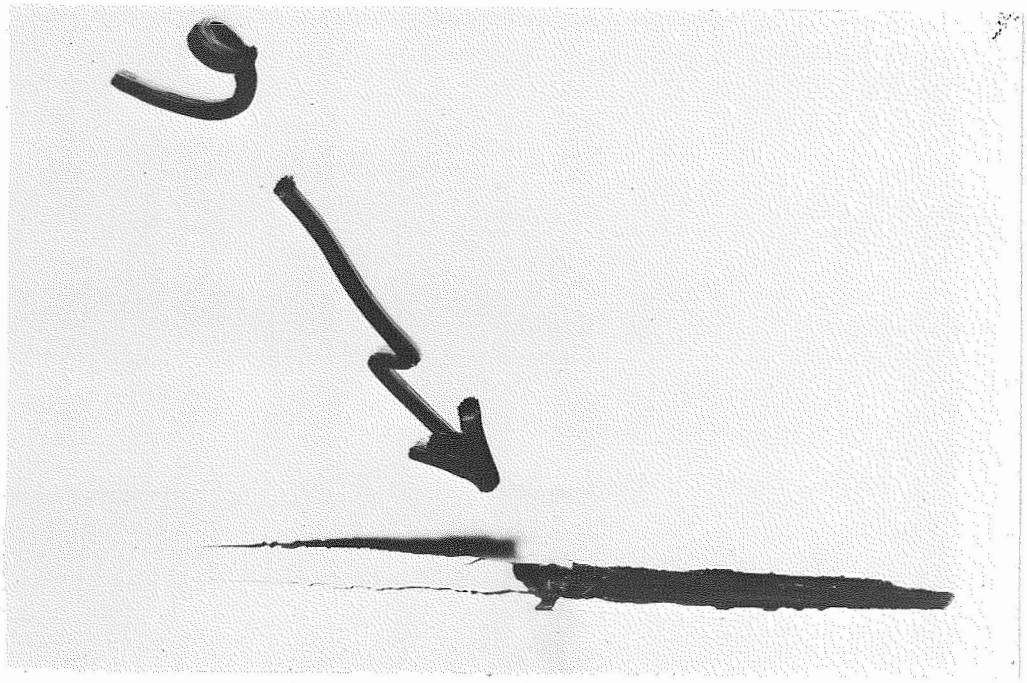

(A) PUNCTURED AREA (MAGNIFIED 2X)

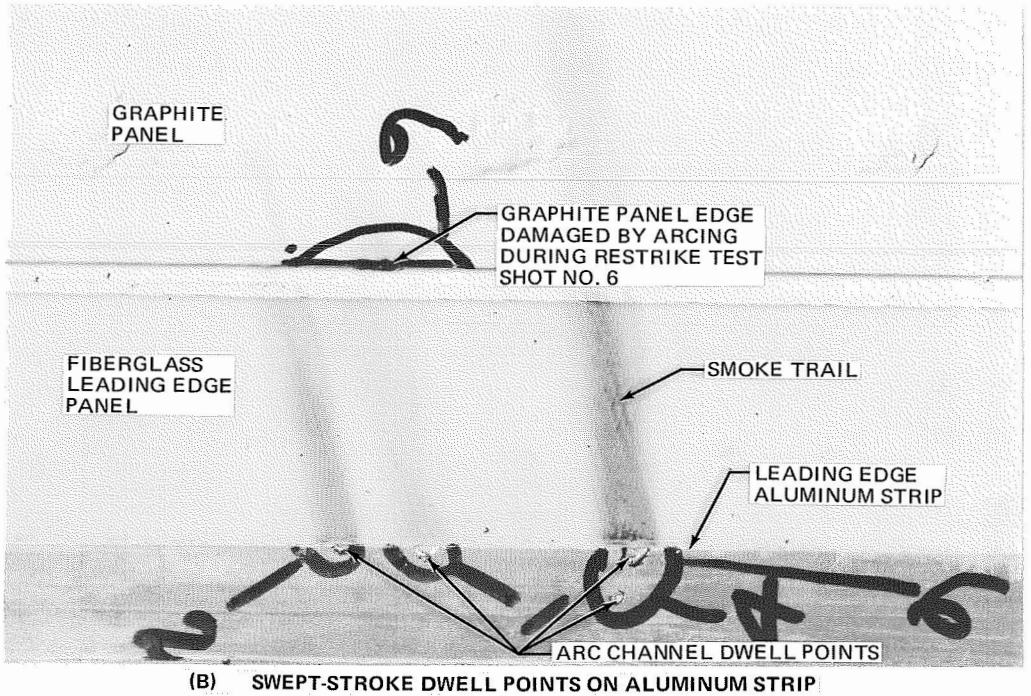

(B) SWEPT-STROKE DWELL POINTS ON ALUMINUM STRIP

FIGURE 36. LIGHTNING TEST PANEL CLOSE-UP VIEWS AFTER TESTING

The additional dielectric shielding strength provided adequate safety margin for the protection system and no further swept-stroke tests were considered necessary.

Direct Strike Attachment Tests. - These tests were conducted on a component representing the tip region of the rudder approximately 0.35 meters long and incorporating the aluminum alloy conductor strips along the fiberglass trailing edge and tip assemblies, Figure 37. The test component also incorporated two precipitation-static (p-static) discharger installations mounted on the trailing edge conductor strip and the upper hinge fitting mounted on the front spar. The objective of these tests was to demonstrate the adequacy of the conductor strips to transfer direct lightning strike current.

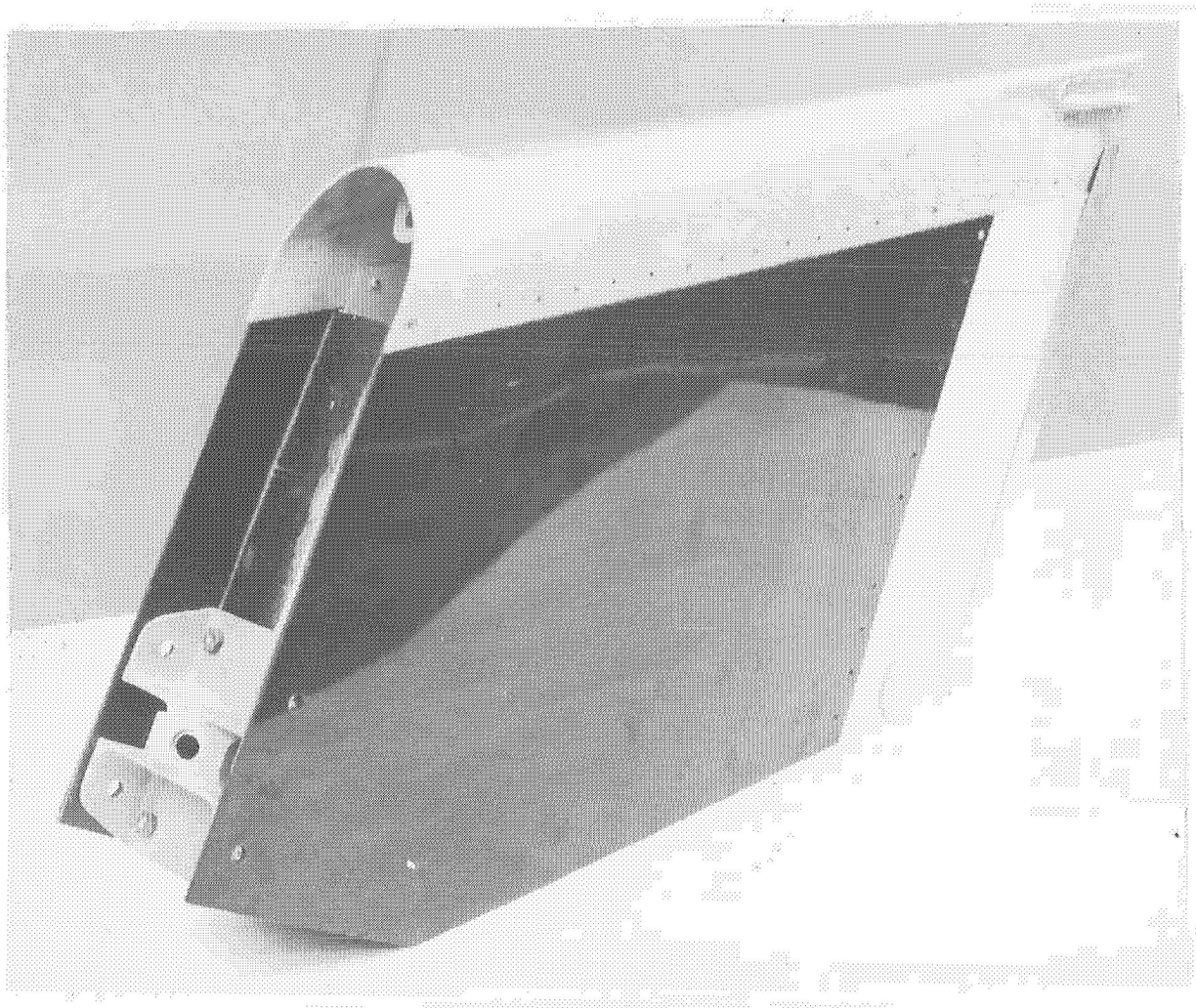

FIGURE 37. LIGHTNING TIP TEST COMPONENT

During each lightning test, the lightning current was directed through both p-static dischargers and through the electrical conductive path which was grounded at the hinge fitting. The test setups are illustrated in Figure 38.

Four preliminary tests were made using peak current amplitudes of 36, 54, 72, and 90 kiloamperes. A typical test current waveform is shown in Figure 39(a). Sparking occurred at the electrical joint between the trailing edge and tip aluminum conductor strips during the 72 kiloampere test as shown in Figure

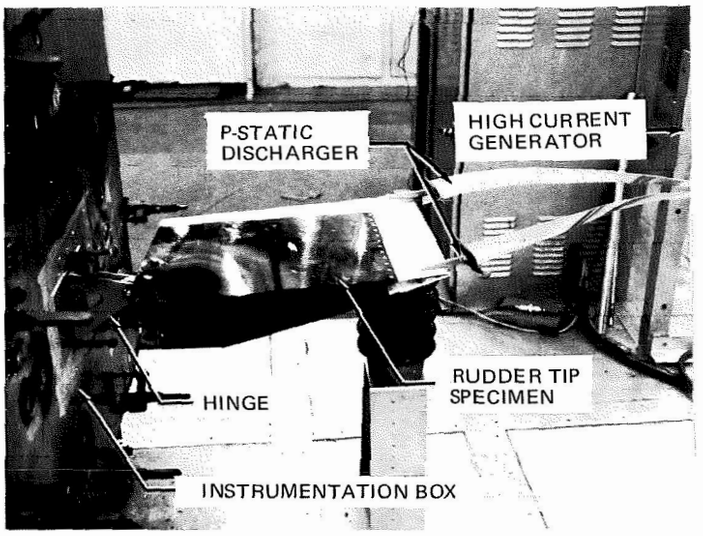

PRELIMINARY TEST SETUP

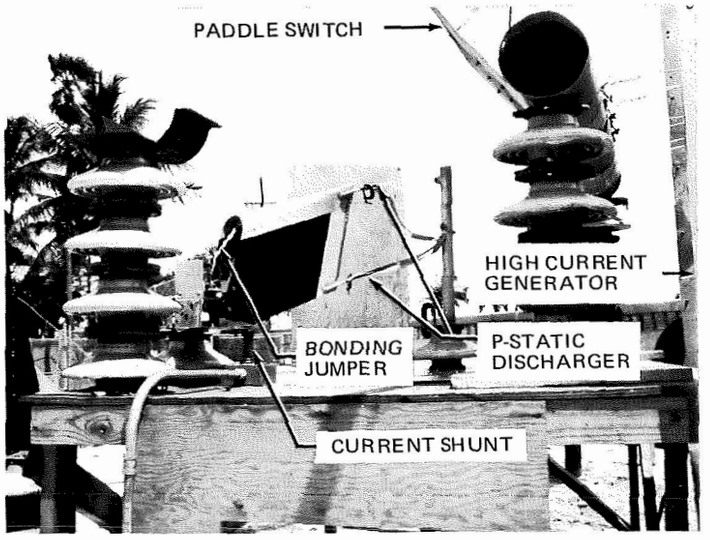

FINAL TEST SETUP

FIGURE 38. LIGHTNING TEST SETUPS

GENERATOR:	C = 8.68 μf, V = 50 KV
CALIBRATION:	45 Ka/DIV, 50 μSEC/DIV
ACTION INTEGRAL:	$\int i^2 t = 0.11 \times 10^6$ AT 29 μSEC

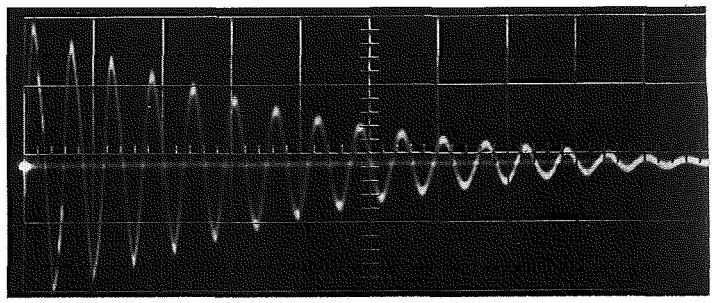

(a) TYPICAL LIGHTNING TEST CURRENT WAVEFORM

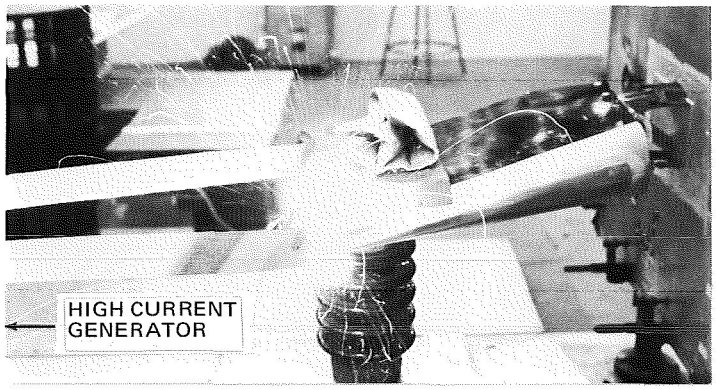

(b) 72 Ka TEST RESULT – SPARKING AT ELECTRICAL JOINT

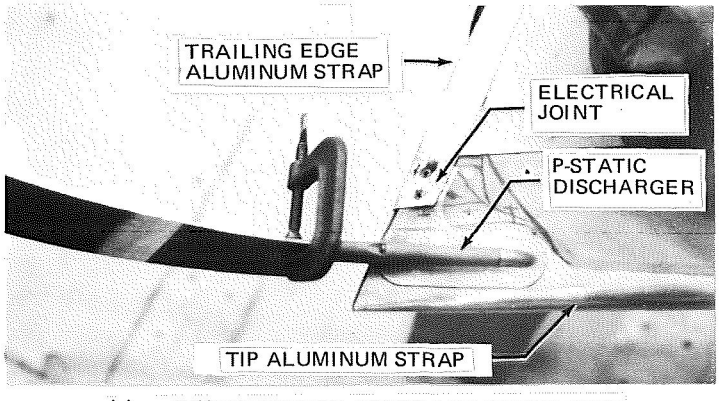

(c) TEST SPECIMEN AFTER LIGHTNING TEST

FIGURE 39. PRELIMINARY LIGHTNING TEST RESULTS

39(b). During the 90 kiloampere test, the electrical joint between the trailing edge and tip conductor strips was rendered ineffective as shown in Figure 39(c). This joint was subsequently redesigned to improve electrical contact by addition of a splice doubler, Figure 40, and several additional universal head rivets of larger diameter.

The final lightning strike test was conducted at a peak current of 195 kiloamperes. The test current waveform, Figure 40(a), supplied an energy level conforming to the requirements of the proposed SAE Aerospace Recommended Practice "Lightning Effects Tests on Aerospace Vehicles and Hardware". This energy level exceeded the requirements of specifications Mil-B-5087 add FAA AC20-53.

The lightning protection system successfully transferred the current but the tip assembly conductor strip sustained some damage as shown in Figures 40(b) and 40(c) due to mechanical loads caused by the electromagnetic fields around the contoured conductor. A drawing change was issued against the flight rudder tip installation drawing to increase the material gage of the tip conductor from 0.40 to 0.63 millimeters and to add several attach rivets to secure the conductor to the fiberglass tip.

GENERATOR:	C = 189 μf, V = 25 KV
CALIBRATION:	80 Ka/DIV, 100 μSEC/DIV
ACTION INTEGRAL:	$\int i^2 t = 2.04 \times 10^6$ AT 135 μSEC

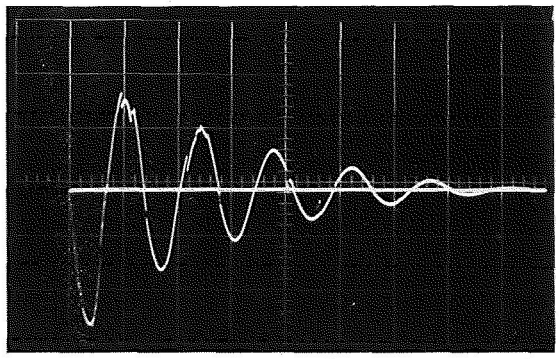

(a) LIGHTNING TEST CURRENT WAVEFORM

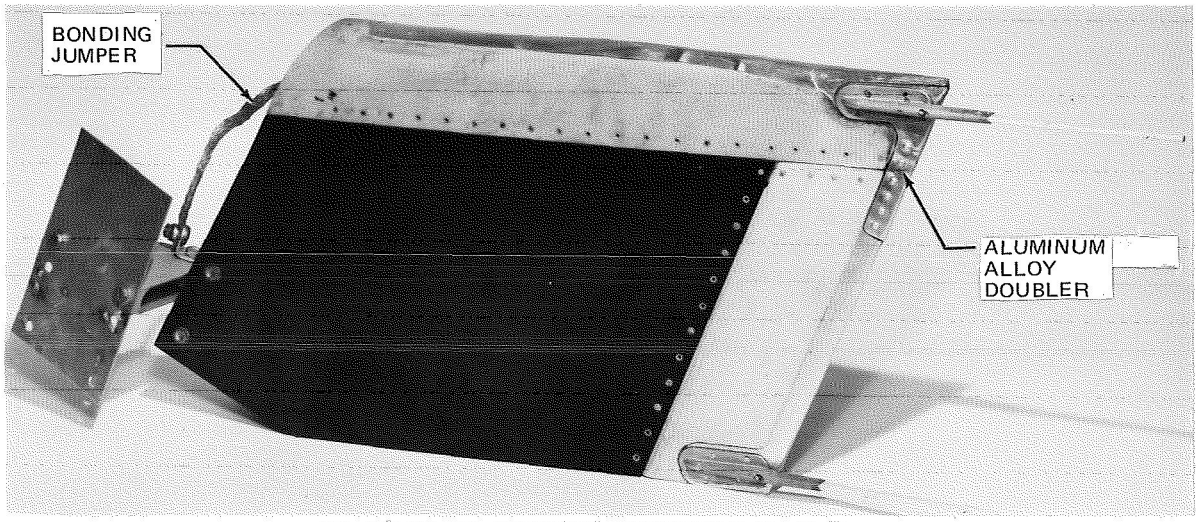

(b) TEST SPECIMEN AFTER LIGHTNING TEST

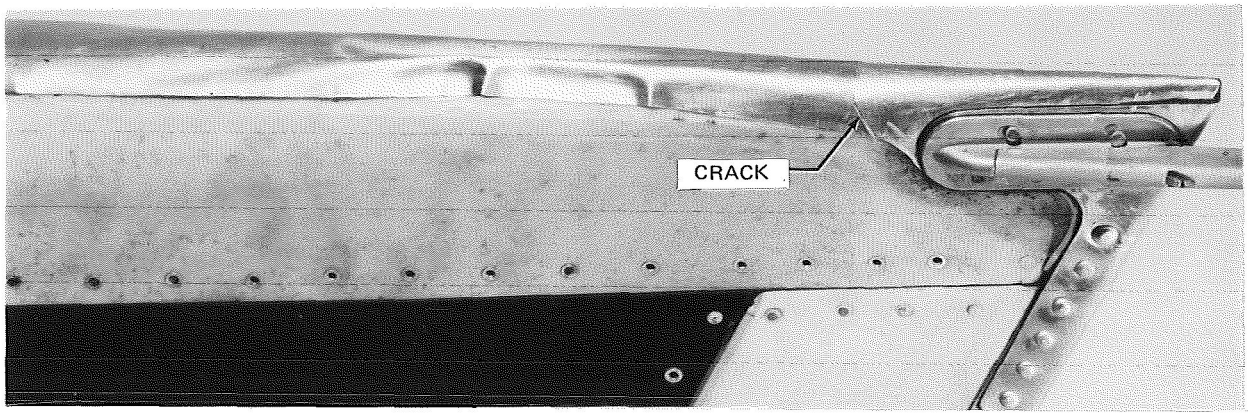

(c) CLOSEUP VIEW

FIGURE 40. FINAL LIGHTNING TEST RESULTS

RUDDER DEVELOPMENT

On successful completion of the eighth three-bay manufacturing development component, the full-scale rudder tooling was completed and manufacturing of prototype rudders was begun. A series of four rudder units was produced during which detailed tooling and processing problems were identified and follow-up solutions were developed. The fourth unit produced was accepted for ground test after completion of tag-end quality control tests and non-destructive inspection. Manufacturing of the ten flight-service rudders followed successful completion of the rudder ground tests. Details of the tooling and manufacturing experience are described in this section.

Tooling

The rudder tool design was consummated using experience gained during fabrication of the eight manufacturing development components. The form mold die (FMD) for the rudder is illustrated in Figure 41. This tool was a scaled-up version of the three-bay FMD, Figure 24, used to make the manufacturing development components.

A five-piece machined aluminum alloy mandrel was provided in each rib-bay of the FMD. The machined details and a typical assembled metal mandrel are shown in Figure 42. The central piece of each metal mandrel assembly was fixed to the FMD through a cylindrical "stand-off" detail which established the location of the rudder front-spar plane relative to the FMD base beam. The front-spar plane locator, Figure 41, was supported on these "stand-off" details. Each of the fixed metal mandrels was internally heated with an electrical cartridge heater. The electrical wiring was routed through the base beam and up through each cylindrical "stand-off" detail. The remaining four pieces of each metal mandrel were removed together with the rubber mandrel elements after a cure cycle was completed.

The rubber mandrels were cast in the FMD using a dummy part to simulate the skin, rib, and spar thicknesses. The simulated skins were cured fiberglass panels which accurately represented all built-up areas for leading edge,

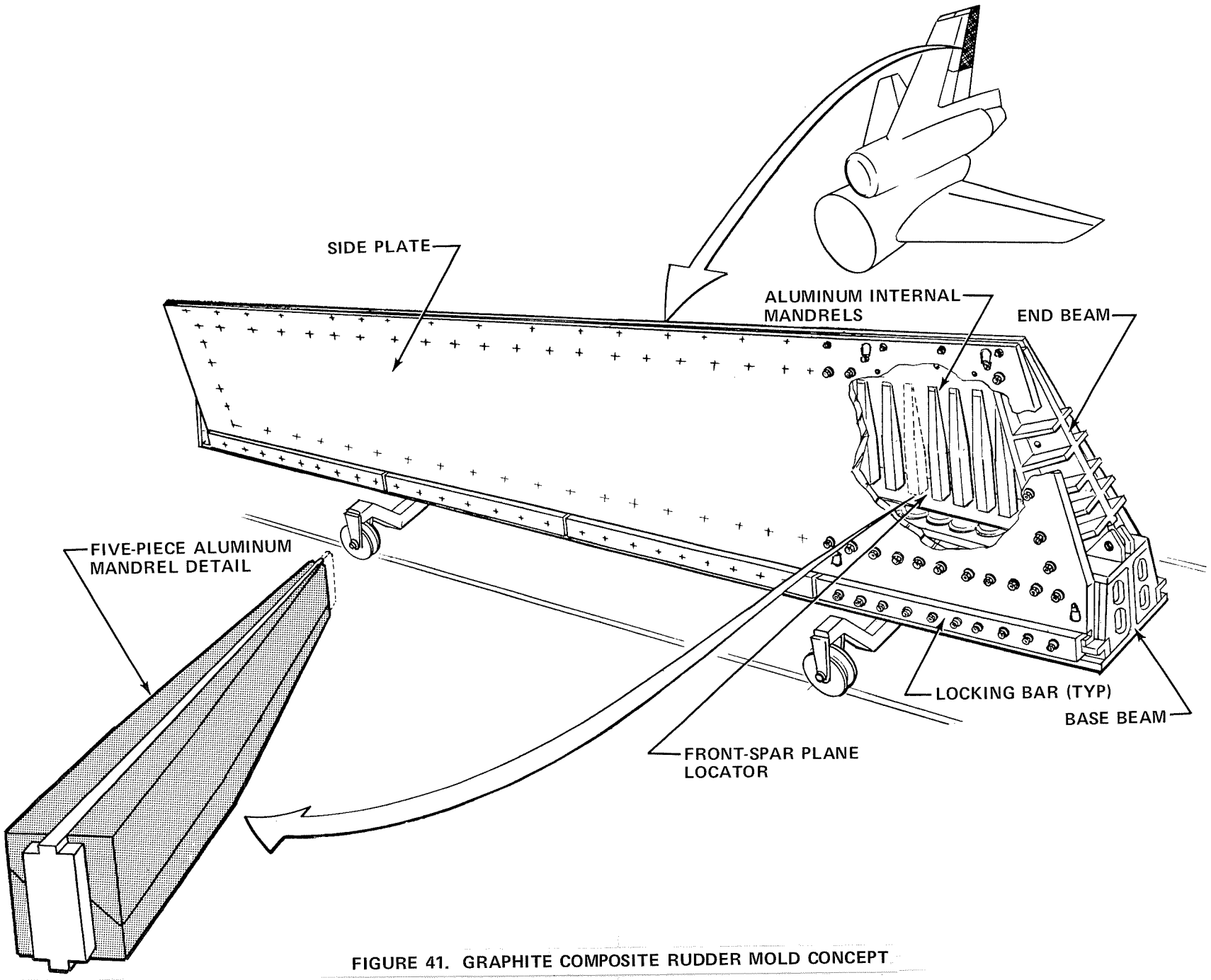

FIGURE 41. GRAPHITE COMPOSITE RUDDER MOLD CONCEPT

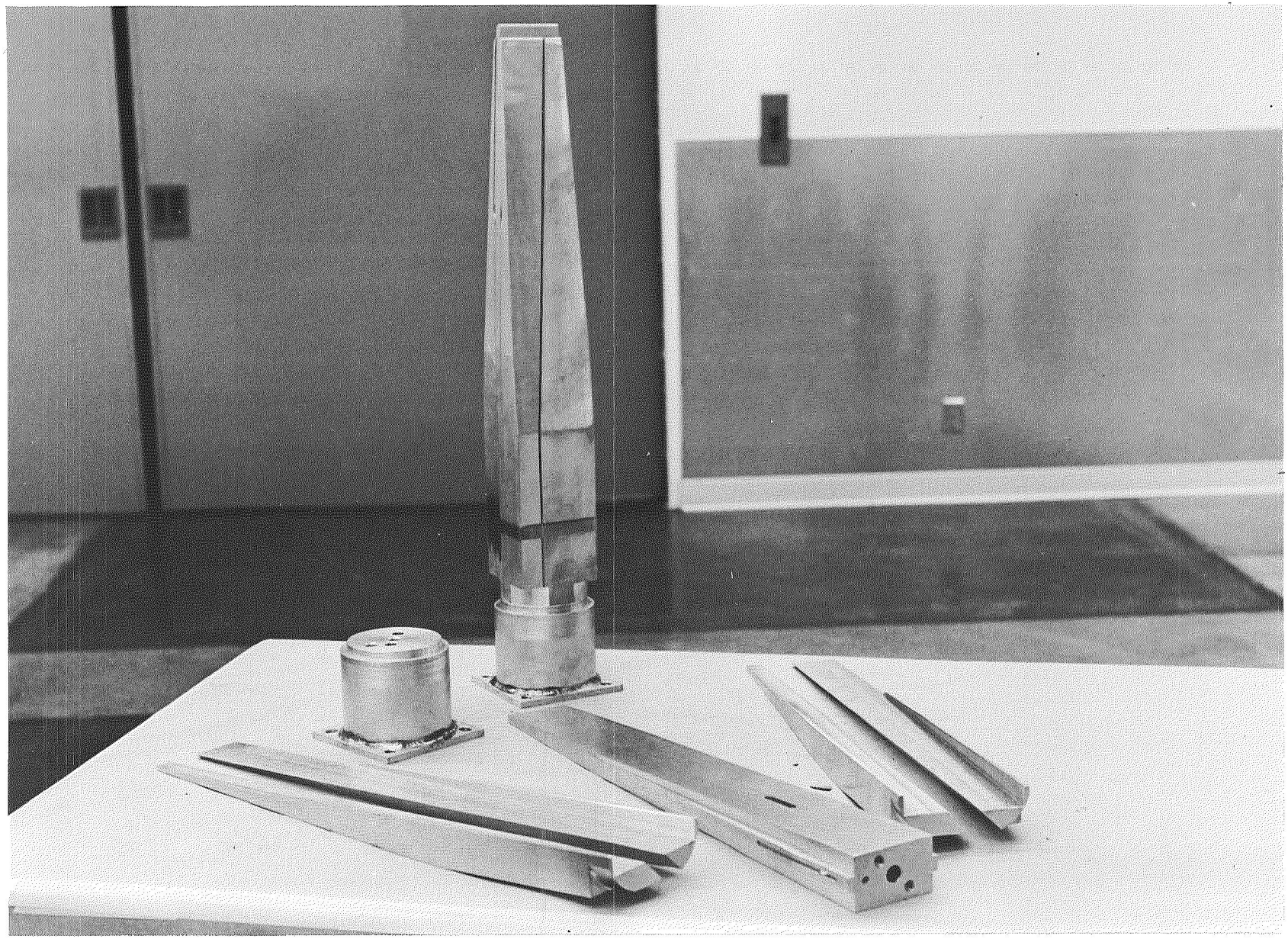

FIGURE 42. RUDDER MOLD ALUMINUM ALLOY MANDRELS

trailing edge, tip, and fitting attachments (see Figure 8). The rib and spar simulations were sheet metal parts of appropriate thicknesses.

The rubber mandrels were cast in place in the dummy part in a three-stage molding operation. The mandrel forward of the front-spar was poured initially, cured overnight at room temperature, and subsequently oven postcured. After positioning the wire screen reinforcing pieces within the mold cavity, the mandrels in the 31 rib-bays between front and rear-spars were poured and similarly cured and post-cured. The front-spar and rib-bay mandrels were made using Dapcocast No. 38-3 rubber. The final pour, aft of the rear-spar, was made using Dow-Corning Silastic J rubber, cured at room temperature and subsequently oven post-cured. The Silastic J rubber, with a greater coefficient of thermal expansion, was used aft of the rear-spar to increase curing pressures in this limited volume region. The 31 rib-bay mandrels were finally cut into segments (six each) and coated with Teflon tape to facilitate removal after a cure cycle. The segments of a completed rib-bay mandrel are shown in Figure 43.

The components of the trailing edge structure were also designed for fabrication using the thermal expansion molding technique. The trailing edge mold is shown in Figure 44, together with a prototype part produced in the mold. The leading edge and tip structures were designed, tooled, and fabricated using conventional autoclave techniques for fiberglass construction. The machined aluminum alloy fittings were also tooled and manufactured using conventional state-of-the-art techniques.

Process Development

Processing experience gained through production of four prototype rudders is summarized in this section. Development problems were encountered in each of the prototype units produced. The severity of the problems was reduced with each subsequent unit as corrective actions were taken. The in-process quality control tests from tag-end specimens and the non-destructive tests performed on the cured units confirmed the overall feasibility of the manufacturing method.

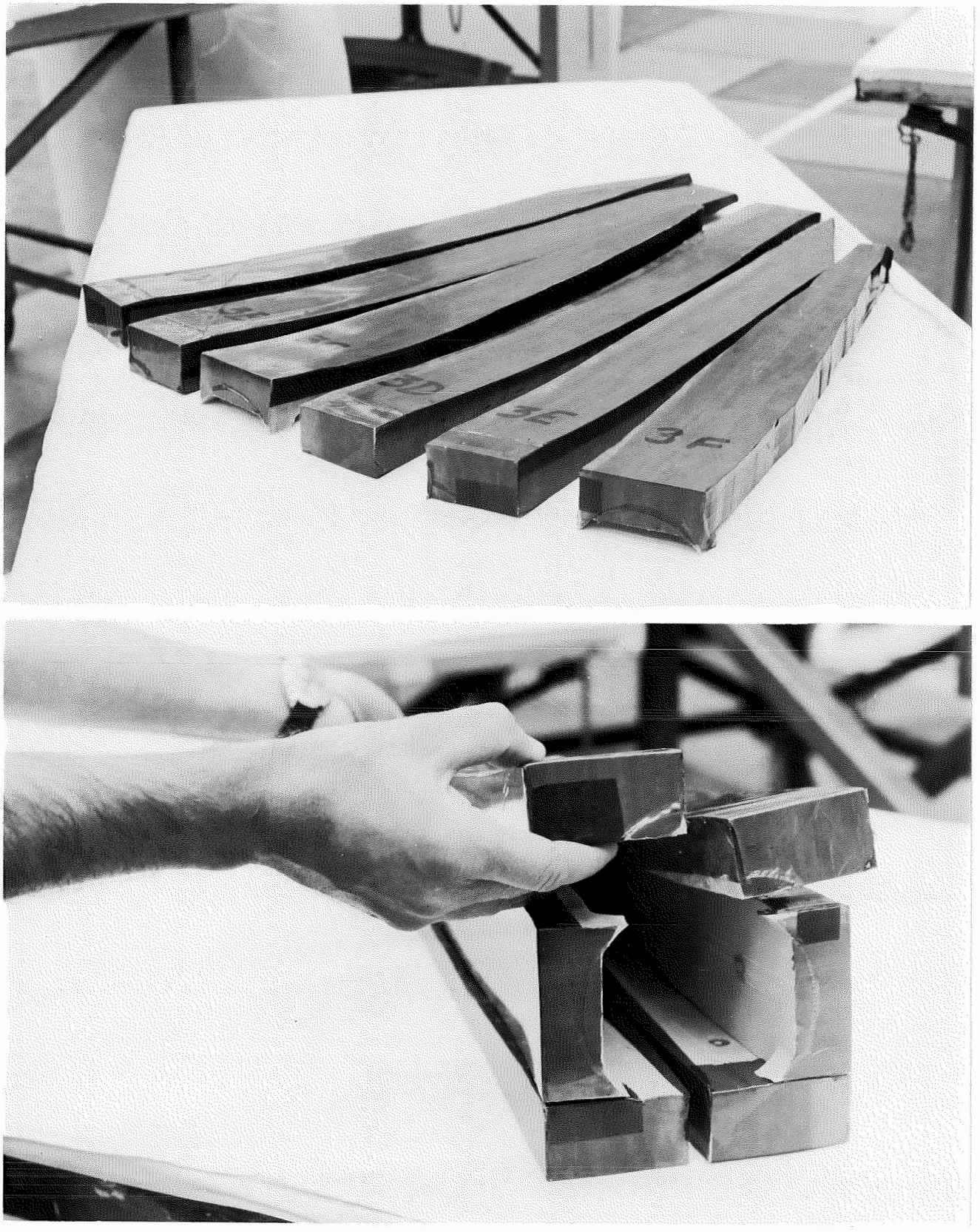

FIGURE 43. SEGMENTED RUBBER MANDREL DETAILS

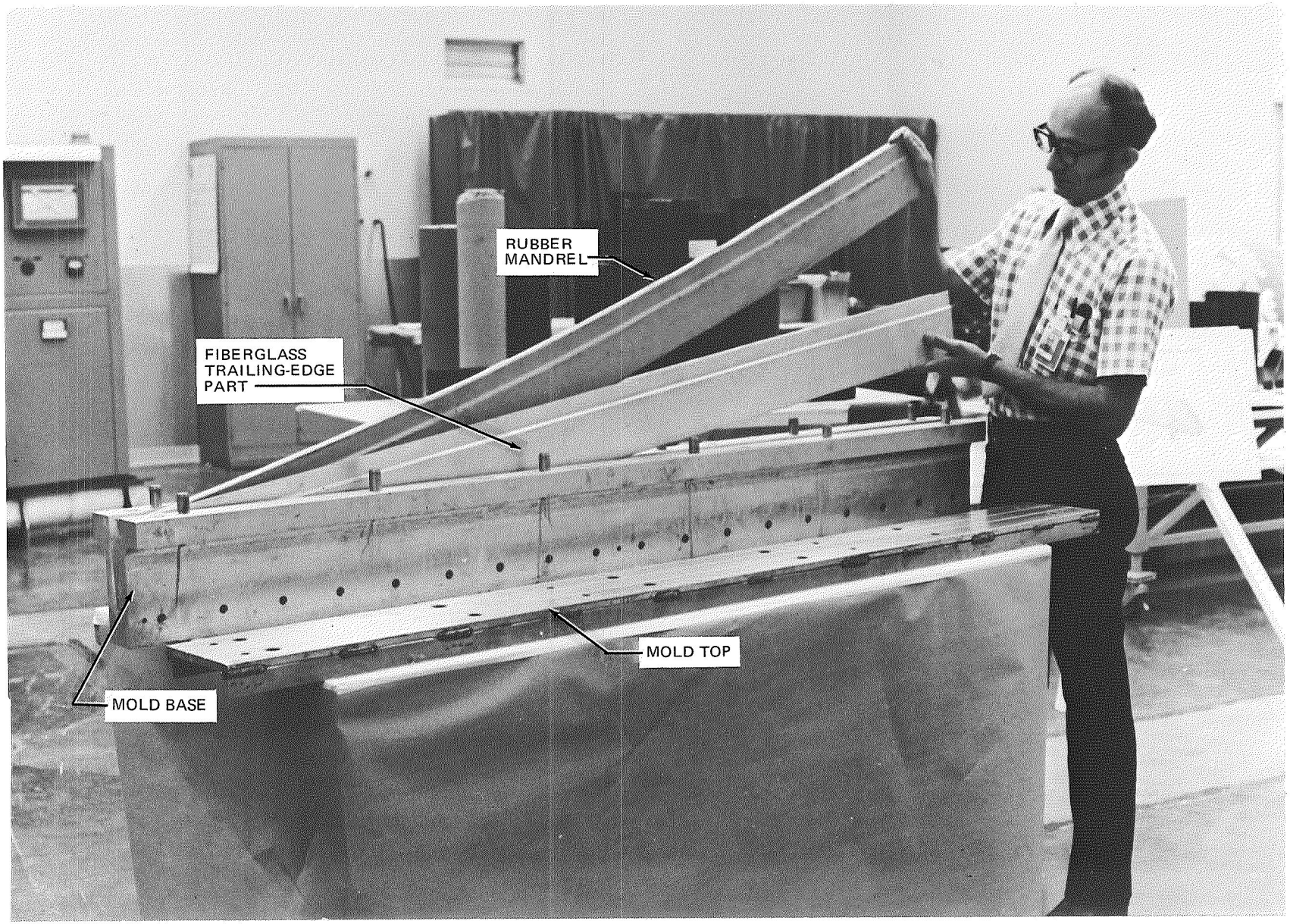

FIGURE 44. TRAILING EDGE MOLDING TOOLS

Rudder Unit 1. - The laminated details for the first graphite rudder mold assembly were laid-up, densified under vacuum pressure, and stored under refrigeration in preparation for the cure cycle. The skins were densified for 30 minutes at 394°K (250°F). Each skin had some additional temperature exposure (10-20 minutes at up to 366°K) during removal of wrinkles caused by buckling of the skins during thermal contraction (cool down) of the aluminum caul plates. This skin wrinkling was subsequently avoided by using a titanium caul plate for the densification cycle. The ribs and spars were densified to a lesser extent (up to 30 minutes at 394°K) since hard densified details had proven more difficult to handle during construction of the three-bay development components.

Each rib element was preformed on wooden form-blocks as shown in Figure 45. The front and rear-spar elements were similarly preformed. The installation of the forward front-spar preform in the FMD is shown in Figure 46. The preformed rib and spar elements were mated with the appropriate rubber mandrels and installed in the FMD as shown in Figure 47.

The lower closing-rib of the rudder was difficult to install in the FMD because of the bulk of the rubber mandrels and laminates and the close fit of a stainless steel tooling shroud around the closing-rib. The end beam of the FMD was finally removed to permit installation of the closing-rib and shroud. The end beam was reinstalled with difficulty using jacks, levers, and clamps to align the beam with adjacent tool members. The tool was subsequently modified (fitted with threaded drawbars) to facilitate this installation.

After the skin panels were located, the FMD side plates were installed and the assembled tool, Figure 48, was rolled into the oven for the cure cycle. Considerable difficulty was encountered in closing the FMD after the mandrels, both metal and rubber, and the laminates were installed. The mold could not be fully closed in the central rear-spar region.

The first cure cycle demonstrated the overall feasibility of the tooling and manufacturing concept. The exterior appearance of the cured rudder was very good (see Figure 49). However, the front-spar and ribs were considered

FIGURE 45. PREFORMED GRAPHITE RIBS AND FORM BLOCKS

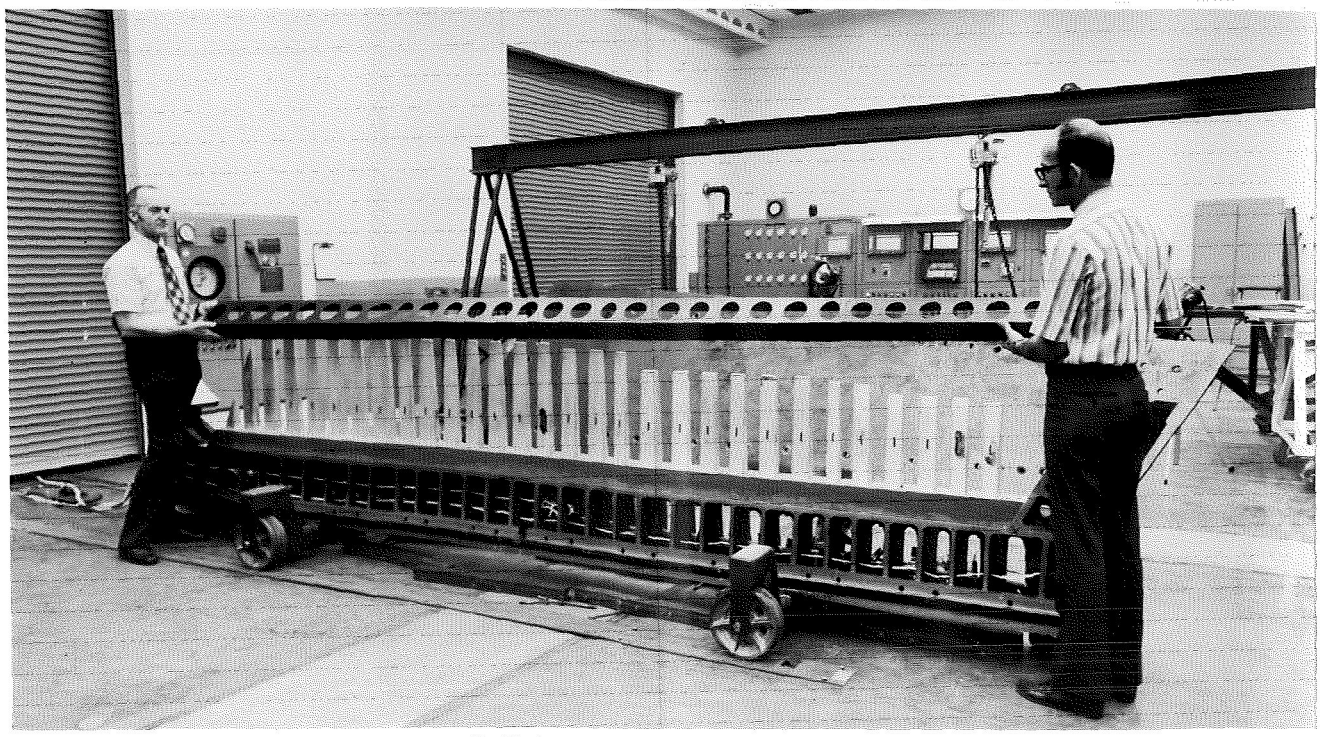

FIGURE 46. INSTALLATION OF FRONT-SPAR PREFORM IN FORM MOLD DIE

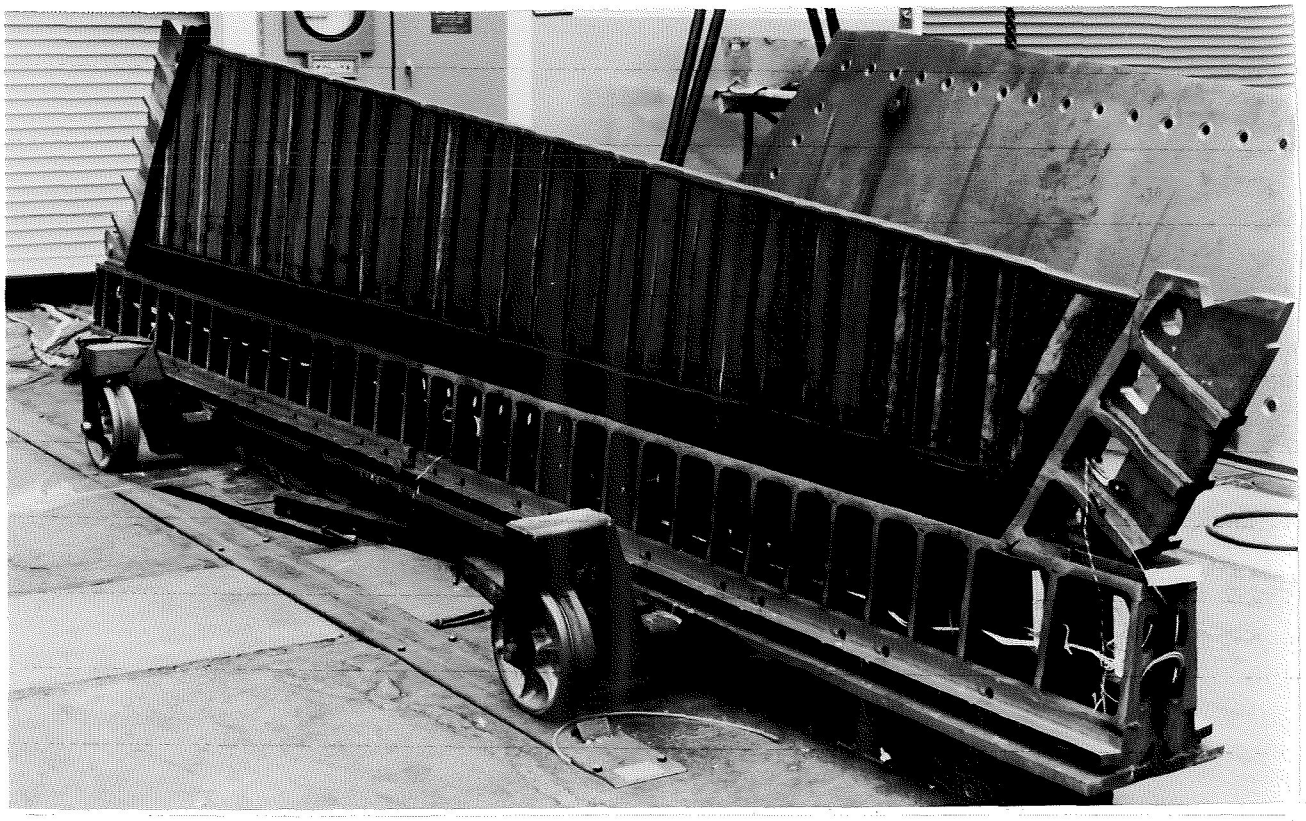

FIGURE 47. RIB AND SPAR PREFORMS AND RIB-BAY MANDRELS INSTALLED IN FORM MOLD DIE

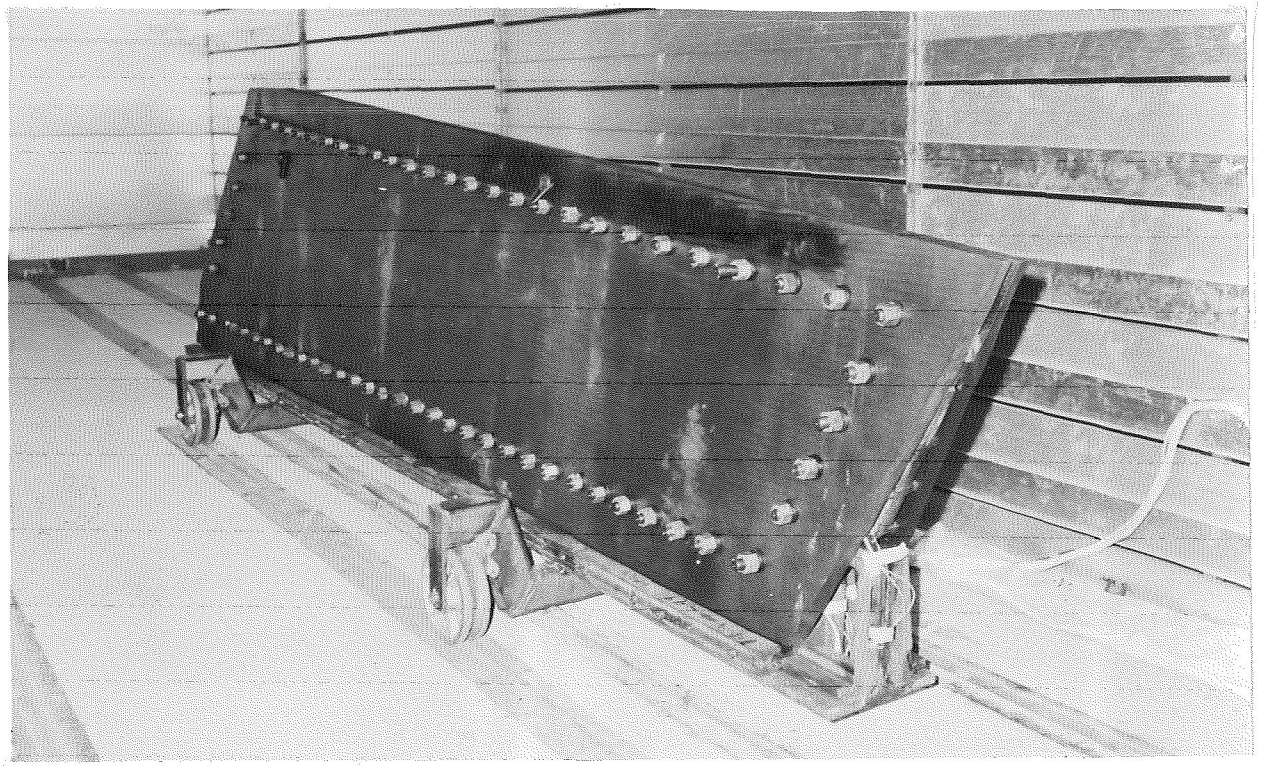

FIGURE 48. ASSEMBLED FORM MOLD DIE IN CURING OVEN

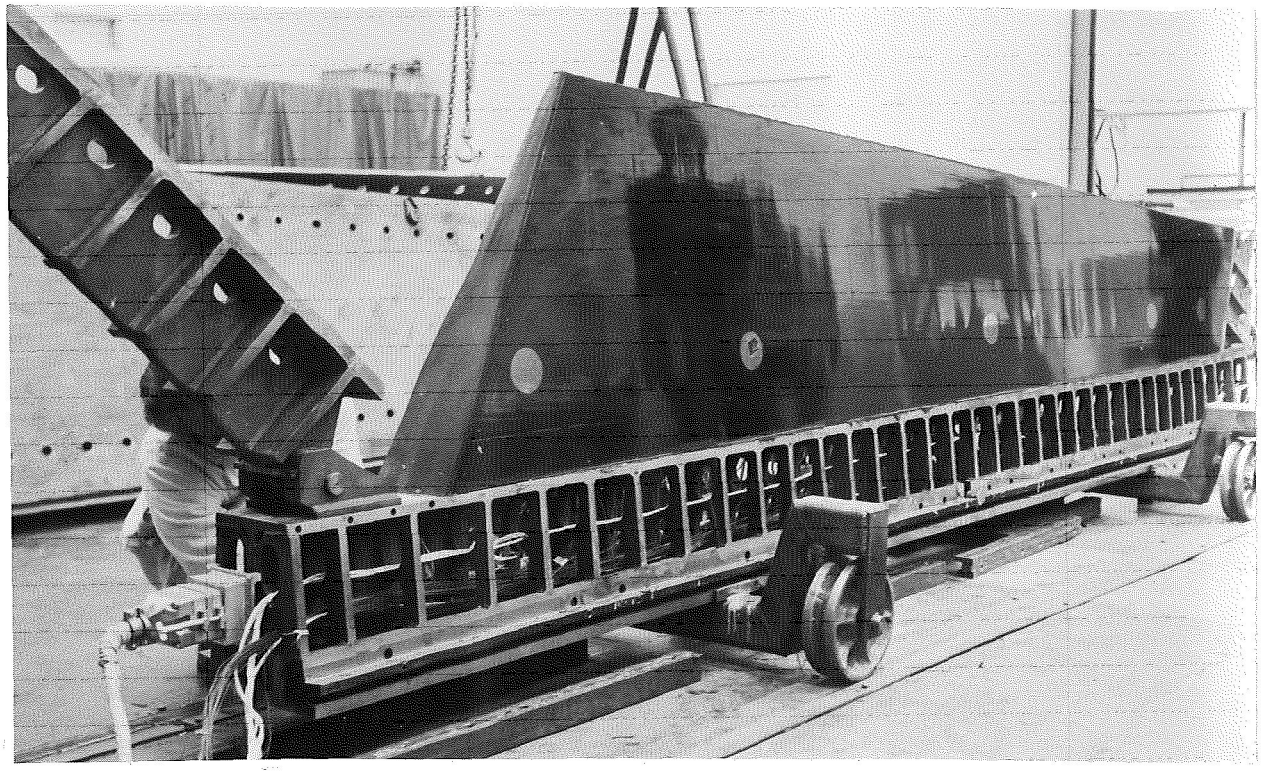

FIGURE 49. CURED GRAPHITE RUDDER LAMINATE ASSEMBLY – DEVELOPMENT RUDDER UNIT 1

unacceptable because of cracks, buckles, and "oilcan" regions at several locations. Dimensional checks along the front-spar indicated that the spar width was oversize up to approximately 5 millimeters and that the rudder side panels were not flat per the loft information. The side panels were cambered to about 2 millimeters at the mid-chord of the rudder.

Quality control test specimens were cut from the peripheral trim of the graphite box from 12 locations (see Appendix B). Flexural strength and modulus, interlaminar shear strength, resin content, and void content were determined at each location. The test results indicated that sound laminates had been produced throughout most of the rudder. One region of porous laminate was detected in the rear central portion of the rudder where the mold was not fully closed. The laminate in this region had excessive ply thickness (about 0.2 millimeter) high resin and void contents, and low mechanical properties. The nondestructive test results (also summarized in Appendix B) confirmed the specimen test results.

Diagnosis of the first cure cycle led to the preliminary conclusion that the front-spar had been cured too quickly with respect to the rest of the rudder. The internal electrical heaters had been turned on before the FMD was rolled into the curing oven to preheat (expand) the rubber mandrels. However, because of the good heat conduction path from the internal metal mandrels to the front-spar, it was postulated that (1) the spar laminate had cured before the rest of the tool was properly heated or pressurized, (2) that the spar cracks resulted from applying full curing pressure after the spar had initially cured in a non-flat configuration, and (3) that the rib-buckles were caused by thermal stress effects of curing the spar before the rest of the FMD had expanded to full size. These conclusions were subsequently changed because the cracks and buckles recurred in the second unit after the cure cycle was changed to eliminate the condition.

Rudder Unit 2. - The densification and cure cycles for the second rudder unit were modified to alleviate the cracking and "oilcanning" of the ribs and spars and to increase resin content in the cured laminates. The external appearance of the cured rudder was again very good, Figure 50, but the rib and spar cracking recurred in regions where the rudder skins were thickened at the upper and lower actuator fitting attachments.

The nominal densification cycled for the skin panels had been increased to 90 minutes at 394°K. This change was effected to inhibit resin flow (increase resin content) because several of the tag-end specimens from Unit 1 indicated relatively low resin content. The actual densification cycle was stopped two hours after the oven temperature had stabilized at 394°K even though the thicker parts of the laminate had not fully attained the specified conditions.

As in the first cure cycle, full closure of the FMD was not attained along the rear-spar. The through-bolts on the FMD were carefully torqued in an unsuccessful attempt to close the gaps, and a pressure of approximately 862 kilopascals (125 psi) was developed in the rubber mandrels, even though no temperature had been applied. It was later concluded that the rubber mandrels were simply too large and that the internal forces applied during torquing of the bolts were sufficiently large to damage the spar laminates and buckle the rib-webs prior to curing.

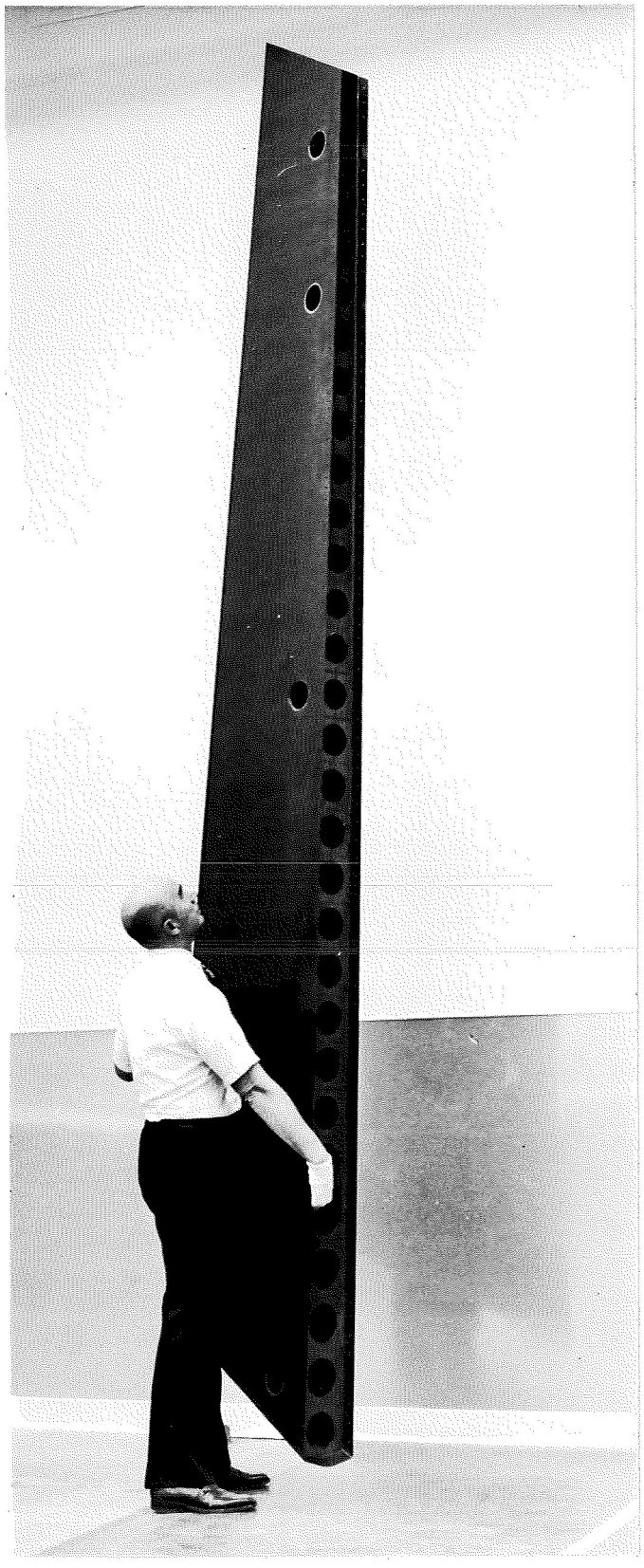

FIGURE 50. GRAPHITE DEVELOPMENT RUDDER UNIT 2

During the cure cycle, the electrical heaters were regulated to minimize thermal gradients throughout the FMD. A two-hour hold period at 366°K was included to expand the rubber prior to cure initiation in the laminates.

The quality control, non-destructive inspection, and dimensional checks of the second rudder were similar in results to the first. Laminate properties were generally good (see Appendix B), but specification requirements were again not attained in the central rear region. Dimensional characteristics were the same as the first rudder.

As a result of the manufacturing experience of the second rudder, a decision was made to remake the rubber mandrels to permit proper closure of the FMD without damage to the preformed rib and spar laminates.

Rudder Unit 3. - The third rudder unit was cured after the rubber mandrels were remade. The skin panels were hard densified for a full 90 minutes at 394°K. Total oven time for the full densification cycle was about three hours. When the edges of the skin panels were trimmed prior to installation in the FMD, the laminate was observed to be dry and boardy. Minor delaminations could not be repaired with a heat-gun and finger pressure.

The rear flange of the front-spar was densified flat and not subsequently preformed prior to installation in the FMD. The flat configuration facilitated installation of the rib preforms in the FMD but required handwork to form the spar-to-skin flange. This flange was subsequently formed somewhat oversize because of the joggles in the regions of skin thickness buildup.

The FMD was fully closed with no difficulty and the prescribed cure cycle was achieved routinely. However, when the FMD was opened, there were porous regions of the skin panel which gave the appearance of curing with inadequate pressure, Figure 51, and six cracked sections at the lower end of the front-spar between the access holes provided for mandrel removal, Figure 52.

Dimensional checks along the front-spar and across the chord of the side panels indicated good agreement with loft information. The camber of the

FIGURE 51. SKIN SURFACE POROSITY IN DEVELOPMENT RUDDER UNIT 3

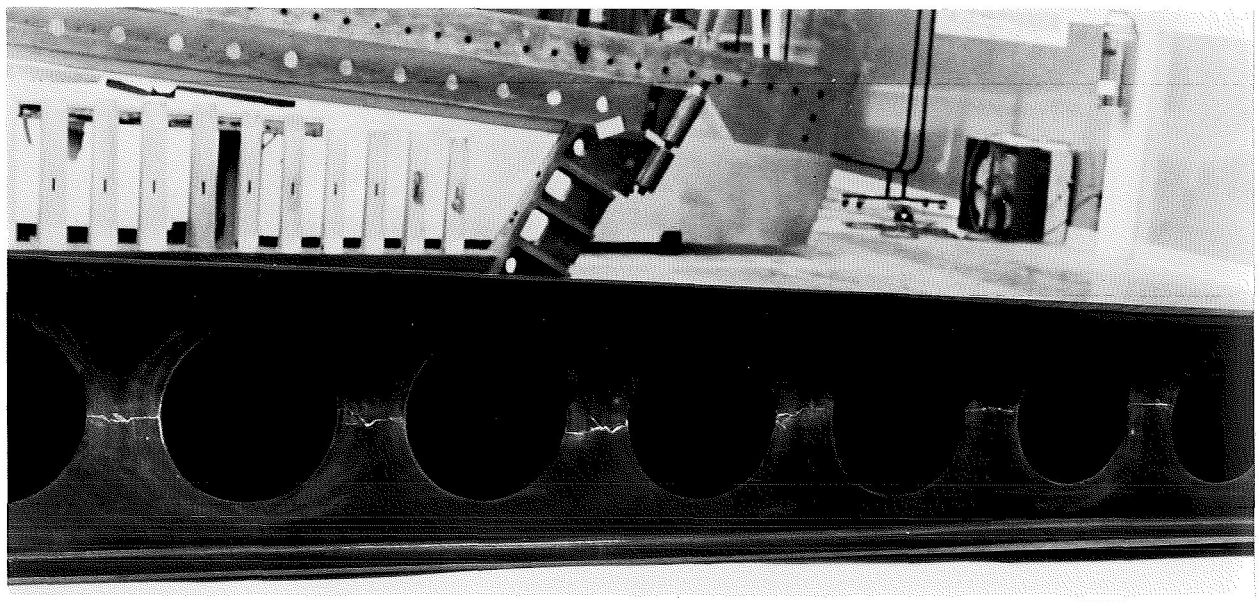

FIGURE 52. CRACKS IN FRONT-SPAR OF DEVELOPMENT RUDDER UNIT 3

side panels was reduced to an acceptable level (0.75 millimeter maximum). Definition of the rib webs for both location and flatness was very good.

The tag-end quality control tests indicated generally improved results (see Appendix B). The resin and void contents were excellent and the mechanical properties indicated improved scatter although the flexural strengths were somewhat low as a result of the hard densification cycle.

Diagnosis of the third cure cycle resulted in the following conclusions:

- Recasting the rubber mandrels attained dimensional precision in the cured graphite rudder, improved the rib definition, reduced the spar cracking, and improved resin content.

- The porous regions in the skin panels resulted from excessive densification which left insufficient time to gelation in the prepreg to attain adequate pressure from thermal expansion of the rubber mandrels during the cure cycle.

- The cracks in the front-spar were eliminated at the upper end, but recurred at the lower end because of insufficient accuracy in preforming the laminated rib and spar details and because of thermal stress effects during tool cool-down.

Rudder Unit 4. - Unit 4 was cured after corrective actions were taken to improve the curing and cracking problems encountered in Unit 3. The densification cycle for all laminated details was reduced to 30 minutes in a 394°K oven under vacuum pressure. The rib form-blocks were modified slightly for dimensional consistency with the FMD and an additional form-block was made to preform the joggles in the aft flange of the front-spar. Eight additional transverse plies of graphite were interspersed in the lower end of the front-spar shear web to reduce thermal stresses in that region during tool cool-down.

During fabrication of the development rudders, the back faces of the graphite laminates tended to delaminate around the edges of drilled holes. This problem was resolved by including a layer of 120 style dry fiberglass cloth in drill breakout regions and cocuring it into the laminate. The close weave of the fabric eliminated the tendency to delaminate and obviated the need for any type of rigid block as a backup member.

The time, temperature, and pressure records for the cure cycle are summarized in Figure 53. An average heat-up rate of 0.45°K (0.80°F) per minute was achieved in the assembled tool. The cure cycle required a total of 12 elapsed hours; 6 hours for heat-up, 2 hours at 450°K (350°F), and 4 hours for cool-down. The mold was opened when the part temperature reached 325°K (125°F).

Visual examination of the cured rudder indicated a significant reduction in the surface porosity, Figure 54, and the elimination of cracked rib and spar elements. The porous regions were subsequently sealed with an epoxy spray coat, Figure 55. The non-destructive inspections (ultrasonic and Fokker bond tests) indicated that a sound laminate had been produced. The molding assembly was free of cracks and delaminations in the spar regions and excellent resin bonds were achieved at all rib, spar, and skin panel interfaces.

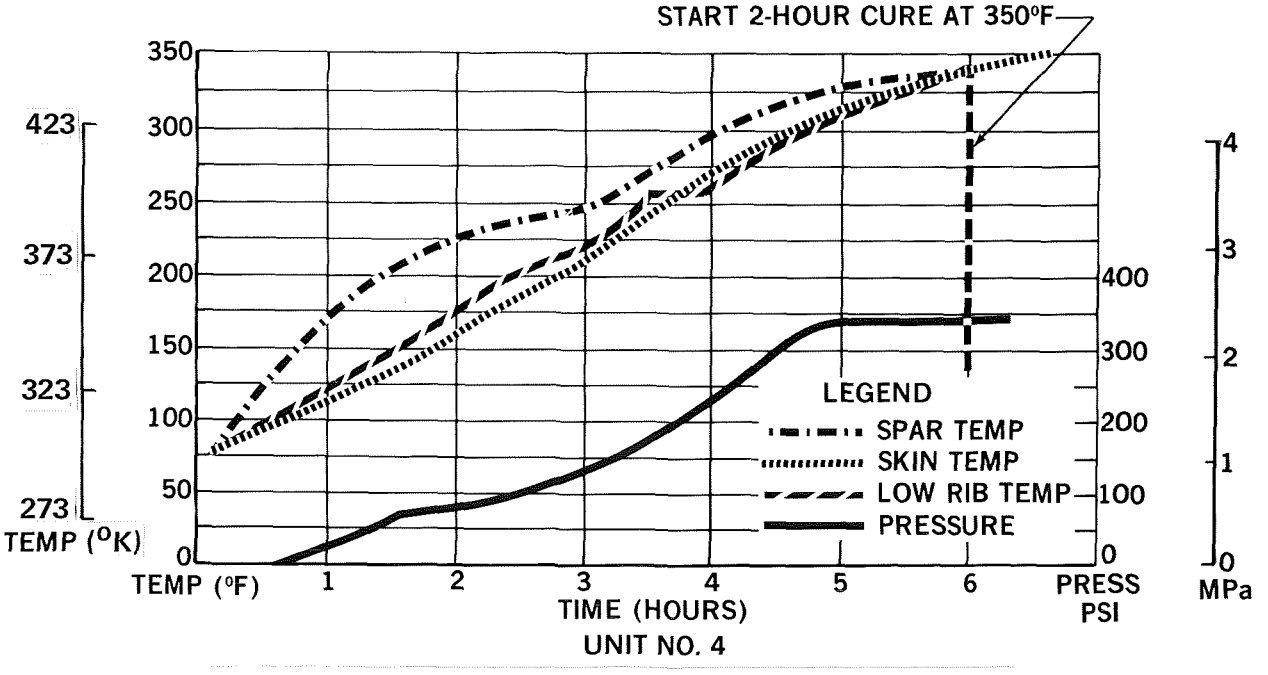

FIGURE 53. CURE CYCLE FOR DEVELOPMENT RUDDER UNIT 4

FIGURE 54. SKIN SURFACE POROSITY DEVELOPMENT RUDDER UNIT 4

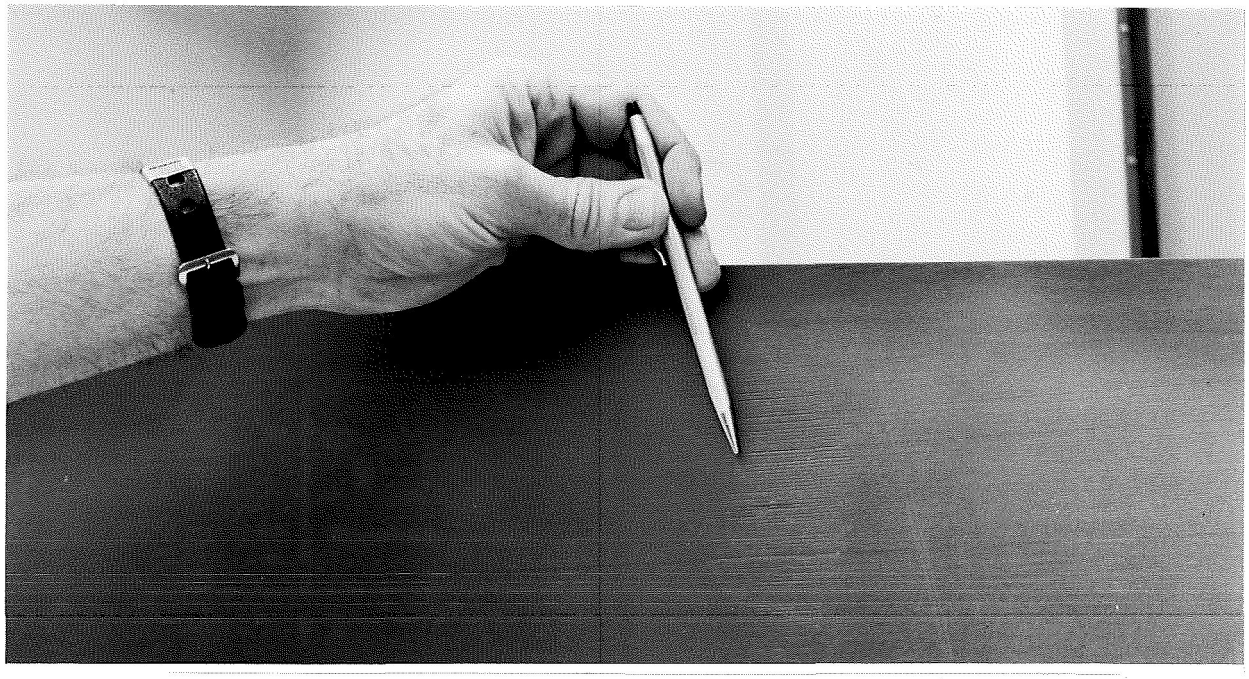

FIGURE 55. SKIN SURFACE AFTER EPOXY SPRAY COATING APPLICATION

The fourth rudder unit was accepted for static tests after satisfactory completion of the tag-end tests and non-destructive inspection. The graphite molding assembly was trimmed net and installed in the final assembly jig for installation of the hinge fittings, leading and trailing edges, and tip structure. The completed static test rudder is shown in Figure 56.

FIGURE 56. RUDDER STATIC TEST COMPONENT

Rudder Manufacturing

The ten flight-service rudders were manufactured after successful completion of the rudder static-test program (see the following section). The manufacturing phase started using essentially the same methods and processes used for the static test rudder. Minor problems were encountered involving the skin surface porosity observed on the static test rudder, waviness of the front-spar plane, and randomly located "oilcan" regions in rib shear-webs and skin panels. The problems were resolved with method and process improvements, local shimming at fitting installations, and local doubler reinforcing as required.

The first problem addressed was the occurrence of the dry and porous areas of the skin panels (see Figure 54). These regions had the appearance of curing with inadequate pressure so the volume of the tool cavity was decreased by replacing the cold-rolled steel tooling shroud with one of increased material gage (1.27 rather than 0.76 millimeters). The side pieces of the new shroud were fastened to the steel side-plates of the PLM with flush-head machine screws, thereby reducing tool assembly time and eliminating the possibility of mislocating the shroud elements.

In the ensuing cure cycle, the regions of skin surface porosity were reduced in size but not eliminated. It was observed that among the several cured rudders the region of surface porosity occurred in a random pattern rather than in the same skin panels. It was finally concluded that trapped air and/or volatiles released during the cure cycle were contributing to the surface porosity phenomenon. One layer of perforated Armalon material (TFE coated glass cloth) was included at the mold surface of each skin panel. This layer provided an escape path for trapped gasses and eliminated the surface porosity on subsequent rudder units.

The manufacturing and tooling approach for the graphite rudder required that the steel locator for the front-spar plane, Figure 41, be capable of movement in the aft direction during removal of a cured graphite box assembly. During fabrication of the four development rudders, it was observed that the spar

locator assumed a bowed shape during the cure cycle since it was not physically restrained against aft movement.

The initiation of the front-spar bowing was attributed to temperature gradients in the tooling during heat-up. In early cure cycles, the internal heaters increased the temperature of the metal mandrels in the rib-bays more quickly than the oven heated the base-beam and side plates of the PLM. The front-spar locator was in good thermal contact with the metal mandrels but was restrained against thermal expansion by the "stand-off" details, Figure 42, attached to the base-beam. The front-spar locator therefore buckled elastically and assumed the bowed configuration with a maximum amplitude between 2 and 3 millimeters from the theoretical spar plane. This bow was not objectionable from a strength standpoint, but required shimming at the hinge and actuator fitting stations to maintain a straight hinge-line for the static test rudder.

A modification was made to the tool which permitted bolting of the spar locator during the cure cycle. These bolts were located near the hinge and actuator fitting stations to minimize the amplitude of the bowing at these points. The spar locator was accurately leveled and securely bolted against the jack-screws prior to a cure cycle. The bolts were removed after the cure cycle so the spar locator was capable of the required aft movement during removal of the cured box assembly.

In addition to the tool modification to restrain the spar locator, temperature gradients during the cure cycle were reduced through increased operator experience with the internal heater and oven temperature controls. Cure times for the initial development rudders were as long as 12 hours (heat-up plus 2 hours at 450°K). Cure time was reduced to 6 hours for flight-rudder number 10. The reduction in cure time was accomplished through better manual control of the internal heaters in conjunction with external (oven) temperatures. Temperature gradients throughout the box assembly were maintained within a 22°K (40°F) range during heat-up. An average heat-up rate of 0.65°K (1.20°F) per minute was achieved in the later cure cycles.

The tooling modification and improved cure cycle reduced the front-spar bowing to an acceptable level. Straight hinge-lines were maintained on the flight-service rudders with nominal shim thicknesses (0 to 1 millimeter) at the front-spar interface with the hinge fittings.

Some isolated cases of rib shear-web and skin-panel "oilcanning" were experienced during manufacture of the flight-service rudders. This problem was also attributed to thermal gradients in the laminating mold during the cure cycle. When thermal gradients were maintained with a 22°K range, the problem was eliminated. The "oilcan" regions were satisfactorily repaired by the application of locally bonded four-ply graphite-epoxy doublers, (45°, -45°)S.

The ten flight-service composite rudders were manufactured without major difficulties. The rudder assembly jig and several cured rudder assemblies are shown in Figure 57. Rudder unit 1 was inadvertantly cured with the wrong fiber orientation in the six-ply ribs. The rib strength was restored by secondarily bonding three-ply (0°, 90°, 0°) graphite-epoxy doublers to each side of the affected ribs. One graphite box-assembly was rejected because the front-spar was damaged during removal from the laminating mold. The damage was caused by stuck metal mandrels which were improperly coated with release agent during the tool preparation. Although the damage was considered repairable, the assembly was rejected because the cost of replacement was determined to be less than the cost of repair.

Cost Summary

An overall summary of non-recurring and recurring labor involved in designing, tooling, and manufacturing the graphite rudders is presented in Table 17. The costs of developing and testing development components and ground test rudders were excluded.

The actual direct recurring labor for manufacturing the ten flight-service rudders is summarized in Table 18. The sheet metal and machined parts were fabricated in two separate shop-order releases of five aircraft each. The direct labor charges for these parts were distributed on a pro-rata basis. Fabrication man-hour accumulations for the leading edge assemblies were not

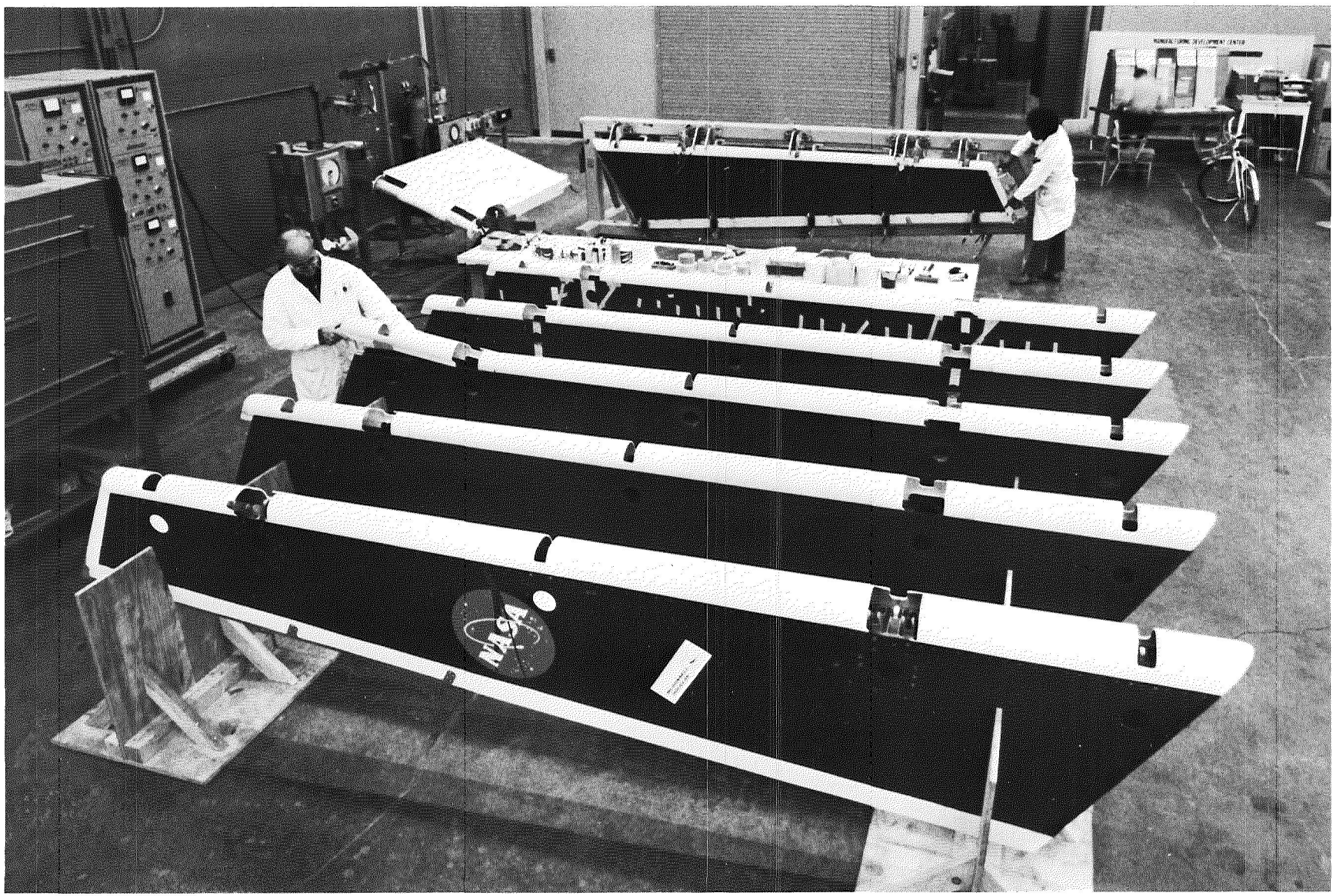

FIGURE 57. CURED GRAPHITE BOX STRUCTURES AND RUDDER ASSEMBLY JIG

TABLE 17

SUMMARY OF NONRECURRING AND RECURRING LABOR FOR DC-10 COMPOSITE RUDDER

LABOR ELEMENT	NONRECURRING LABOR MAN-HOURS	RECURRING LABOR MAN-HOURS
ENGINEERING	4,520	830
TOOLING	17,800	1,100
PLANNING	550	335
MANUFACTURING	NONE	16,765
INSPECTION	NONE	1,900
NONDESTRUCTIVE TESTING	NONE	220

TABLE 18

SUMMARY OF DIRECT MANUFACTURING RECURRING LABOR FOR DC-10 COMPOSITE RUDDER

OPERATION \ UNIT NO.	RECURRING DIRECT LABOR (MAN-HOURS)										
	1	2	3	4	5	6	7	8	9	10	TOTAL
GRAPHITE COMPOSITE LAYUP	441	459	451	382	312	369	368	287	323	312	3,704
GRAPHITE MOLD ASSEMBLY (WMC 7012-3)	500	207	102	258	204	202	236	282	172	172	2,362
NONDESTRUCTIVE TESTING	20	20	20	20	20	30	30	20	20	20	220
FIBERGLASS FABRICATION											
a. LEADING EDGE	163	131	121	115	110	107	105	102	99	96	1,149
b. TRAILING EDGE	114	61	44	69	71	90	43	72	54	98	716
c. TIP ASSEMBLY	79	43	35	94	50	44	43	40	48	50	526
SHEET METAL AND MACHINED PARTS FABRICATION	470	470	470	470	470	354	354	354	354	354	4,120
MISCELLANEOUS FABRICATION (FAIRING, SEALS, DOORS, ETC.)	88	88	88	88	88	88	88	88	88	88	880
FINAL ASSEMBLY (WMC 7012-4901 AND -1)	408	429	359	468	341	272	218	299	257	257	3,308
INSPECTION	259	216	192	217	190	175	168	167	156	160	1,900
TOTAL	2,542	2,124	1,882	2,208	1,856	1,731	1,652	1,711	1,571	1,608	18,885
CUM TOTAL	2,542	4,666	6,548	8,756	10,612	12,343	13,995	15,706	17,277	18,885	
CUM AVERAGE	2,542	2,333	2,183	2,189	2,122	2,057	1,999	1,963	1,920	1,889	

tracked individually, so the total hours for leading edge fabrication were distributed statistically in accordance with an estimated learning curve slope (90 percent).

Estimated labor hours at the detailed operation level are shown in Tables 19 through 24. These estimates were statistically developed using industrial engineering standard values as a basis. The man-hour totals agree in each case with those recorded in Table 18.

TABLE 19
DIRECT LABOR RECURRING MAN-HOURS FOR LAYUP AND DENSIFICATION OF "B" STAGE GRAPHITE-EPOXY DETAILS

PART AND OPERATION / UNIT NO.	RECURRING DIRECT LABOR (MAN-HOURS)											
	1	2	3	4	5	6	7	8	9	10	10R	TOTAL
RIB PREFORMS												
1. LAYUP AND TRIM	86	117	114	76	68	79	59	51	48	75	48	
2. VACUUM BAG AND DENSIFY	14	20	19	12	11	13	10	8	8	12	8	
3. FORM FLANGES, IDENTIFY AND STORE	54	75	72	48	43	51	37	32	30	48	31	
SUBTOTAL	154	212*	205*	136	122	143	106	91	86	135	87	1,477
SPAR PREFORMS												
1. LAYUP AND TRIM	69	47	57	65	34	54	68	43	78	45	41	
2. FORM FLANGES	22	16	19	22	11	18	22	14	26	15	14	
3. VACUUM BAG AND DENSIFY	10	8	9	10	6	9	11	7	13	7	7	
4. PUNCH ACCESS HOLES	6	4	5	5	3	5	6	4	6	4	3	
5. IDENTIFY AND STORE	5	3	5	5	2	4	5	3	6	4	3	
SUBTOTAL	112	78	95	107	56	90	112	71	129*	75	68	993
SKIN PANELS												
1. LAYUP AND TRIM	150	145	128	119	115	116	129	107	92	87	66	
2. VACUUM BAG AND DENSIFY	21	20	19	17	16	17	17	15	13	12	10	
3. IDENTIFY AND STORE	4	4	4	3	3	3	4	3	3	3	2	
SUBTOTAL	175	169	151	139	134	136	150	125	108	102	78	1,467
TOTAL	441	459	451	382	312	369	368	287	323	312	233	3,937

*INDICATES PARTIAL OR TOTAL REMAKE REQUIRED

TABLE 20
DIRECT LABOR RECURRING MAN-HOURS FOR CURING, TRIMMING, AND PILOT-DRILLING THE GRAPHITE-EPOXY MOLD ASSEMBLY

OPERATION / UNIT NO.	RECURRING DIRECT LABOR (MAN-HOURS)											
	1	2	3	4	5	6	7	8	9	10	10R	TOTAL
1. LOAD INTO TOOL	58	38	19	43	38	37	41	37	32	36	32	
2. UNLOAD	34	23	11	26	23	22	24	22	20	20	20	
3. REMOVE MANDRELS	16	10	4	11	10	10	10	10	9	11	9	
4. DRILL FOR TRIM OPERATION	7	5	3	5	4	5	5	4	4	0	4	
5. TRIM	15	9	4	10	9	8	9	9	7	0	,	
6. PREPARE TAG-END SPECIMEN	14	9	4	10	9	8	9	9	7	0	7	
7. DRILL PILOT HOLES	7	5	3	6	4	4	5	4	4	0	4	
8. INSTALL SALVAGE AND REPAIR	183	0	0	51	0	8	21	81	0	0	0	
9. TOOL CLEANUP	166	108	54	123	107	101	113	105	89	85	89	
TOTAL	500	207	102	285	204	202	236	282	172	152*	172	2,514

*NO TRIM OR DRILL OPERATIONS ACCOMPLISHED

TABLE 21
DIRECT LABOR RECURRING MAN-HOURS FOR FIBERGLASS-EPOXY LEADING EDGE FABRICATION

OPERATION / UNIT NO.	RECURRING DIRECT LABOR (MAN-HOURS)										
	1	2	3	4	5	6	7	8	9	10	TOTAL
1. LAYUP	115	92	85	81	78	75	74	72	69	68	
2. CURE – BAG AND WRAP	14	12	11	10	10	10	9	9	9	8	
3. REMOVE FROM TOOL	11	9	8	8	7	7	7	7	7	6	
4. ROUT AND NET TRIM	22	17	16	15	14	14	14	13	13	13	
5. SUBMIT FOR INSPECTION	1	1	1	1	1	1	1	1	1	1	
TOTAL	163	131	121	115	110	107	105	102	99	96	1,149

TABLE 22
DIRECT LABOR RECURRING MAN-HOURS FOR FIBERGLASS-EPOXY TRAILING EDGE FABRICATION

OPERATION / UNIT NO.	RECURRING DIRECT LABOR (MAN-HOURS)										
	1	2	3	4	5	6	7	8	9	10	TOTAL
1. LAYUP AND CURE	26	14	10	16	16	21	10	17	12	23*	
2. TRIM	18	9	7	11	11	14	7	11	8	15	
3. INSTALL FILLER, PLUGS AND SPLICE	24	13	9	15	15	19	9	15	12	21	
4. BOND CONDUCTOR	9	5	4	5	6	7	3	6	4	8	
5. INSTALL RETAINER	35	19	13	21	22	28	13	22	17	30	
6. SUBMIT FOR INSPECTION	2	1	1	1	1	1	1	1	1	1	
TOTAL	114	61	44	69	71	90	43	72	54	98	716

*PARTIAL OR TOTAL REMAKE REQUIRED

TABLE 23
DIRECT LABOR RECURRING MAN-HOURS FOR FIBERGLASS-EPOXY TIP FABRICATION

OPERATION / UNIT NO.	RECURRING DIRECT LABOR (MAN-HOURS)										
	1	2	3	4	5	6	7	8	9	10	TOTAL
1. LAYUP AND CURE	4	3	2	5	3	2	2	2	2	3	
2. TRIM AND DRILL HOLES	3	1	1	3	2	2	2	1	2	2	
3. BOND FILLER	1	1	1	2	1	1	1	1	1	1	
4. BOND CONDUCTOR	64	34	28	76	39	36	35	32	39	40	
5. INSTALL RETAINER	4	2	2	5	3	2	2	2	3	3	
6. INSTALL CLIP AND BUSHINGS	3	2	1	3	2	1	1	2	1	1	
TOTAL	79	43	35	94	50	44	43	40	48	50	526

TABLE 24
DIRECT LABOR RECURRING MAN-HOURS
FOR FINAL ASSEMBLY OF COMPOSITE RUDDERS

OPERATION	UNIT NO.	RECURRING DIRECT LABOR (MAN-HOURS)										
		1	2	3	4	5	6	7	8	9	10	TOTAL
WMC 7012-4901 SUBASSEMBLY												
1. LOCATE HINGE AND CRANK ASSY (5 PLACES) AND DEVELOP SHIMS AS REQUIRED		119	126	105	137	101	78	65	88	76	76	
2. BOND ON SHIMS		3	2	3	4	3	3	1	3	2	2	
3. DRILL 1/4-IN. HOLES FOR SPAR PLANE BOLTS		36	37	31	41	30	24	20	27	23	23	
4. INSTALL BOLTS (HINGE AND CRANK ASSEMBLIES)		13	13	12	14	10	8	7	9	8	8	
5. APPLY DJ AND DRILL 5/16-IN. HOLES FOR SLIDES OF HINGE AND CRANK ASSEMBLY – REQUEST INSPECTION		13	13	10	14	10	8	7	8	7	7	
6. INSTALL 5/16-IN. HI-LOK BOLTS		6	6	5	7	5	4	3	5	4	4	
7. INSTALL LEADING AND TRAILING EDGE TO BACK DRILL PILOT HOLES FOR ATTACHMENTS		36	37	31	41	30	24	20	27	23	23	
8. BOND WMC 7015-15 RIB, -17 RIB AND -21 CLIP TO WMC 7012-3 BOX ASSEMBLY		8	10	8	10	7	6	5	6	6	6	
9. INSTALL TIP ASSEMBLY – BACK DRILL FOR PILOT HOLES		6	6	5	7	5	3	3	5	4	4	
10. REMOVE LEADING EDGE, TRAILING EDGE AND TIP ASSY		2	2	3	3	3	3	1	2	1	1	
11. CLEAN UP ASSEMBLY		2	2	3	3	2	2	1	2	1	1	
12. COUNTERSINK ALL ATTACHMENT HOLES FOR LEADING EDGE AND TRAILING EDGE		8	10	8	10	7	6	5	6	6	6	
13. CLEAN UP ASSEMBLY		2	2	2	3	2	2	1	2	1	1	
14. CUT LEADING EDGE INTO SEGMENTS		2	2	2	3	2	2	1	2	1	1	
15. LOCATE, BOND AND RIVET SPLICE – JOINTS ON LEADING EDGE – INSTALL NUT PLATES		59	63	53	68	50	40	31	43	38	38	
16. INSTALL GANG CHANNELS ON LEADING EDGE – SEGMENTS		24	26	21	28	20	16	13	17	15	15	
17. COUNTERSINK ATTACHMENT HOLES AND INSTALL TIP ASSY		13	13	10	13	9	8	6	8	7	7	
WMC 7012-1 FINAL ASSEMBLY												
18. FINAL INSTALLATION OF TRAILING EDGE (INSPECTION REQUIRED)		24	26	21	28	20	15	13	17	15	15	
19. FINAL INSTALLATION OF LEADING EDGE		19	20	16	21	15	12	9	14	12	12	
20. INSTALL WMC 7025-1 DOOR ASSEMBLIES AND SUBMIT FOR FINAL INSPECTION		13	13	10	13	10	8	6	8	7	7	
TOTAL		408	429	359	468	341	272	218	299	257	257	3,308

There were significant variations in recurring man-hours from rudder to rudder which would not be expected from normal learning curve trends because the rudders were manufactured in an advanced development department rather than in a true production mode. Because of the relatively few rudders involved, repetitive operations could not be fully exploited. The learning curve trends were also influenced by the manufacturing labor involved in hand-fitting (shimming) of hinges brackets and reworking of "oilcanned" regions on an individual rudder basis.

The cumulative average man-hours per rudder as a function of the number produced is shown in Figure 58. The learning curve slopes at the conclusion of the ten rudder program were 89.4, 87.4, and 93.8 percent, respectively, for composite rudder assemblies complete, graphite composite box fabrication, and fiberglass component fabrication (i.e., leading and trailing edges, and tip assemblies).

The operations requiring relatively high recurring labor costs were machined part fabrication, graphite composite "B" stage layup, and rudder final assembly. These costs could be reduced significantly in production through the use of precision forgings for hinge brackets, the use of woven and broadgoods forms of graphite prepreg layup, and tool and process improvements to reduce the hand-work involved in shim installations and localized "oilcan" region repairs.

Total manufacturing costs of the composite rudder consisted of fabrication - 82 percent, inspection - 10 percent, sustaining tooling - 5 percent, planning - 2 percent, and NDI - 1 percent. Fabrication costs consisted of graphite-epoxy parts - 36 percent, machined parts - 25 percent, final assembly - 20 percent, fiberglass parts - 14 percent, and miscellaneous fabrication - 5 percent.

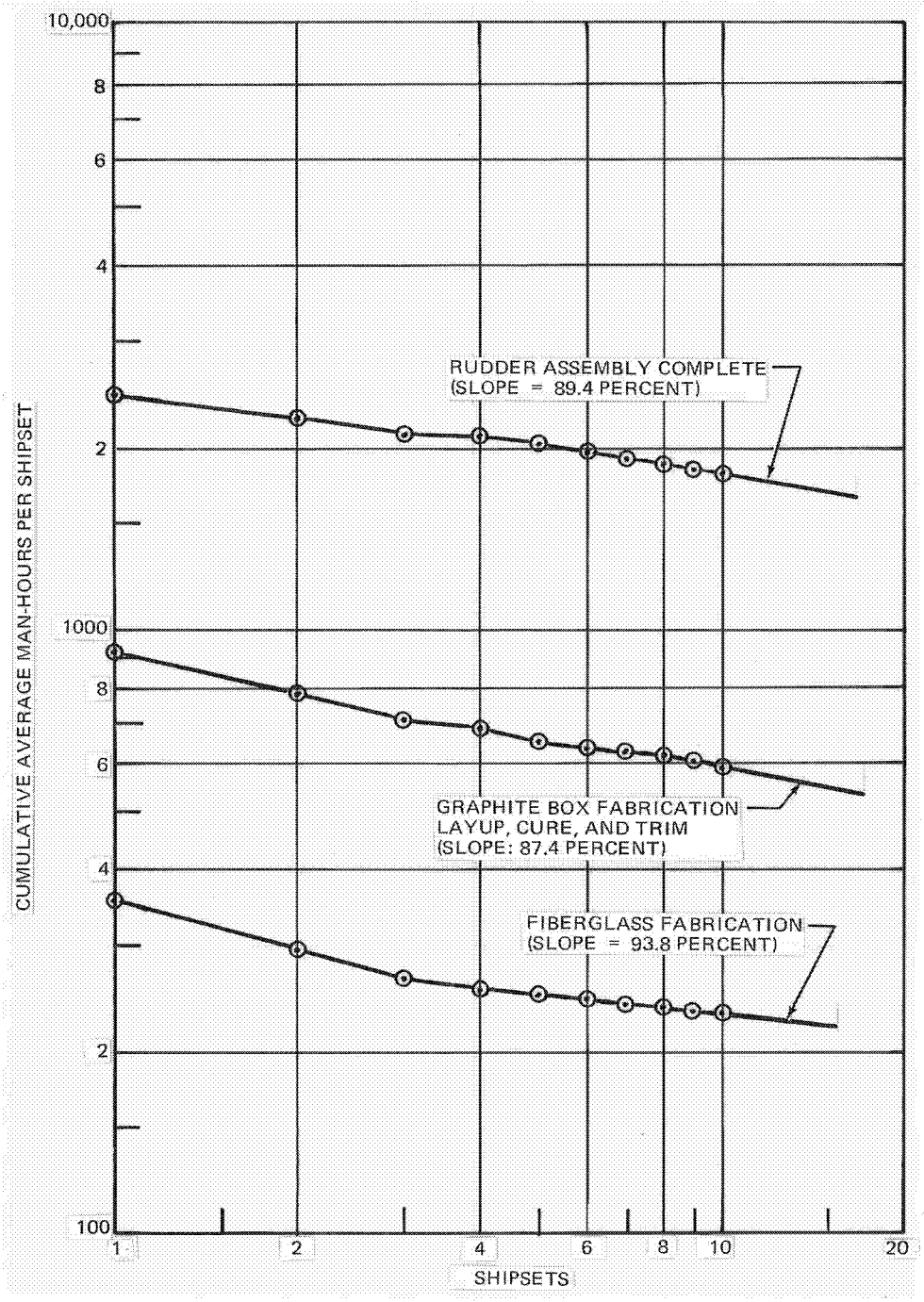

FIGURE 58. COMPOSITE RUDDER CUMULATIVE AVERAGE RECURRING MANUFACTURING MAN-HOURS PER SHIPSET

RUDDER GROUND TESTS

The graphite composite rudder was thoroughly ground tested to verify the structural integrity under critical static and dynamic design load conditions. Thermal expansion characteristics were determined experimentally and all critical static load conditions and failsafe variations were successfully sustained in ground tests. Natural vibration mode shapes and frequencies of the forward and aft rudder assembly were determined experimentally and compared with metal rudder data to verify flutter integrity of the rudder installation. Analysis indicated that flutter speeds with the graphite rudder were equal to or greater than those with the metal rudder. The ground test setups, methods, and results are described in this section.

Thermal Expansion Test

The thermal expansion characteristics of the graphite rudder molding assembly and an equivalent length aluminum alloy bar were determined experimentally at 225°K and 344°K to verify the data used in the stress analysis of the forward rudder "A" frame hinge brackets. Flexible hinge brackets were designed to accommodate the differential thermal expansions between the graphite aft rudder and the aluminum alloy forward rudder. The measured coefficients of thermal expansion, summarized in Table 25, were in agreement with the data used in analysis. On conclusion of testing, the graphite molding assembly returned to its original length. The latter fact was verified by checking overall dimensions against the fabrication tooling.

Static Tests

The static test program on the graphite composite rudder was successfully completed without a structural failure of any kind. The critical flight loads were simulated including loads induced from forward rudder bending and applied airloads but neglecting the minor effects of thermal stresses. The rudder structure was substantiated under critical ultimate stress conditions and failsafe variations through a series of nine test sequences (see Table 26).

TABLE 25

COEFFICIENTS OF THERMAL EXPANSION FOR GRAPHITE RUDDER AND ALUMINUM ALLOY BAR

ITEM	REFERENCE LENGTH		ORIGINAL TEMPERATURE		FINAL TEMPERATURE		TEMPERATURE DIFFERENTIAL		LENGTH DIFFERENTIAL		COEFFICIENT OF THERMAL EXPANSION	
	cm	IN.	^{o}K	^{o}F	^{o}K	^{o}F	^{o}K	^{o}F	cm	IN.	mm/mm/^{o}K	IN./IN./^{o}F
GRAPHITE EPOXY RUDDER	349.57	137.63	295 294	71 70	230 345	−55 162	325 313	126 92	0.073 0.042	0.0288 0.0166	2.99×10^{-6} 2.36×10^{-6}	1.66×10^{-6} 1.32×10^{-6}
ALUMINUM ALLOY BAR 7075-T651	348.93	137.38	295	71	230	−55	325	126	0.555	0.2185	22.72×10^{-6}	12.62×10^{-6}

TABLE 26

SUMMARY OF ADVANCED COMPOSITE RUDDER STATIC TESTS

CRITICAL CONDITION	TEST SEQUENCE	RUDDER CONFIGURATION				LOAD LEVEL (% DLL)	REMARKS
		ALL WELL	DRIVE ROD OUT	FITTING ATTACH BOLT OUT	RUDDER HINGE BOLT OUT		
RUDDER KICK	1	X				150	NO FAILURE.
	2				X	100	LOWER DRIVE HINGE OUT. NO FAILURE.
	3	X				100	LOWER DRIVE HINGE ROD OUT. NO FAILURE.
	4			X		100	LOWER DRIVE FITTING ATTACHMENT OUT. NO FAILURE.
ONE ENGINE OUT	5	X				150	NO FAILURE.
	6			X		100	UPPER DRIVE FITTING ATTACHMENT OUT. NO FAILURE.
	7				X	100	CENTER HINGE OUT. NO FAILURE.
CRITICAL REAR-SPAR STRESS	8					100	LOCAL CONDITION ON REAR-SPAR. NO FAILURE.
ONE ENGINE OUT. UPPER DRIVE HINGE STRESS	9			X		100	UPPER DRIVE FITTING ATTACHMENT OUT. NO FAILURE.
RUDDER KICK	10	X				415	ATTEMPTED FAILURE TEST. TEST SUSPENDED BECAUSE OF IMPENDING WHIFFLING INSTABILITY.

Two critical static load conditions were tested using the test setup shown in Figure 59. The test rudder was supported in a horizontal plane by a set of five forward rudder hinge brackets and four dummy control rods. A structural steel test jig duplicated the upper forward rudder interfaces for the hinge brackets and control rods. Deflection of the aft rudder hinge line was achieved using fixed mounts for the lower and upper hinge brackets and movable mounts for the three intermediate brackets. Simulated airloads were generated by a 32.26 square centimeter (five square inch) hydraulic actuator acting through compression whiffling to 71 load points on the surface of the graphite rudder.

Details of the interface between the whiffling and the graphite rudder are shown in Figure 60. Point-loads were applied on alternate ribs of the rudder at mid-rib and at the rib intersections with the front and rear spars. The relatively small size of the aluminum alloy bearing blocks at the graphite surface afforded excellent visibility of the rudder surface during the tests.

The structural tests were conducted either in an all-well configuration or in a failed configuration in which a single structural element (i.e., a drive rod or attach bolt) was intentionally omitted from the structure. In the all-well configurations, design ultimate loads (150 percent design limit loads) were applied. In the failed configurations, design limit loads were applied in accordance with design criteria requirements. Either limit or ultimate hinge line deflections were pre-set at the aft rudder hinge line depending on the appropriate load level for the test sequence. Governing airloads were applied in increments and strain and deflection data were recorded after each load application. No structural failures were experienced through the nine test sequences.

The tenth test sequence duplicated one of the ultimate stress conditions, but the applied loads were increased above ultimate in an attempt to determine the failure load and mode for the rudder. The load was increased to 415 percent design limit load without failure. At this point the test was suspended because the compression whiffletree system was near critical load conditions. Load-deflection characteristics of the rudder were determined as a comparison basis for future tests on rudders retrieved from flight-service.

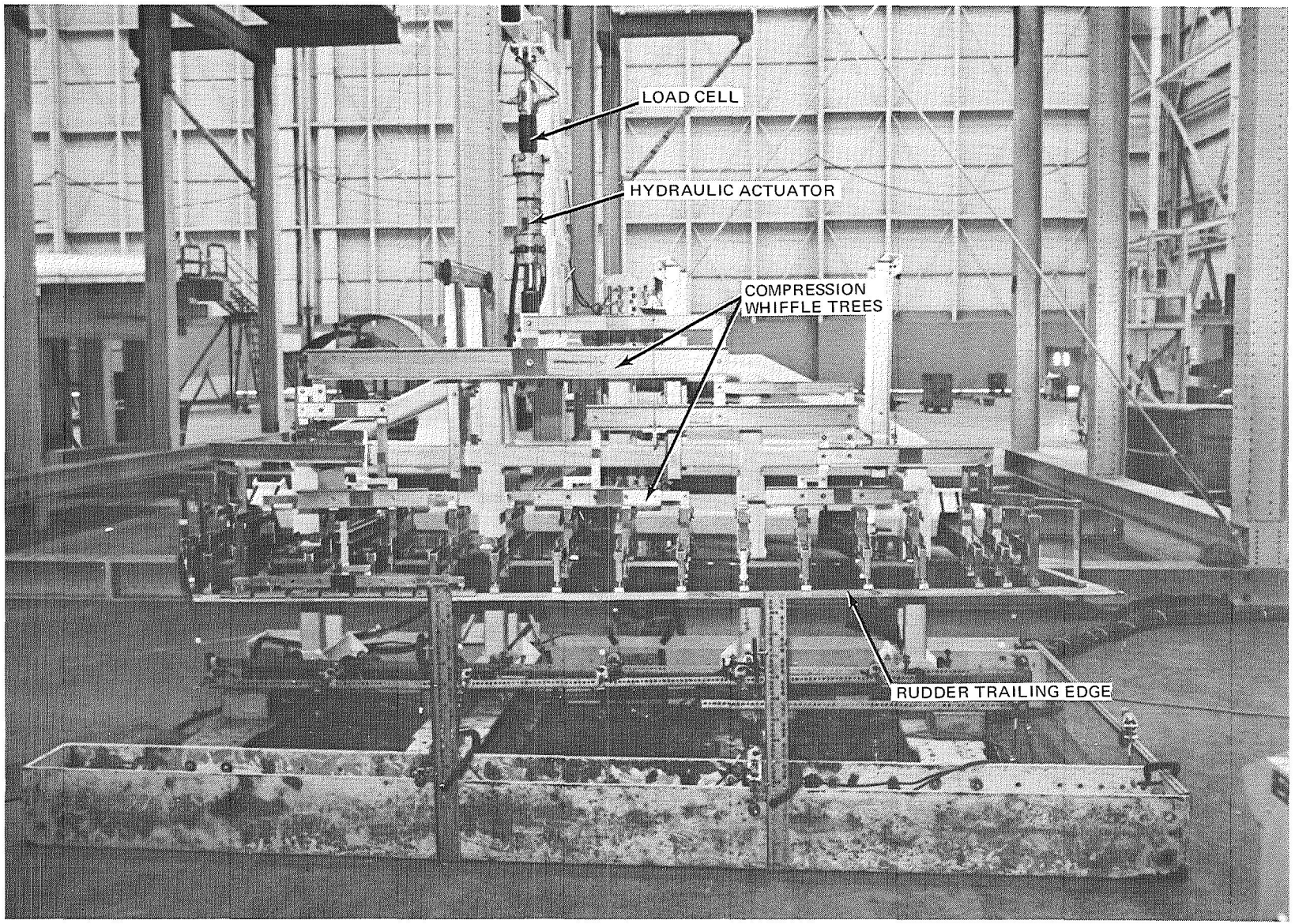

FIGURE 59. RUDDER STATIC TEST SETUP

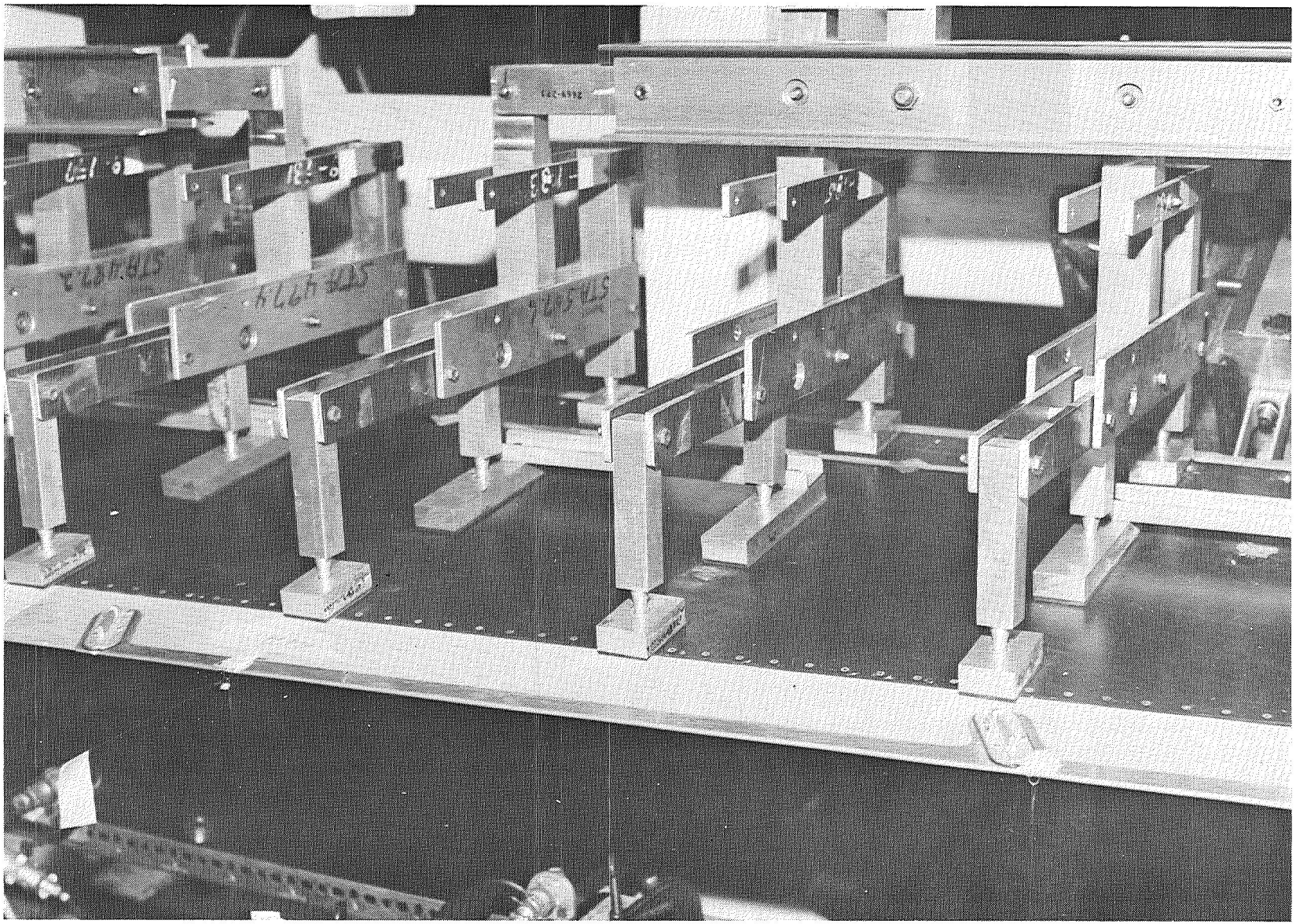

FIGURE 60. DETAILS OF COMPRESSION WHIFFLING AND BEARING BLOCKS

Modal Vibration Tests and Flutter Analysis

Laboratory modal vibration survey tests were conducted on the first flight-service composite rudder and a metal forward rudder modified to accommodate the differential thermal expansions between the two rudders. The rudders were assembled and the test installation was completed with production push-rods, hinges, brackets, and attaching hardware. The forward rudder was mounted to a rigid support fixture, Figure 61, similar to a previous test conducted with the all-metal assembly. Vibration modes were excited with a shaker system as shown in Figure 62. Resonant frequencies and mode shapes were determined for the basic design and six fail-safe variations involving hinge bolts or pushrod failures. The resonant frequency results are shown in Table 27 and are compared with previously obtained results for the production all metal assembly.

A flutter evaluation was performed in accordance with FAA regulations to determine the effect of the composite rudder installation on the flutter characteristics. The criteria for flutter safety on the DC-10 is FAR 25, Section 25.629 which requires a minimum design flutter speed of 1.2 times the design dive speed (V_D) for the all-well rudder configuration and V_D for any probable single failure.

Relevant flutter mechanisms for the composite rudder installation are the following:

- Fin bending - rudder rotation coupled flutter. This mode is prevented by sufficient actuator rigidity or, in the event of actuator failure, by forward rudder mass balance.

- Flutter involving rotation of the unbalanced aft rudder coupling with the rotation of the forward rudder. This mode is prevented by maintaining an adequately high aft rudder rotation frequency.

The fin bending rudder rotation mode was avoided by retaining the basic mass balance design which resulted in a favorable increase in overbalance for the composite aft rudder compared to the heavier metal aft rudder.

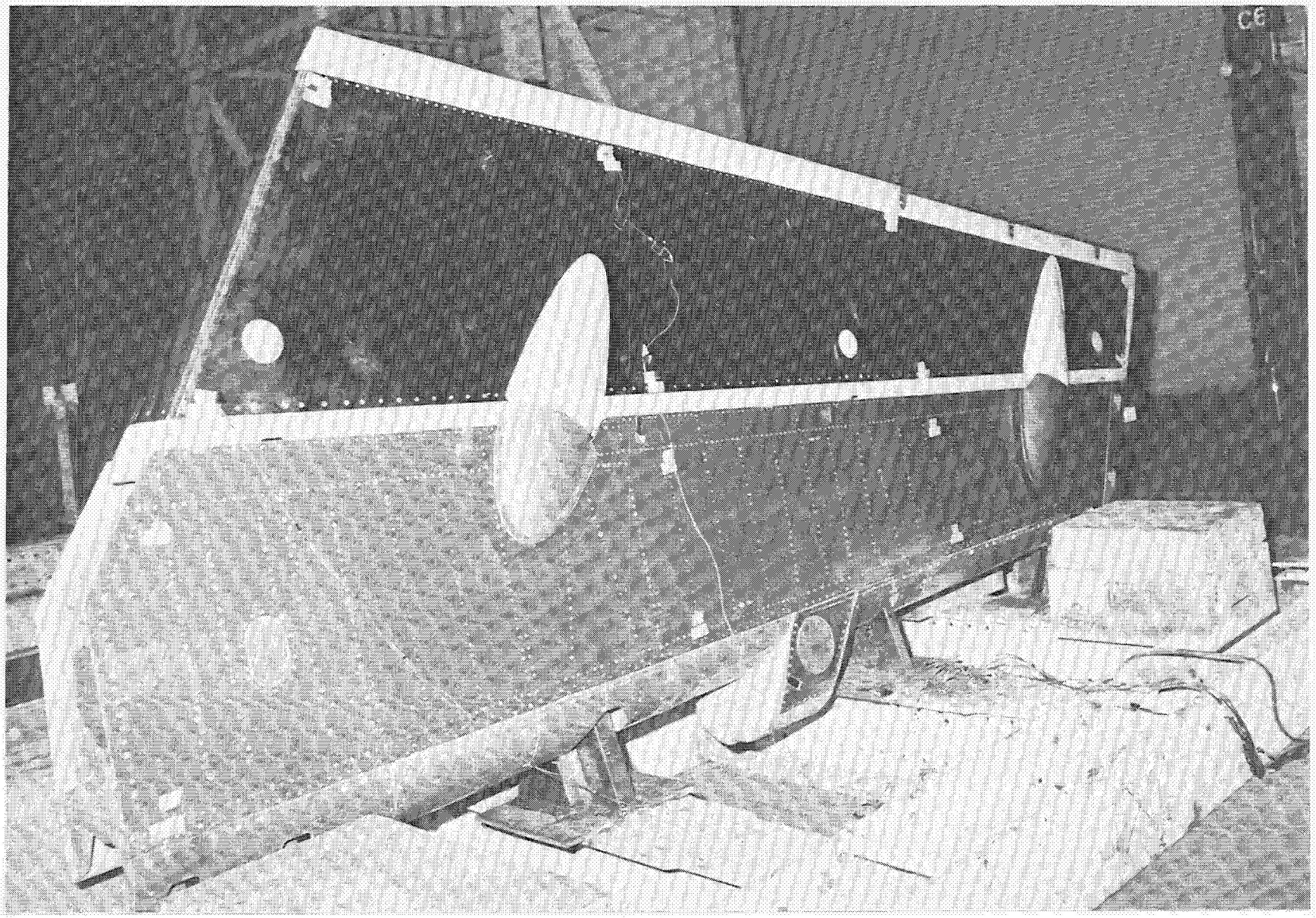

FIGURE 61. RUDDER MODAL VIBRATION TEST SETUP

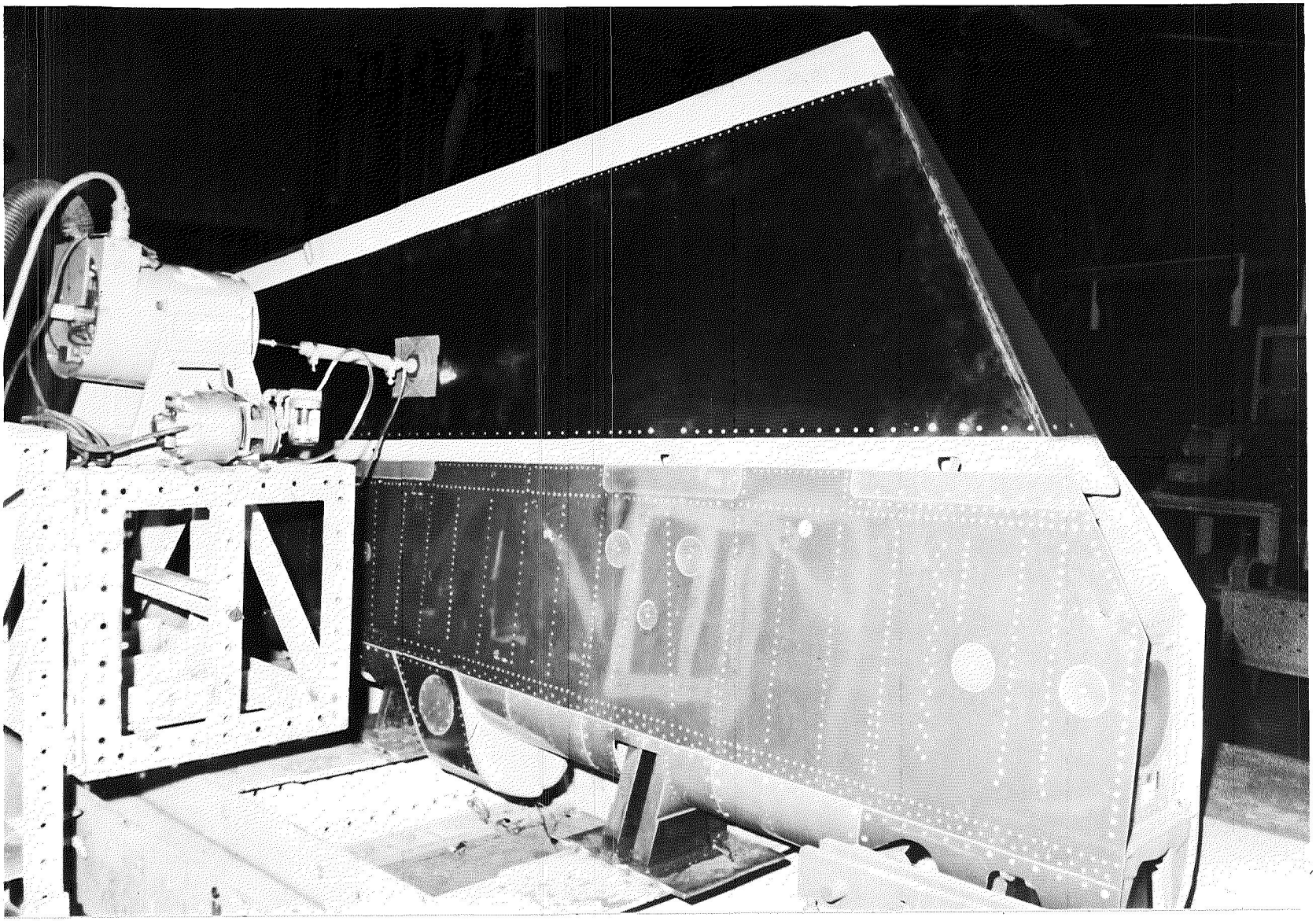

FIGURE 62. VIBRATION TEST SHAKER INSTALLATION

TABLE 27

DC-10 UPPER RUDDER MODAL FREQUENCY SUMMARY

PRODUCTION ALUMINUM UPPER AFT RUDDER VERSUS COMPOSITE MATERIAL UPPER AFT RUDDER

CONFIGURATION	FIRST MODE f (Hz)		SECOND MODE f (Hz)		THIRD MODE f (Hz)	
	AL	COMP	AL	COMP	AL	COMP
BASIC	30.1	33.2	48.8	47.3	68.6	58.3
ONE LOWER DRIVE ROD OFF	30.2	31.6	43.2	45.0	65.1	56.0
ONE UPPER DRIVE ROD OFF	29.6	30.8	45.6	45.3	68.0	57.0
UPPER HINGE BOLT OUT	29.7	31.2	43.7	46.8	68.6	
ONE LOWER AND ONE UPPER DRIVE RODS OUT	29.3	31.3	40.4	44.8	63.4	55.5
BOTH UPPER DRIVE RODS OUT	26.5	26.6	39.8	39.0	64.5	
BOTH LOWER DRIVE RODS OUT	25.3	27.9	32.0	33.8	62.1	

The primary flutter investigation was directed toward insuring that the aft rudder rotational frequency, controlled by pushrod backup structural rigidity, was sufficiently large for the composite structure. An accurate evaluation of the aft rudder rotation frequency was obtained from the modal vibration test.

Analysis of the test data showed the composite graphite design to have modal characteristics similar to those of the metal design but with differences in pushrod backup rigidity. Test results indicated a 28 percent and 18 percent reduction in the pushrod backup rigidity of the lower and upper pushrods, respectively, compared to the metal backup structure. However, the composite rudder reduced weight and inertia more than compensated for this loss in backup rigidity and resulted in higher rotational frequencies. The minimum frequency of 26.6 Hz exceeded the level required for flutter safety.

Based on analysis and supporting tests, it was concluded that the flutter speeds of the DC-10 with the composite graphite aft upper rudder are equal or greater than those with the metal aft rudder for both design and failure cases. By similarity to the previous tests of the production rudder, this conclusion is applicable for certifying DC-10 series airplanes fitted with the upper aft composite rudder under Federal Aviation Regulations, Part 25, Seciton 25.629.

CONCLUDING REMARKS

An advanced composite rudder for the DC-10 was designed and developed using a unique manufacturing approach. The rudder was extensively ground tested to demonstrate the structural integrity of all critical details of the design concept. A 33 percent weight reduction of 13.58 kg (30 pounds) was attained in the composite rudder.

The manufacturing approach utilized the thermal expansion characteristics of trapped rubber mandrels to generate curing pressures, thereby eliminating the need for autoclave curing and secondary bonding during consolidation of the structural box. Rubber mandrel development problems were solved by adjustments to the rubber formulation for control of curing pressures, metal screening inclusions to prevent shrinkage, and Teflon coatings to prevent sticking. Process development required the incorporation of internal heaters to expand the rubber mandrels early in the cure cycle. Adjustments to the densification cycle of "B" state laminates were required to control resin flow and gelation during the cure cycle. Thermal stress cracks in the cured laminates were eliminated through care in preforming the "B" stage laminate details and through local reinforcement of critical sections.

Actual production progress (learning) curve slopes for metal rudders typically range from 75 to 82 percent depending on the number of units produced. During manufacuturing of the 10 flight-service composite rudders, production progress curve slopes of 87.4 and 89.4 percent, respectively, were attained for fabrication of the graphite-epoxy molding assemblies and the composite rudder assemblies complete. There were significant variations in recurring labor man-hours from rudder to rudder which would not be expected from normal learning curve trends because the rudders were manufactured in an advanced development mode rather than a true production mode. If repetitive manufacturing operations were fully exploited, it is anticipated that competitive learning curve slopes and manufacturing costs would result.

The composite rudder successfully sustained all critical ground-test requirements. Documentation showing compliance with all Federal Aviation Requirements

was submitted to the Federal Aviation Agency (FAA) and certification was received. The first composite rudder was flight tested at the Douglas Aircraft Company on an experimentally certified aircraft. A five-year flight-service period on commercial aircraft was begun in June 1976. Flight-service experience will be reported at annual intervals during the flight-service period.

APPENDIX A

INCOMING MATERIAL QUALITY CONTROL TEST DATA

The graphite-epoxy prepreg material was purchased to the requirements of Douglas Material Specification (DMS) 1936. A total of 384.3 kilograms (846.6 pounds) or graphite-epoxy prepreg was purchased for the program in the form of 7.62 centimeter (3-inch) wide unidirectional tape on paper backing. Prepreg and laminate properties routinely determined during incoming quality control checks were prepreg resin and volatile content; cured laminate flexural strength, modulus, and interlaminar shear strength; and cured laminate ply thickness. The test data determined during these checks are tabulated in this appendix.

TABLE A1

INCOMING MATERIAL QUALITY CONTROL TEST RESULTS FOR THORNEL 300/5208 MATERIAL

BATCH NO.	QUANTITY RECEIVED (kg)	QUANTITY RECEIVED (LB)	UNIT IDENTITY	PREPREG PROPERTIES: RESIN CONTENT WEIGHT %	PREPREG PROPERTIES: VOLATILE CONTENT WEIGHT %	LAMINATE PROPERTIES: FLEXURAL STRENGTH (MPa)	FLEXURAL STRENGTH (KSI)	FLEXURAL MODULUS (GPa)	FLEXURAL MODULUS (MSI)	INTERLAMINAR SHEAR STRENGTH (MPa)	INTERLAMINAR SHEAR STRENGTH (KSI)	THICKNESS PER PLY (mm)	THICKNESS PER PLY (MILS)
–	–	–	DMS REQ'T	39 TO 45	3.0 MAX	1345 MIN	195 MIN	120.6 MIN	17.5 MIN	96.5 MIN	14 MIN	–	–
179	14.6	32.2	ROLL 1C	40.46	0.70	2125 2164 2104 2136	308.2 313.8 305.1 309.8	155.1 152.1 148.0 152.7	22.50 22.06 21.47 22.15	137.2 134.0 141.1 132.1	19.90 19.44 20.47 19.16	0.122 0.129 0.131 0.128	4.84 5.08 5.16 5.03
			ROLL 2D	39.61	0.70	2252 2184 2224 2090	326.6 316.8 322.6 303.2	163.4 163.6 159.8 155.0	23.70 23.73 23.18 22.48	121.3 147.8 145.8 136.5	17.60 21.43 21.14 19.80	0.119 0.122 0.123 0.121	4.69 4.81 4.84 4.78
			ROLL 4D	40.55	0.55	2201 2232 2035 2157	319.2 323.7 295.2 312.8	167.7 160.0 149.9 157.5	24.32 23.20 21.74 22.85	132.5 139.3 138.9 133.4	19.22 20.21 20.14 19.35	0.122 0.123 0.130 0.129	4.79 4.83 5.12 5.08
180	10.3	22.8	ROLL 1A	41.92	0.70	2129 2031 2025 2040	308.8 294.5 293.7 295.9	155.7 142.5 146.7 153.8	22.58 20.67 21.28 22.31	139.8 152.7 138.8 149.5	20.28 22.15 20.13 21.68	0.126 0.127 0.126 0.124	4.95 5.00 4.97 4.89
186	3.8	8.4	ROLL 3	43.6	–	2023 2230 2159 1966	293.4 323.5 313.2 285.1	159.3 160.6 157.2 151.7	23.1 23.3 22.8 22.0	128.9 142.7 135.1 137.2	18.7 20.7 19.6 19.9	0.116 0.121 0.123 0.123	4.58 4.75 4.84 4.85
202	9.1	20.0	ROLL 12	42.2	0.7	2208 2212 2122	320.3 320.8 307.7	163.4 165.5 164.1	23.7 24.0 23.8	146.9 123.4 145.5	21.3 17.9 21.1	0.128 0.128 0.120	5.02 5.05 4.71
			ROLL 13	40.0	1.9	2200 2137 2115	319.1 309.9 306.8	155.8 163.4 166.2	22.6 23.7 24.1	117.9 126.2 124.8	17.1 18.3 18.1	0.127 0.120 0.132	5.00 4.74 5.19
312	9.3	20.4	ROLL 2C1	44.5	0.3	1904 2032 2000	276.2 294.8 290.1	128.9 133.1 131.0	18.7 19.3 19.0	131.7 134.4 137.9	19.1 19.5 20.0	0.127 0.131 0.131	5.01 5.14 5.16
			ROLL 2D2	43.6	0.4	1860 1972 2035	269.8 286.0 295.1	133.8 135.8 135.1	19.4 19.7 19.6	129.6 135.1 133.8	18.8 19.6 19.4	0.132 0.132 0.138	5.18 5.19 5.43
324	28.6	62.9	ROLL 1B	40.45		2337 2304 2292	338.9 334.1 332.4	173.0 182.0 182.7	25.1 26.4 26.5	140.0 140.6 103.4	20.3 20.4 15.0	0.131 0.137 0.124	5.14 5.38 4.88
			ROLL 4C	43.07 43.02		2390 2460 2356	346.7 356.8 341.7	161.3 186.8 167.5	23.4 27.1 24.3	130.3 124.8 134.4	18.9 18.1 19.5	0.129 0.119 0.131	5.08 4.70 5.17
			ROLL 5C	41.64 43.29		2387 2401 2378	346.2 348.2 344.9	182.0 173.0 175.8	26.4 25.1 25.5	136.5 133.1 125.5	19.8 19.3 18.2	0.121 0.126 0.128	4.75 4.95 5.05
352	28.0	61.7	ROLL 1D	44.33 44.14		2228 2281 2375	323.2 330.9 344.4	176.5 178.6 173.7	25.6 25.9 25.2	104.8 134.4 122.0	15.2 19.5 17.7	0.126 0.118 0.116	4.95 4.64 4.55
			ROLL 3B	45.59 44.27		2304 2337 –	334.2 339.0 –	173.1 177.2 –	25.1 25.7 –	133.1 131.7 129.6	19.3 19.1 18.8	0.123 0.125 0.126	4.86 4.93 4.96
			ROLL 4C	43.69 43.56		2199 2290 2221	318.9 332.2 322.2	171.7 163.4 167.5	24.9 23.7 24.3	120.0 122.0 107.6	17.4 17.7 15.6	0.124 0.127 0.127	4.89 4.99 5.01
359	14.4	31.8	ROLL 1D	44.1 45.9		2210 2184 1962	320.5 316.8 284.5	175.8 173.7 153.8	25.5 25.2 22.3	114.4 104.8 121.3	16.6 15.2 17.6	0.127 0.118 0.113	5.01 4.63 4.43
			ROLL 2C	46.2 46.9		2257 2279 2175	327.4 330.5 315.5	182.7 171.7 173.1	26.5 24.9 25.1	126.9 142.0 129.6	18.4 20.6 18.8	0.109 0.114 0.119	4.30 4.47 4.67
			ROLL 3B	40.2 40.3		2283 2326 2307	331.1 337.4 334.6	171.0 168.2 168.2	24.8 24.4 24.4	130.3 122.0 124.1	18.9 17.7 18.0	0.131 0.128 0.128	5.14 5.04 5.04
			ROLL 4D	42.0 42.0		2110 2241 2179	306.0 325.0 316.0	164.8 177.2 175.1	23.9 25.7 25.4	120.0 125.5 127.6	17.4 18.2 18.5	0.115 0.114 0.114	4.53 4.49 4.48

TABLE A1

INCOMING MATERIAL QUALITY CONTROL TEST RESULTS FOR THORNEL 300/5208 MATERIAL (CONTINUED)

BATCH NO.	QUANTITY RECEIVED (kg)	QUANTITY RECEIVED (LB)	UNIT IDENTITY	PREPREG PROPERTIES: RESIN CONTENT WEIGHT %	PREPREG PROPERTIES: VOLATILE CONTENT WEIGHT %	LAMINATE PROPERTIES: FLEXURAL STRENGTH (MPa)	FLEXURAL STRENGTH (KSI)	FLEXURAL MODULUS (GPa)	FLEXURAL MODULUS (MSI)	INTERLAMINAR SHEAR STRENGTH (MPa)	INTERLAMINAR SHEAR STRENGTH (KSI)	THICKNESS PER PLY (mm)	THICKNESS PER PLY (MILS)
379	53.7	118.3	ROLL 2A	41.4 42.3	0.6	2250 2266 2176	326.4 328.3 315.6	175.8 180.6 171.7	25.5 26.2 24.9	148.9 130.3 157.2	21.6 18.9 22.8	0.131 0.131 0.133	5.17 5.14 5.25
			ROLL 3B	41.3 41.4	0.4	2330 2295 2752	337.9 332.8 399.1	177.9 175.1 184.1	25.8 25.4 26.7	138.6 133.8 134.4	20.1 19.4 19.5	0.125 0.126 0.124	4.94 4.96 4.88
			ROLL 5C	43.3 44.3	1.0	2258 2374 2195	327.5 344.3 318.4	177.2 184.1 180.0	25.7 26.7 26.1	140.7 146.9 124.8	20.4 21.3 18.1	0.123 0.123 0.124	4.83 4.85 4.88
			ROLL 6A	42.7 42.8	1.2	2282 2237 2382	331.0 324.4 345.5	177.2 174.4 185.5	25.7 25.3 26.9	144.1 122.0 137.9	20.9 17.7 20.0	0.129 0.126 0.121	5.06 4.97 4.75
			ROLL 6D	43.8 43.5	0.5	2419 2371 2293	350.8 343.9 332.5	187.5 173.7 181.3	27.2 25.2 26.3	146.9 148.9 130.3	21.3 21.6 18.9	0.121 0.125 0.123	4.78 4.93 4.83
			ROLL 7C	43.8 43.7	0.6	2312 2427 2292	335.3 352.0 332.4	180.6 182.7 176.5	26.2 26.5 25.6	135.8 128.2 144.8	19.7 18.6 21.0	0.123 0.127 0.129	4.86 5.00 5.06
			ROLL 8C	42.4 42.3	0.4	2290 2367 2197	332.2 324.4 318.7	165.5 168.9 162.7	24.0 24.5 23.6	126.9 142.0 142.0	18.4 20.6 20.6	0.127 0.128 0.128	5.00 5.05 5.06
			ROLL 9B	40.5 40.7	0.4	2250 2256 2236	326.4 327.2 324.3	167.5 168.2 168.9	24.3 24.4 24.5	128.9 140.0 133.1	18.7 20.3 19.3	0.123 0.123 0.120	4.83 4.83 4.73
			ROLL 10A	43.9 43.7	0.5	2121 2178 2098	307.6 315.9 304.3	168.2 168.2 161.3	24.4 24.4 23.4	140.0 143.4 137.9	20.3 20.8 20.0	0.130 0.130 0.128	5.13 5.11 5.04
385	51.7	113.9	ROLL 1C	42.02 42.52	0.6	2040 2177 2308	295.9 315.8 334.7	157.2 156.5 165.5	22.8 22.7 24.0	135.8 136.5 142.7	19.7 19.8 20.7	0.125 0.128 0.126	4.93 5.05 4.97
			ROLL 4A	43.98 43.35	0.6	2253 2208 2219	326.7 320.3 321.8	154.4 151.0 148.2	22.4 21.9 21.5	139.3 144.1 128.2	20.2 20.9 18.6	0.123 0.123 0.122	4.84 4.84 4.81
			ROLL 7B	41.56 41.62	0.8	2275 2261 2138	329.9 327.9 310.1	159.3 160.0 157.2	23.1 23.2 22.8	137.9 142.7 131.0	20.0 20.7 19.0	0.123 0.127 0.128	4.89 5.00 5.06
			ROLL 9B			2219 2188 2240	321.8 317.3 324.9	166.2 166.2 166.2	24.1 24.1 24.1	140.0 135.1 141.3	20.3 19.6 20.5	0.130 0.125 0.130	5.13 4.93 5.13
409	8.3	18.2	ROLL 1D	45.6 43.9	0.3	2079 2128 2169	301.6 308.7 314.6	150.3 149.6 157.2	21.8 21.7 22.8	132.4 142.0 131.7	19.2 20.6 19.1	0.127 0.125 0.120	5.01 4.94 4.73
			ROLL 3A	44.5 43.6	0.3	2163 2358 2246	313.7 342.0 325.7	155.8 160.0 163.4	22.6 23.2 23.7	141.3 117.2 138.6	20.5 17.0 20.1	0.118 0.116 0.122	4.63 4.58 4.81
			ROLL 6B			2091 2209 2130	303.3 320.4 308.9	157.2 151.7 155.1	22.8 22.0 22.5	140.0 133.1 140.0	20.3 19.3 20.3	0.127 0.130 0.132	4.99 5.13 5.19
			ROLL 9C	41.7 42.2	0.5	2109 2199 2275	305.9 318.9 330.0	160.6 166.2 168.2	23.3 24.1 24.4	135.1 126.9 134.4	19.6 18.4 19.5	0.132 0.128 0.125	5.19 5.05 4.93
			ROLL 12A	42.2 41.0	0.4	2103 2102 2208	305.0 304.9 320.2	160.0 165.5 161.3	23.2 24.0 23.4	146.9 131.7 131.0	21.3 19.1 19.0	0.111 0.119 0.121	4.36 4.70 4.76
440	30.0	66.2	ROLL 7A	42.8 43.0		2203 2160 2236	319.5 313.3 324.3	151.7 164.1 160.0	22.0 23.8 23.2	138.6 142.7 132.4	20.1 20.7 19.2	0.127 0.125 0.125	4.99 4.91 4.93
			ROLL 10C	42.4 43.6	0.7	2035 2221 2132	295.2 322.2 309.2	160.0 177.2 159.3	23.2 25.7 23.1	130.3 143.4 146.9	18.9 20.8 21.3	0.129 0.129 0.124	5.08 5.08 4.90
			ROLL 13A	43.3 43.1		2181 2136 2098	316.3 309.8 304.3	163.4 164.1 160.6	23.7 23.8 23.3	153.1 138.6 142.0	22.2 20.1 20.6	0.125 0.130 0.126	4.92 5.10 4.95
			ROLL 17A	44.1 43.8		2060 2193 2093	298.8 318.1 303.6	158.6 157.2 164.1	23.0 22.8 23.8	132.4 133.1 114.5	19.2 19.3 16.6	0.146 0.135 0.116	5.74 5.31 4.58

TABLE A1

INCOMING MATERIAL QUALITY CONTROL TEST RESULTS FOR THORNEL 300/5208 MATERIAL (CONTINUED)

BATCH NO.	QUANTITY RECEIVED (kg)	QUANTITY RECEIVED (LB)	UNIT IDENTITY	PREPREG PROPERTIES: RESIN CONTENT WEIGHT %	PREPREG PROPERTIES: VOLATILE CONTENT WEIGHT %	FLEXURAL STRENGTH (MPa)	FLEXURAL STRENGTH (KSI)	LAMINATE PROPERTIES: FLEXURAL MODULUS (GPa)	FLEXURAL MODULUS (MSI)	INTERLAMINAR SHEAR STRENGTH (MPa)	INTERLAMINAR SHEAR STRENGTH (KSI)	THICKNESS PER PLY (mm)	THICKNESS PER PLY (MILS)
446	32.7	72.0	ROLL 1D	48.0	0.43	2082	301.9	151.0	21.9	148.9	21.6	0.130	5.10
				44.3		2143	310.8	157.9	22.9	140.0	20.3	0.127	5.00
						2044	296.5	153.1	22.2	143.4	20.8	0.127	5.00
						2574	373.3	155.8	22.6	157.9	22.9	0.127	5.00
						2550	369.9	175.1	25.4	157.9	22.9	0.130	5.10
						2221	322.1	177.9	25.8	166.9	24.2	0.127	5.00
			ROLL 4B	45.4		2110	306.0	160.0	23.2	132.4	19.2	0.127	5.00
				42.8		2102	304.9	158.6	23.0	158.6	23.0	0.130	5.10
						2096	304.0	149.6	21.7	123.4	17.9	0.132	5.20
			ROLL 5B	43.1		2064	299.3	153.6	22.3	148.9	21.6	0.127	5.00
				43.7		2097	304.1	160.0	23.2	147.5	21.4	0.130	5.10
						2130	308.9	148.9	21.6	148.2	21.5	0.132	5.20
						2172	315.0	184.8	26.8	162.0	23.5	0.122	4.80
						2076	301.1	173.7	25.2	152.4	22.1	0.132	5.20
						2380	345.2	133.1	19.3	166.9	24.2	0.132	5.00
			ROLL 6C	40.0		2125	308.2	158.6	23.0	132.4	19.2	0.135	5.30
				41.5		2143	310.8	151.0	21.9	154.4	22.4	0.130	5.10
						2153	312.3	151.0	21.9	151.0	21.9	0.135	5.30
467	26.8	59.0	ROLL 1B	42.4	0.60	2199	318.9	165.5	24.0	135.8	19.7	0.124	4.90
				41.7		2244	325.5	160.1	23.3	138.6	20.1	0.124	4.90
						2066	299.6	186.8	27.1	140.0	20.3	0.124	4.90
						2143	310.8	164.8	23.9	140.0	20.3	0.122	4.80
						1831	265.6	188.9	27.4	138.6	20.1	0.119	4.70
						2475	359.0	191.7	27.8	142.0	20.6	0.132	5.20
			ROLL 2A	43.1		2144	310.9	160.0	23.2	142.7	20.7	0.127	5.00
				43.3		2308	334.7	165.5	24.0	129.6	18.8	0.127	5.00
						2210	320.6	165.5	24.0	119.3	17.3	0.127	5.00
			ROLL 2D	39.5		2201	319.3	163.4	23.7	133.1	19.3	0.130	5.10
				42.7		2301	333.8	166.2	24.1	129.6	18.8	0.130	5.10
						2110	306.0	157.2	22.8	135.8	19.7	0.127	5.00
						2522	365.8	191.7	27.8	127.6	18.5	0.130	5.10
						2504	363.2	183.4	26.6	122.7	17.8	0.135	5.30
						2368	343.5	177.2	25.7	131.7	19.1	0.124	4.90
			ROLL 3C	42.1		2110	306.1	153.1	22.2	128.2	18.6	0.124	4.90
				41.7		2124	308.1	157.9	22.9	133.1	19.3	0.127	5.00
						2062	299.0	146.9	21.3	135.1	19.6	0.127	5.00
						2682	389.0	208.2	30.2	132.4	19.2	0.130	5.10
						2490	361.2	200.6	29.1	135.1	19.6	0.124	4.90
						2230	323.4	164.1	23.8	122.0	17.7	0.119	4.70
			ROLL 7D			2508	363.8	195.1	28.3	145.5	21.1	0.127	5.00
						2523	365.9	192.4	27.9	142.0	20.6	0.130	5.10
						2446	354.7	184.8	26.8	143.4	20.8	0.127	5.00
624	63.0	138.8	ROLL 1A	39.1	0.50	2091	303.3	183.4	26.6	133.1	19.3	0.112	4.4
				39.4		2155	312.5	181.3	26.3	131.0	19.0	0.119	4.7
						2361	342.4	208.2	30.2	146.2	21.2	0.124	4.9
			ROLL 2D	40.0	0.50	1948	282.6	160.6	23.3	142.0	20.6	0.119	4.7
				37.6		2076	301.1	168.9	24.5	147.5	21.4	0.122	4.8
						2104	305.2	173.1	25.1	142.0	20.6	0.122	4.8
			ROLL 5B	40.3	0.40	1958	284.0	157.2	22.8	140.0	20.3	0.109	4.3
				43.0		2119	307.4	172.4	25.0	148.9	21.6	0.117	4.6
						2277	330.3	182.0	26.4	146.9	21.3	0.114	4.5
			ROLL 6C	39.6	0.50	2147	311.4	171.7	24.9	147.5	21.4	0.117	4.6
				39.7		2166	314.1	171.0	24.8	138.6	20.1	0.114	4.5
						2063	299.2	168.2	24.4	133.1	19.3	0.122	4.8

APPENDIX B

IN-PROCESS QUALITY CONTROL AND NON-DESTRUCTIVE TEST DATA

Quality control test specimens were cut from the peripheral trim of each graphite molding assembly at the locations shown in Figure B1. Flexural strengths and moduli, interlaminar shear strengths, resin and void contents, and average ply thicknesses were determined at each of these locations on both left and right-hand sides of each rudder. Acceptance levels were determined from samples obtained from the process development rudders. The following acceptance levels were established:

Type of Test	Units	Forward Trim	Aft Trim
Minimum Flexural Strength	MPa KSI	730.8 106.0	627.4 91.0
Minimum Interlaminar Shear Strength	MPa KSI	46.05 6.68	46.05 6.68
Resin Content by Weight	%	21 to 31	21 to 31
Maximum Void Volume	%	2.0	2.0
Ply Thickness	mm mils	0.122 $\pm$ 0.013 4.8 $\pm$ 0.5	0.122 $\pm$ 0.013 4.8 $\pm$ 0.5

Test results from the static test rudder and the ten flight-service rudders are summarized in Table B1. The graphite rudder molding assemblies were of uniform good quality and each was accepted for use in the program. In the isolated instances where acceptance test levels were not attained, the assemblies were accepted on the basis of favorable comparisons between the actual test levels and the levels required in the rudders. In most cases, the low test values were caused by non-uniform (tapered) cross-sections of the test specimens.

The graphite rudder mold assemblies were nondestructively inspected using Fokker bondtester and ultrasonic methods. Fokker bondtesting was performed

using Probe No. 3814-0985. Ultrasonic testing was performed using the UM-721 Reflectoscope and a 10 mHz, 4.76 millimeter (3/16-inch) diameter SFZ search unit. The nondestructive inspections (NDI) confirmed the general acceptability of the skin panel laminates and the good resin bond achieved at the interface of the skin panels with all rib and spar flanges.

The Fokker bondtester was calibrated initially to a 12-ply graphite laminate standard which contained 50.8 and 25.4 millimeter (two-inch and one-inch) diameter delaminated regions. Various areas of the rudder had different numbers of plies and the Fokker presentation changed at each area (see Figure B2). The rudders were checked completely for discontinuities. Figure B3 shows the Fokker bondtester and UM-721 Reflectoscope response for porosity at the rear-spar left hand flange of the first two development rudder units. Ultrasonic presentations for different areas of the rudder are shown in Figure B4. After recasting the rubber mandrels for fabrication of the third and subsequent rudders, the porous regions were eliminated and NDI indicated acceptable mold assemblies in all cases.

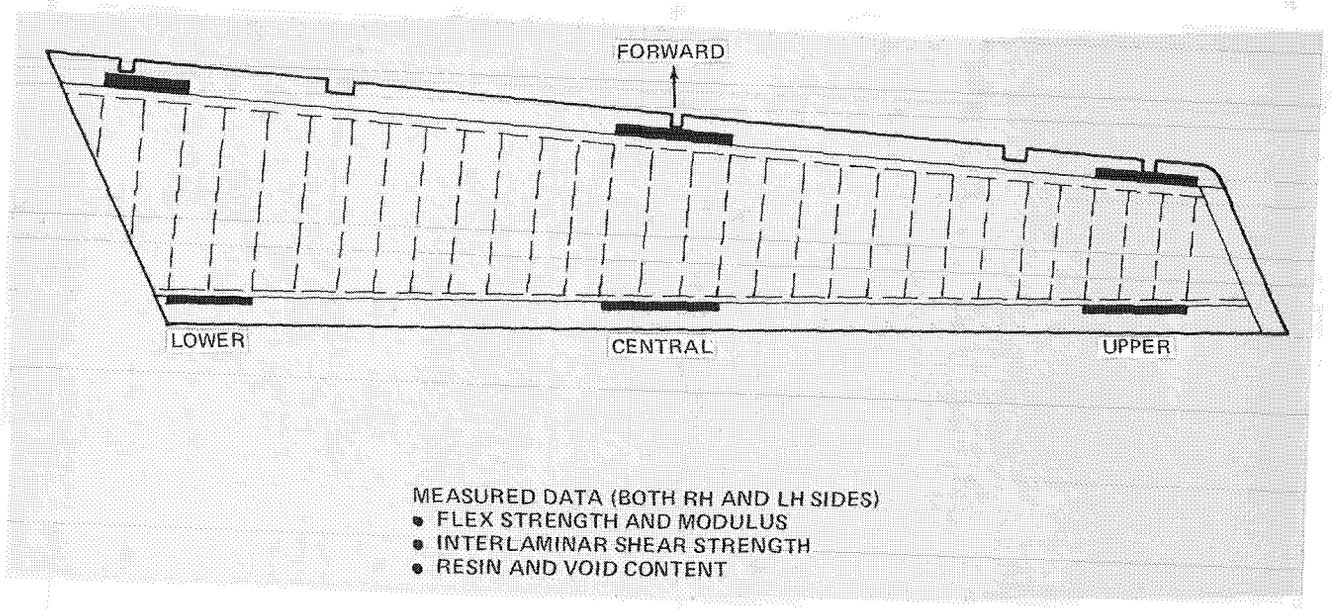

FIGURE B1. LOCATIONS OF IN-PROCESS QUALITY CONTROL TEST SPECIMENS

TABLE B1
IN-PROCESS QUALITY CONTROL TEST RESULTS

RUDDER IDENTITY	PROPERTY \ SPECIMEN LOCATION													
		FWD	X	X	X	X	X	X						
		AFT							X	X	X	X	X	X
		UPR			X			X			X			X
		CTR		X			X			X			X	
		LWR	X			X			X			X		
		RH				X	X	X				X	X	X
		LH	X	X	X				X	X	X			
DEVELOPMENT RUDDER NO. 1	FLEXURAL STRENGTH (MPa)		965	938	1000	862	896	945	1014	586	1062	903	786	979
	FLEXURAL MODULUS (GPa)		77.4	75.0	80.4	78.0	71.4	77.8	88.0	52.0	96.0	74.2	63.5	87.6
	INTERLAMINAR SHEAR STRENGTH (MPa)		46.5	51.3	56.8	58.5	63.6	53.9	58.8	39.0	47.6	57.9	54.8	57.1
	RESIN CONTENT (WT %)		23.97	22.40	22.44	23.21	25.87	25.28	30.52	48.40	22.10	28.09	36.19	23.68
	VOID CONTENT (VOL %)		0	0.21	0	0.12	0.20	0.18	0.01	1.69	0.18	0.32	0.97	0.17
	AVG PLY THICKNESS (mm)		0.124	0.124	0.119	0.123	0.127	0.123	0.140	0.204	0.123	0.138	0.169	0.125
DEVELOPMENT RUDDER NO. 2	FLEXURAL STRENGTH (MPa)		800	758	934	807	820	876	883	552	848	869	689	834
	FLEXURAL MODULUS (GPa)		64.9	55.0	70.5	64.0	66.2	68.5	73.5	41.1	77.1	72.9	69.3	72.1
	INTERLAMINAR SHEAR STRENGTH (MPa)		81.3	68.5	57.9	59.0	54.4	55.9	60.3	43.4	61.9	60.5	67.6	59.5
	RESIN CONTENT (WT %)		40.75	26.84	22.01	32.70	34.97	22.14	25.35	44.68	23.24	34.51	29.64	33.70
	VOID CONTENT (VOL %)		0.59	0.24	0.34	0.47	0.83	0.75	0.52	—	0.79	0.10	0.38	0.02
	AVG PLY THICKNESS (mm)		0.135	0.135	0.120	0.139	0.130	0.123	0.144	0.203	0.124	0.140	0.169	0.139
DEVELOPMENT RUDDER NO. 3	FLEXURAL STRENGTH (MPa)		738	758	772	772	779	807	834	814	745	641	738	752
	FLEXURAL MODULUS (GPa)		67.6	64.1	73.8	71.0	72.4	73.8	64.1	67.6	62.7	68.9	66.2	62.7
	INTERLAMINAR SHEAR STRENGTH (MPa)		73.1	67.9	56.9	52.4	55.2	51.8	73.2	63.8	49.3	55.8	57.2	62.9
	RESIN CONTENT (WT %)		30.3	27.5	28.2	28.9	29.2	27.4	30.7	28.3	25.6	29.5	31.8	29.8
	VOID CONTENT (VOL %)		0.50	0.50	0.40	0.30	0.40	0.40	0	0.50	0.50	0.40	0.60	0.10
	AVG PLY THICKNESS (mm)		0.142	0.141	0.137	0.139	0.140	0.137	0.132	0.134	0.116	0.125	0.134	0.132
DEVELOPMENT RUDDER NO. 4	FLEXURAL STRENGTH (MPa)		779	834	855	800	820	820	738	758	793	607	724	758
	FLEXURAL MODULUS (GPa)		68.9	69.6	73.8	70.3	73.8	73.1	62.1	62.7	70.3	60.7	64.8	67.6
	INTERLAMINAR SHEAR STRENGTH (MPa)		55.8	62.6	65.7	61.1	57.1	64.1	65.6	53.6	51.4	52.2	58.3	57.0
	RESIN CONTENT (WT %)		19.59	20.65	20.86	20.97	21.00	21.31	25.26	23.51	24.78	23.40	23.79	24.09
	VOID CONTENT (VOL %)		0.83	0.64	0.58	0.52	0.50	0.65	0.65	0.79	0.60	0.80	0.99	0.50
	AVG PLY THICKNESS (mm)		0.124	0.125	0.126	0.124	0.124	0.124	0.129	0.128	0.124	0.126	0.122	0.123
FLIGHT RUDDER NO. 1	FLEXURAL STRENGTH (MPa)		869	876	814	945	986	910	945	979	889	1048	965	1027
	FLEXURAL MODULUS (GPa)		80.7	80.0	80.7	80.0	85.5	77.9	86.9	85.5	84.1	81.4	93.1	92.4
	INTERLAMINAR SHEAR STRENGTH (MPa)		66.5	66.1	66.3	59.0	66.4	52.9	72.0	62.0	59.4	77.5	66.3	64.1
	RESIN CONTENT (WT %)		23.33	23.47	24.49	21.81	22.07	23.57	24.28	23.17	22.54	23.42	23.50	23.16
	VOID CONTENT (VOL %)		0.74	0.31	0.30	0.40	0.34	0.33	0.51	0.34	0.57	0.49	0.72	0.18
	AVG PLY THICKNESS (mm)		0.125	0.125	0.125	0.124	0.122	0.123	0.122	0.122	0.116	0.120	0.121	0.126
FLIGHT RUDDER NO. 2	FLEXURAL STRENGTH (MPa)		910	796	965	908	776	848	896	953	898	894	920	863
	FLEXURAL MODULUS (GPa)		80.4	80.0	86.3	69.9	74.7	79.2	76.7	79.3	81.8	83.2	92.7	88.5
	INTERLAMINAR SHEAR STRENGTH (MPa)		57.9	46.7	51.7	60.6	61.1	61.6	55.3	58.9	52.8	62.7	46.7	76.6
	RESIN CONTENT (WT %)		21.17	20.84	21.51	20.91	20.65	21.54	20.97	20.71	19.87	21.53	21.07	20.27
	VOID CONTENT (VOL %)		0.44	0.03	0.52	0.34	0.83	0.34	0.61	0.57	0.48	0.43	0.21	0.55
	AVG PLY THICKNESS (mm)		0.126	0.123	0.125	0.125	0.126	0.127	0.120	0.120	0.119	0.121	0.120	0.121
FLIGHT RUDDER NO. 3	FLEXURAL STRENGTH (MPa)		836	898	994	843	894	938	810	883	866	837	786	833
	FLEXURAL MODULUS (GPa)		62.8	67.4	69.6	68.2	72.1	70.7	65.0	76.9	75.0	71.0	63.8	71.1
	INTERLAMINAR SHEAR STRENGTH (MPa)		54.7	59.3	49.6	52.0	46.5	53.0	44.5	48.1	48.1	58.2	64.4	43.4
	RESIN CONTENT (WT %)		24.21	22.69	22.23	22.48	22.06	22.14	22.25	21.13	20.72	21.98	21.84	20.51
	VOID CONTENT (VOL %)		0	0	0	0	0	0	0.06	0.12	0.07	0.08	0.16	0.12
	AVG PLY THICKNESS (mm)		0.123	0.122	0.119	0.123	0.121	0.121	0.124	0.120	0.121	0.124	0.120	0.122

TABLE B1

IN-PROCESS QUALITY CONTROL TEST RESULTS (CONTINUED)

RUDDER IDENTITY	PROPERTY \ SPECIMEN LOCATION													
		FWD	X	X	X	X	X	X						
		AFT							X	X	X	X	X	X
		UPR			X			X			X			X
		CTR		X			X			X			X	
		LWR	X			X			X			X		
		RH				X	X	X				X	X	X
		LH	X	X	X				X	X	X			
FLIGHT RUDDER NO. 4	FLEXURAL STRENGTH (MPa)		983	958	974	966	951	966	964	935	868	1145	1060	939
	FLEXURAL MODULUS (GPa)		82.7	82.0	82.0	80.7	77.9	78.6	94.4	86.2	104.1	113.1	108.9	95.1
	INTERLAMINAR SHEAR STRENGTH (MPa)		62.1	55.7	62.0	66.9	67.7	67.2	63.1	75.5	65.5	70.1	53.1	63.0
	RESIN CONTENT (WT %)		21.78	21.32	20.90	21.27	21.67	21.33	22.08	21.42	21.50	22.22	20.95	21.62
	VOID CONTENT (VOL %)		0	0	0.12	0	0.02	0.16	0.19	0.11	0	0	0.35	0.53
	AVG PLY THICKNESS (mm)		0.125	0.124	0.120	0.122	0.121	0.122	0.116	0.116	0.113	0.116	0.116	0.121
FLIGHT RUDDER NO. 5	FLEXURAL STRENGTH (MPa)		1052	989	1030	1050	1016	1109	1006	958	854	1109	1145	885
	FLEXURAL MODULUS (GPa)		68.0	68.2	69.9	72.0	73.9	77.8	85.9	81.2	83.7	85.4	92.9	83.6
	INTERLAMINAR SHEAR STRENGTH (MPa)		85.8	69.6	61.3	78.7	72.3	64.5	55.2	71.7	79.9	55.1	78.5	61.1
	RESIN CONTENT (WT %)		22.65	22.50	22.22	22.46	22.16	21.56	22.09	21.64	21.76	21.07	20.72	20.68
	VOID CONTENT (VOL %)		0	0	0	0	0.32	0	0	1.67	0.97	0.90	1.59	0
	AVG PLY THICKNESS (mm)		0.124	0.125	0.124	0.123	0.125	0.123	0.119	0.122	0.121	0.120	0.121	0.120
FLIGHT RUDDER NO. 6	FLEXURAL STRENGTH (MPa)		829	841	849	885	867	992	717	709	715	749	658	747
	FLEXURAL MODULUS (GPa)		83.2	79.6	84.8	86.1	84.5	85.4	52.1	52.8	50.9	55.7	54.1	56.3
	INTERLAMINAR SHEAR STRENGTH (MPa)		50.7	62.3	56.4	62.5	76.9	64.9	51.8	55.1	47.4	57.0	52.2	51.8
	RESIN CONTENT (WT %)		22.73	22.47	22.71	21.84	21.92	22.39	24.30	24.97	22.42	23.55	23.26	22.26
	VOID CONTENT (VOL %)		0	0	0	0	0	0	0	0	0	0	0	0
	AVG PLY THICKNESS (mm)		0.123	0.120	0.116	0.122	0.122	0.121	0.118	0.119	0.116	0.121	0.119	0.120
FLIGHT RUDDER NO. 7	FLEXURAL STRENGTH (MPa)		914	863	907	831	818	783	891	1004	962	853	931	960
	FLEXURAL MODULUS (GPa)		67.7	69.1	71.6	72.8	71.6	72.2	75.6	77.3	73.1	73.4	72.6	74.6
	INTERLAMINAR SHEAR STRENGTH (MPa)		64.0	56.0	51.9	56.7	64.4	66.1	48.8	62.4	57.5	48.0	62.9	54.0
	RESIN CONTENT (WT %)		22.22	22.19	22.10	22.26	21.29	21.47	21.76	22.09	21.53	21.25	21.40	22.13
	VOID CONTENT (VOL %)		0	0	0	0	0	0.02	0.24	0.26	0.21	0.46	0.25	0.64
	AVG PLY THICKNESS (mm)		0.130	0.129	0.130	0.129	0.130	0.128	0.119	0.121	0.127	0.119	0.120	0.124
FLIGHT RUDDER NO. 8	FLEXURAL STRENGTH (MPa)		894	934	925	754	890	891	1053	1094	1014	956	1095	981
	FLEXURAL MODULUS (GPa)		67.9	76.5	78.5	71.0	72.0	76.7	72.3	76.0	73.2	75.8	81.6	67.8
	INTERLAMINAR SHEAR STRENGTH (MPa)		62.7	52.1	52.9	53.6	57.2	54.4	60.1	54.5	47.7	47.6	52.4	54.4
	RESIN CONTENT (WT %)		21.80	21.81	22.42	21.87	22.68	21.20	23.81	27.09	22.29	23.34	22.72	21.60
	VOID CONTENT (VOL %)		0.51	0.55	0.49	0.54	0.29	0.66	0.71	0.85	0.63	0.68	0.64	0.67
	AVG PLY THICKNESS (mm)		0.127	0.127	0.125	0.130	0.130	0.129	0.121	0.120	0.113	0.122	0.122	0.124
FLIGHT RUDDER NO. 9	FLEXURAL STRENGTH (MPa)		852	841	916	862	945	887	826	880	903	874	864	891
	FLEXURAL MODULUS (GPa)		68.0	65.5	70.0	80.4	66.5	78.4	58.7	74.1	77.3	60.5	78.5	77.2
	INTERLAMINAR SHEAR STRENGTH (MPa)		71.6	62.8	74.0	57.7	57.5	55.9	45.9	49.3	49.2	49.6	69.9	57.1
	RESIN CONTENT (WT %)		22.99	22.20	22.71	22.13	22.02	22.07	23.05	23.11	23.71	22.50	22.25	22.90
	VOID CONTENT (VOL %)		0.70	0.77	0.56	0.70	0.65	0.69	0.33	0.85	0.27	0.55	0.94	0.49
	AVG PLY THICKNESS (mm)		0.128	0.130	0.128	0.127	0.129	0.128	0.123	0.126	0.124	0.124	0.126	0.123
FLIGHT RUDDER NO. 10	FLEXURAL STRENGTH (MPa)		833	845	884	933	944	919	896	936	998	951	922	1013
	FLEXURAL MODULUS (GPa)		68.2	70.8	75.3	75.8	75.4	77.0	73.9	79.7	81.6	77.2	70.3	82.9
	INTERLAMINAR SHEAR STRENGTH (MPa)		48.6	55.5	55.9	49.3	48.2	69.9	40.9	47.3	43.4	39.2	39.4	45.5
	RESIN CONTENT (WT %)		22.25	21.98	21.84	21.32	23.83	21.48	21.38	21.45	20.88	21.87	23.95	20.87
	VOID CONTENT (VOL %)		0.23	0.33	0.40	0.40	0	0.90	0	0.78	0.56	0.74	0	0.75
	AVG PLY THICKNESS (mm)		0.129	0.130	0.134	0.131	0.133	0.130	0.122	0.121	0.120	0.122	0.122	0.125

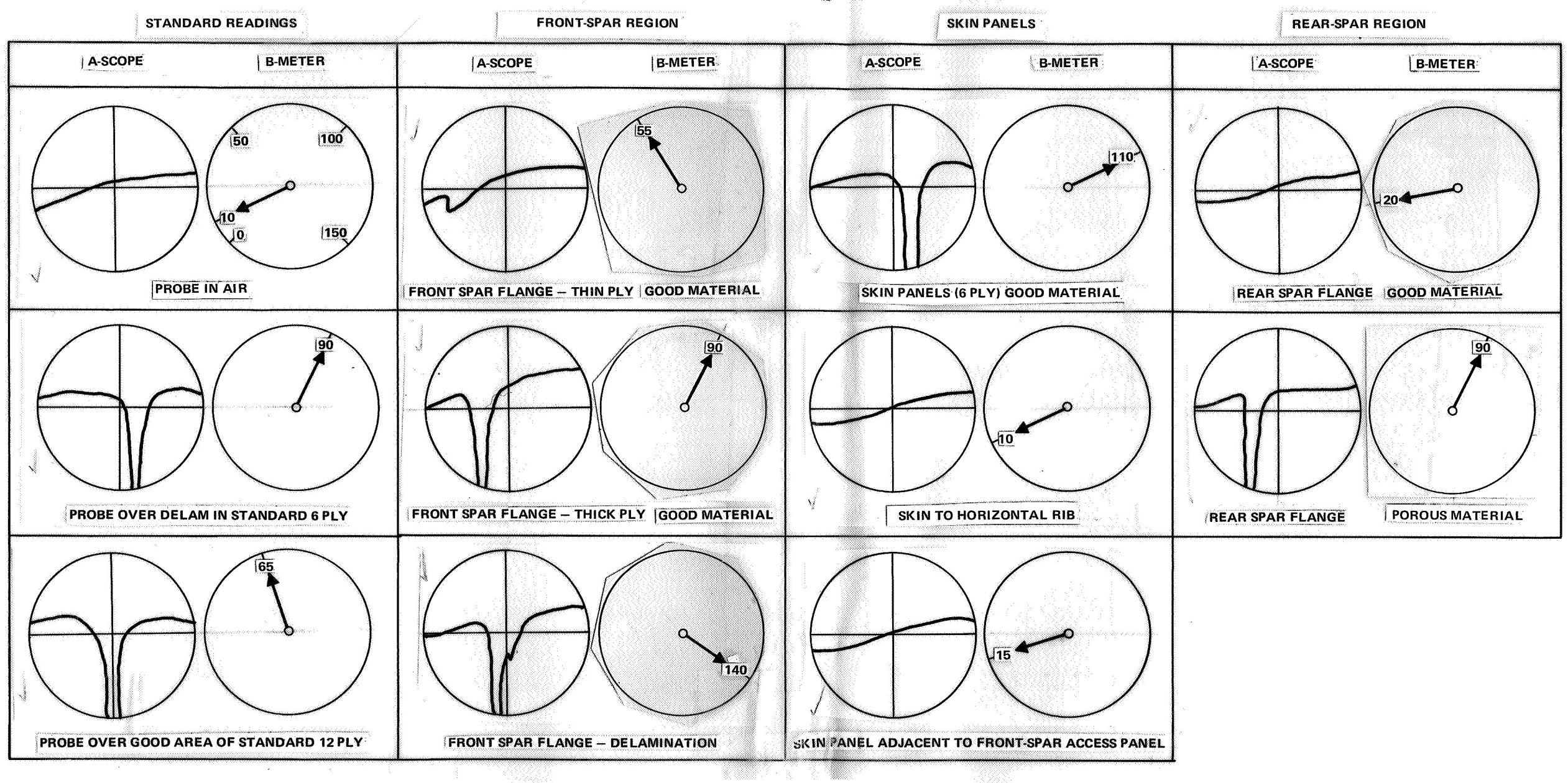

FIGURE B2. FOKKER BONDTEST PRESENTATIONS FOR GRAPHITE RUDDER

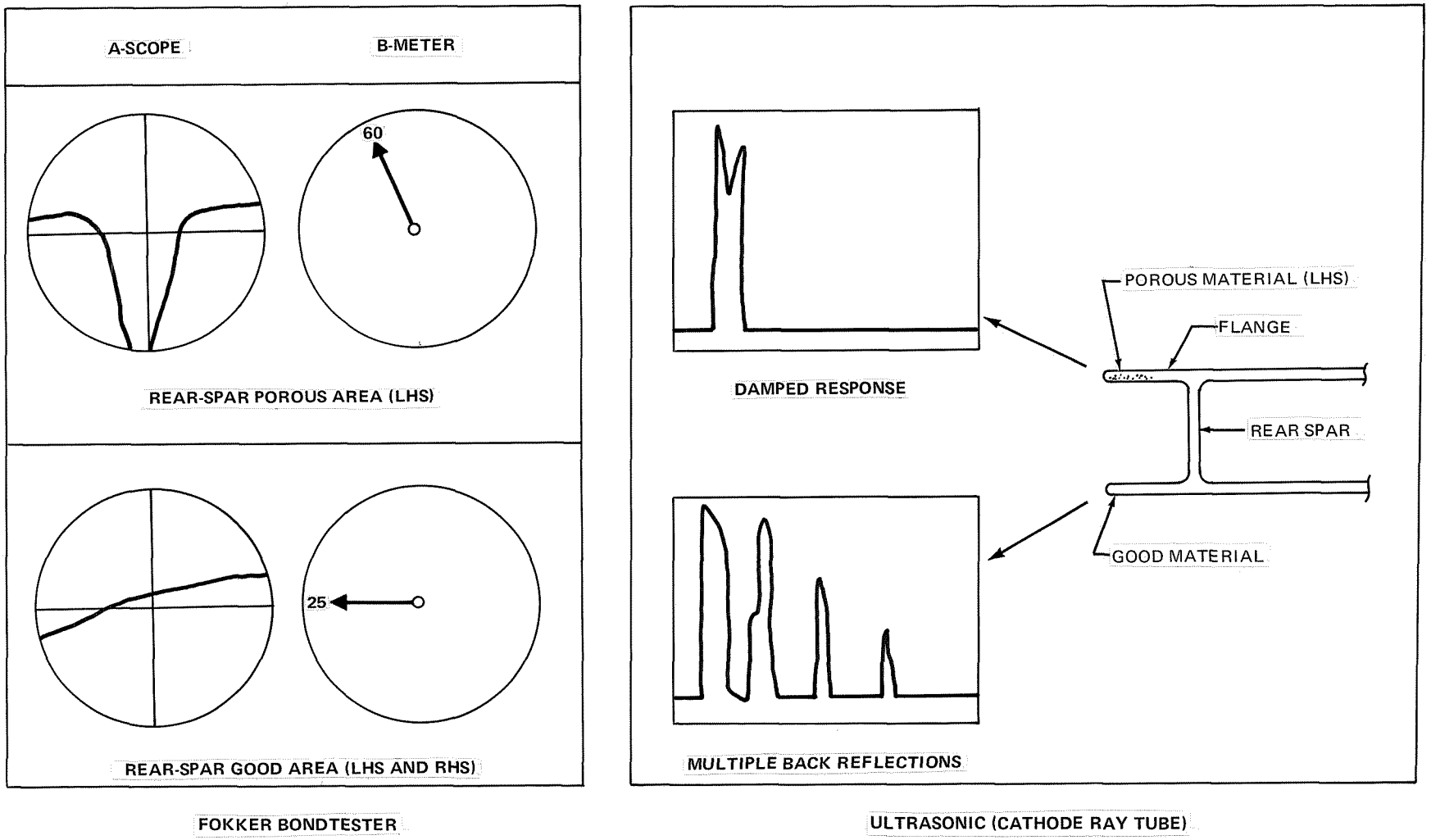

FIGURE B3. FOKKER BONDTEST AND ULTRASONIC PRESENTATIONS FOR REAR-SPAR FLANGES DEVELOPMENT RUDDER UNIT

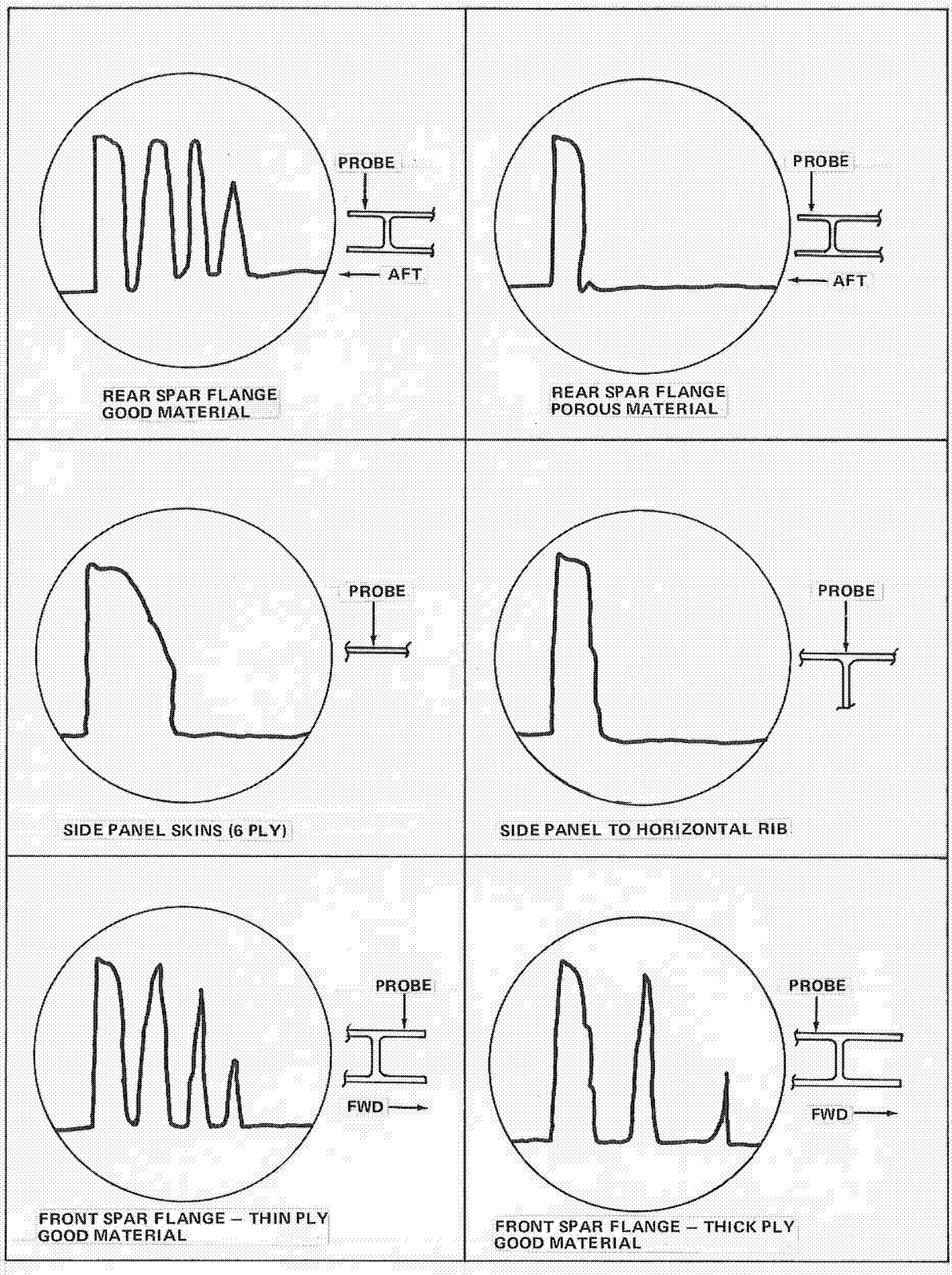

FIGURE B4. ULTRASONIC CATHODE RAY TUBE PRESENTATIONS – DEVELOPMENT RUDDER UNIT 2

APPENDIX C

IN-SERVICE REPAIR PROCEDURES

Repair procedures for the composite rudder are described in this appendix. The major composite components of the rudder are the fiberglass-epoxy leading edge, trailing edge, and tip assemblies, and the graphite-epoxy molding assembly. The repair procedures have been categorized into general procedures which apply to both the fiberglass and graphite-epoxy material systems and into specific procedures for certain types of damage to each of these material systems.

General Repair Procedures

Information on materials, preparations, applications methods, and repair procedures for minor local damage to either fiberglass or graphite-epoxy laminates is presented in this section.

Materials and Sources. - Table C1 summarizes approved repair materials and sources for repair of reinforced plastic parts; equivalent materials may be substituted for the items listed.

Repair Area Preparation and Cleaning. - Any area to be repaired must be prepared and cleaned in accordance with the following requirements, as applicable.

1. Remove all hardware and paint whenever repair resins to be used will require an oven cure.

2. Wash rework area with acetone solvent or methyl ethyl ketone (MEK) to remove grease, dirt, or other foreign materials.

3. Remove surface gloss and paint by scuff sanding area with medium grit sandpaper. Use care to prevent damage to fibers.

TABLE C1
REINFORCED PLASTICS REPAIR MATERIALS

MATERIAL	SOURCE
HETRON 92 RESIN	DUREZ PLASTICS CO. 3350 WILSHIRE BLVD. LOS ANGELES 5, CA
EPON 828 RESIN	SHELL CHEMICAL CORP. 1008 WEST 6TH STREET LOS ANGELES 17, CA
GARAKO NO. 100A (2% COBALT NAPTHANATE) NO. 10A SETTING FLUID (60% METHYL ETHYL KETONE PEROXIDE IN DIMETHYL PTHALATE)	THALCO GLASS PRODUCTS CO. 6431 FLOTILLA STREET LOS ANGELES 22, CA
BENZOIL PEROXIDE PASTE (BZP)	RAM CHEMICAL CO. 210 EAST OLIVE GARDENA, CA
HN-23 HARDENER (DIETHYLENE TRIAMINE; DTA) EPOCAST H-991A	FURANE PLASTICS 4516 BRAZIL STREET LOS ANGELES 39, CA
RP-7A HARDENER	CHEMICAL PROCESS CO. 901 SPRING STREET REDWOOD CITY, CA
APCO 320 HARDENER	APPLIED PLASTICS 130 PENN STREET EL SEGUNDO, CA
NO. 120 VOLAN A GLASS CLOTH, MIL-C-9084 NO. 181 VOLAN A GLASS CLOTH, MIL-C-9084	THALCO GLASS PRODUCTS 6431 FLOTILLA STREET LOS ANGELES 22, CA
ACETONE SOLVENT OR METHYL ETHYL KETONE	INTER CHEMICAL CORPORATION LOS ANGELES, CA
CELLOPHANE SHEET	E. I. DUPONT CO. WILMINGTON, DE
SANDPAPER, MEDIUM GRIT	LOCAL
SEALANT, LOW ADHESION (GUN TYPE) 3C-200 WITH ACCELERATOR 3C-200A	CHURCHILL CHEMICAL CO. LOS ANGELES, CA

4. Remove all dust particles, after sanding, with a clean cloth dampened with acetone solvent or MEK.

Preparation and Mixing of Resins. - Liquid resins are used to impregnate the laminates to form a bond in the repair area. Several resin systems are described; however, for repair of interior parts, Hetron 92 is required because of fire-retardant characteristics, but parts not used in interiors may be repaired with Epon 828. Both resins, Hetron 92 and Epon 828, may be prepared for cold-set or heat-cured applications. Table C2 indicates applicable catalyst, mixing proportions, and pot life for each resin system. Comply with applicable instructions and precautionary information, when preparing resins for application.

1. Weigh required type and quantity of resin. Place in a clean non-absorbent container.

2. Add catalyst, setting agent, or hardener to resin as specified in Table C2. After adding an ingredient, mix thoroughly before adding another.

   WARNING: DO NOT ALLOW #10A SETTING FLUID TO COME INTO CONTACT WITH GARAKO #100A CATALYST, UNTIL CATALYST IS THOROUGHLY MIXED INTO RESIN. AN EXPLOSION COULD RESULT.

   WHEN USING EPOXY CATALYSTS, RUBBER GLOVES AND EYE PROTECTION MUST BE USED TO PREVENT SKIN CONTACT. IF CATALYST DOES CONTACT SKIN, WASH THOROUGHLY WITH WHITE VINEGAR.

Pressure Application Methods. - Repair of reinforced plastic parts requires the application of pressure to repair area. Proper application of pressure assists in affecting a good bond and maintains the contour or alignment. Two methods of applying pressure are recommended.

1. Vacuum bag method

   a. Place repaired part in vacuum bag.

TABLE C2
MIXING OF RESINS

TYPES OF RESIN SYSTEM	APPLICABLE CATALYST(S)	PARTS BY WEIGHT CATALYST TO RESIN	POT LIFE
HETRON 92 COLDSET	GARAKO NO. 100A AND NO. 10A SETTING FLUID	1/2 OR 1 TO 100 1 TO 100	20 TO 30 MINUTES
HETRON 92 HEAT-CURED	BENZOIL PEROXIDE PASTE	2 TO 100	6 TO 8 HOURS
EPON 828 COLDSET	HARDENER HN-23	8 TO 100	20 TO 30 MINUTES
EPON 828 HEAT-CURED	HARDENER, RP-7A OR APCO 320	17 TO 100	6 TO 8 HOURS
EPOCAST H-991A	HARDENER HN-23	6 TO 100	20 TO 30 MINUTES

b. Arrange bag so that as depressurization occurs the resultant external pressure will not be bridged.

NOTE: A minimum of 610 millimeters of mercury (12 psi) vacuum pressure is required to remove air from the bag.

c. Hand squeegee the bag and laminate to remove any excess resin or pockets of air.

2. Mechanical Method

a. Cover repair area with cellophane

b. Use pressure evenly and apply pressure with C-clamps or weights

NOTE: If C-clamps or weights cannot be used, stretch cellophane to exert uniform pressure and secure with tape.

Curing Procedures for Repairs. - Curing times and temperature for repairs depend on type of resin mixture used. Curing times for resin mixtures and times and temperatures for heat cure mixed resin are given in the following steps:

1. Coldset Resin Mixtures (Normal Cure Time): Coldset resin mixtures are cured under normal temperature conditions in a period of 16 hours.

2. Coldset Resin Mixtures (Accelerated Cure Time): Cure cycle for coldset resin mixtures may be accelerated by allowing a minimum of 1 hour for material to gel. Then apply heat for 20 to 30 minutes, using heat gun or lamp capable of maintaining 365 $\pm$ 8°K (200 $\pm$ 15°F) on entire repair area.

3. Heat cure for Epon 828 is accomplished by application of 355 ± 10°K (180 ± 15°F) for 3 hours, followed by 394 ± 10°K (250 ± 15°F) for 2 hours.

Surface Pits and Indentation Repair Procedure. - Surface pits and indentations can be repaired as follows:

1. Prepare area to be repaired.

2. Prepare Epocast H-991A resin.

3. Fill surface pits or indentations which do not penetrate the laminate with mixed material (see Figure C1).

4. Cure material (see preceeding paragraph).

5. Sand repaired area to provide smooth and faired surface.

Blisters and Delamination Repair Procedure. - Blisters and delamination repairs (areas less than 1-inch diameter) may be repaired per the following instructions:

1. Drill at least two 1-millimeter (1/32-inch) diameter holes into edges of blistered area.

2. Prepare applicable coldset resin. Use hypodermic needle to inject resin into blistered or delaminated area (see Figure C1). Inject sufficient quantity to fill area.

3. Apply pressure to blister and allow excess resin to exude out through the 1 millimeter diameter holes. Wipe off excess resin.

4. Apply pressure to area and cure as described previously.

Edge Separation Repair Procedure. - Edge separations may be repaired as follows:

1. Prepare separated area for repair.

2. Prepare applicable coldset resin. Force resin between separated plies (see Figure C1). Make certain that area is completely filled.

3. Apply pressure to area to expel excess material and to close separation. Ensure that proper contour is maintained.

4. Maintain pressure to repair area and cure as described previously.

Fiberglass - Epoxy Repair Procedures

Procedures for repairing holes and multiple lamination damage to fiberglass-epoxy materials are presented in this section.

Hole Repair Procedure. - Holes less than 10 millimeters (3/8-inch) diameter may be repaired in accordance with following instructions and Figure C2.

NOTE: These instructions do not apply to holes to be redrilled in repaired area. See the following paragraph for repair of larger holes or for any portion to be redrilled.

1. Remove one ply of glass cloth from each side of the part (removed cloth to extend beyond edge of hole at least 12 millimeters (1/2 inch) in all directions.

2. Catalyze applicable coldset resin.

3. Set aside a portion of catalyzed resin to be used later for replacement of laminations in Step 6.

1. SURFACE INDENTATION REPAIR PROCEDURE

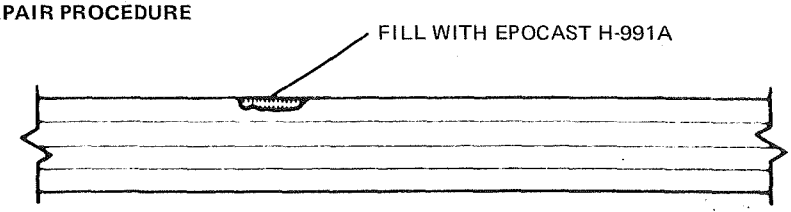

2. BLISTER REPAIR PROCEDURE

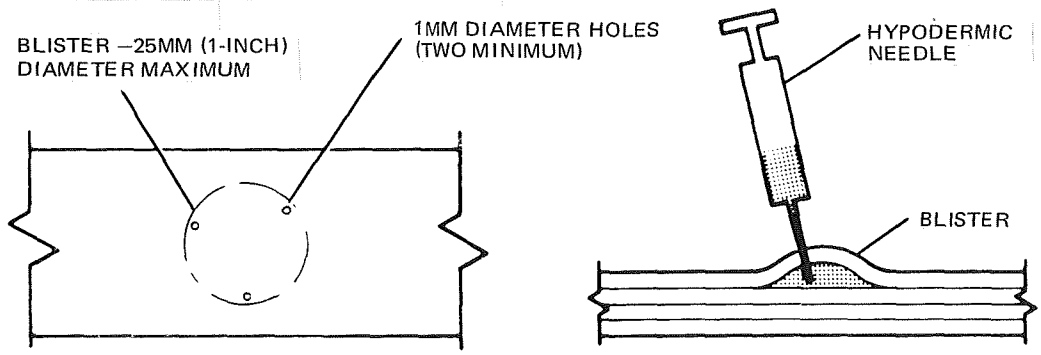

3. EDGE SEPARATION REPAIR PROCEDURE

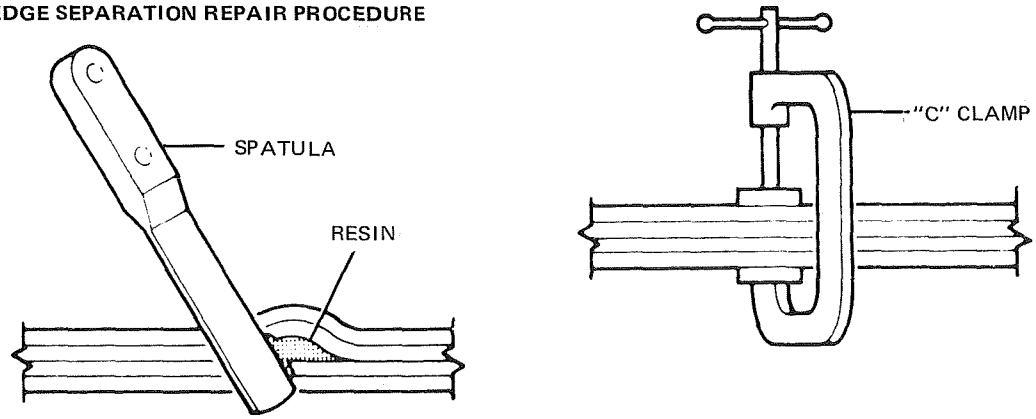

FIGURE C1. REPAIR PROCEDURES FOR SURFACE INDENTATIONS, BLISTERS, AND EDGE SEPARATIONS

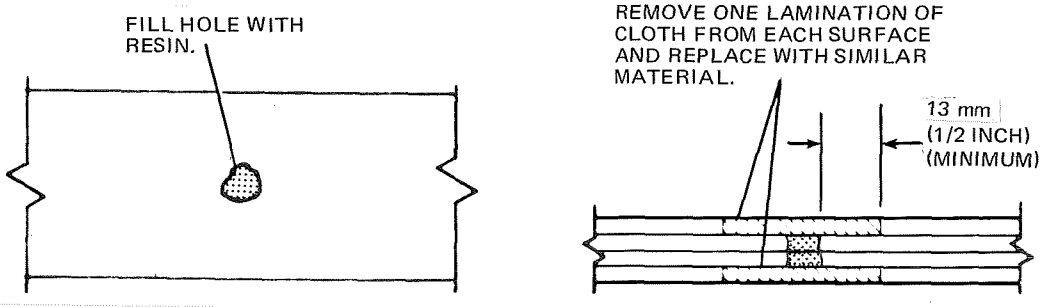

FIGURE C2. HOLE REPAIR PROCEDURE

4. Weigh remaining mixed resin and add 15 parts (by weight) of milled glass fibers to 100 parts (by weight) of catalyzed resin. Mix thoroughly.

5. Fill hole with glass fiber resin mixture.

6. Replace cut out plies with Number 181 glass cloth, and fully impregnate with catalyzed resin.

7. Apply pressure to repair area and cure as described previously.

8. Sand repaired area to obtain smooth and faired surface.

Multiple Lamination Repair Procedure. - Multiple lamination repairs are accomplished as follows:

1. Cut back and remove damaged plies of glass cloth. Each ply must be trimmed a minimum of 12 millimeters (1/2 inch) beyond trim line of ply below (see Figure C3). If damage extends through part, both sides of laminate must be cut back.

2. Prepare repair area.

3. Cut pieces of glass cloth to replace damaged pieces. Each replacement cloth must be cut from same type of cloth being replaced.

4. Prepare applicable resin.

5. Lay in each succeeding layer of glass cloth. Apply resin to each layer as it is installed.

6. Apply pressure to repair area and cure as described previously.

7. Sand repaired area to provide a smooth and faired surface.

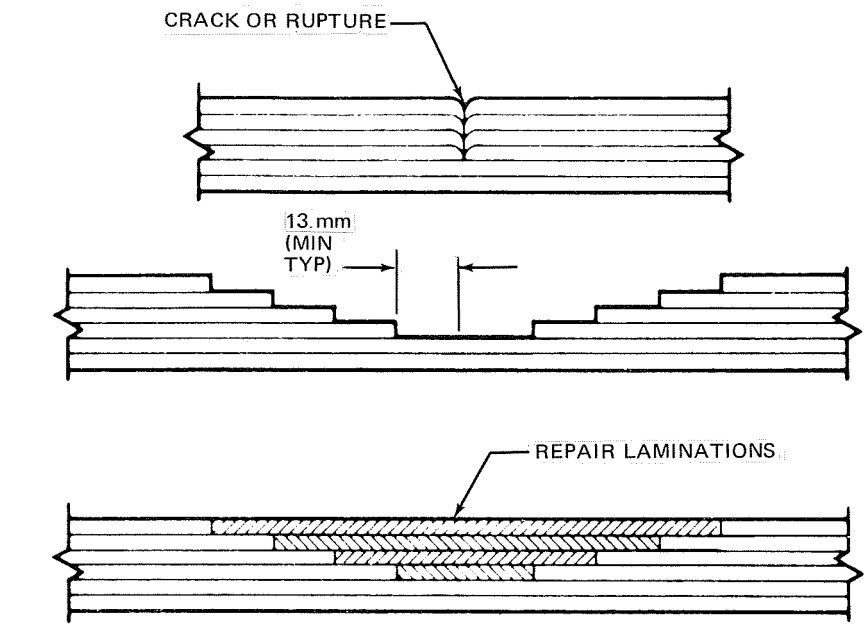

MULTIPLE LAMINATION REPAIR (DAMAGE TO ONE SURFACE ONLY)

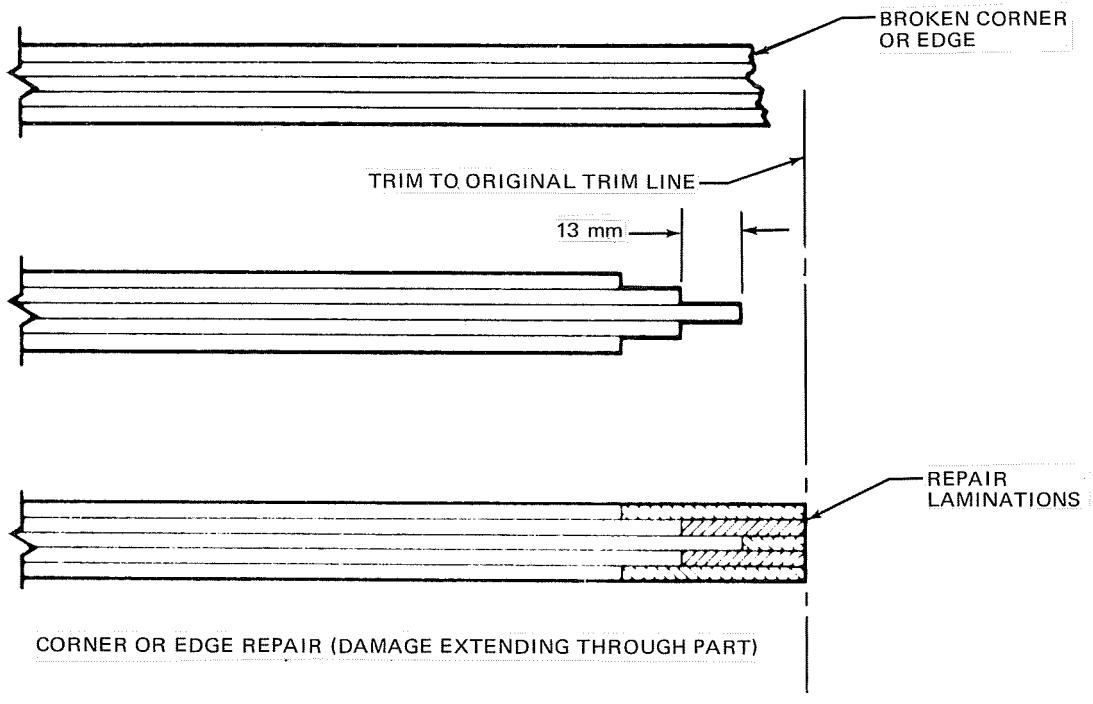

CORNER OR EDGE REPAIR (DAMAGE EXTENDING THROUGH PART)

FIGURE C3. MULTIPLE LAMINATION REPAIRS

Graphite-Epoxy Repair Procedures

The procedure for repairing damage to the graphite-epoxy molding assembly skin panels is presented in this section. The regions of the rudder surface covered by this procedure are shown in Figure C4. If structural damage occurs in regions not covered by this procedure (i.e., the shaded regions of Figure C4 in which the damage involves rib or spar flanges) the composite rudder shall be removed from the aircraft and replaced with a spare rudder. A specific disposition for the composite rudder will be formulated in this event.

Hole Repair Procedure. - Holes (also cracks, punctures or dalaminations) up to 64 millimeters (2.5 inches) diameter may be repaired in accordance with the following instructions.

1. Interim (Field) Repair. (Note: Replace interim repairs with permanent repairs within 6 months of application.)

    a. Laminate, apply pressure, and precure a fiberglass-epoxy disc as shown in Figure C5.

    b. Prepare area to be repaired.

    c. Bond fiberglass-epoxy disc to repair area as shown in Figure C5. Do not trim damaged graphite fibers from damaged area. Apply adhesive in annular region around damage. Do not apply adhesive to damaged fibers during an interim repair.

2. Permanent (Depot) Repair

    a. Laminate, apply pressure, and pre-cure graphite-epoxy discs as shown in Figure C6. The graphite-epoxy material must be cured under vacuum pressure for two hours at 450 $\pm$ 8°K (350 $\pm$ 15°F).

    b. Prepare area to be repaired.

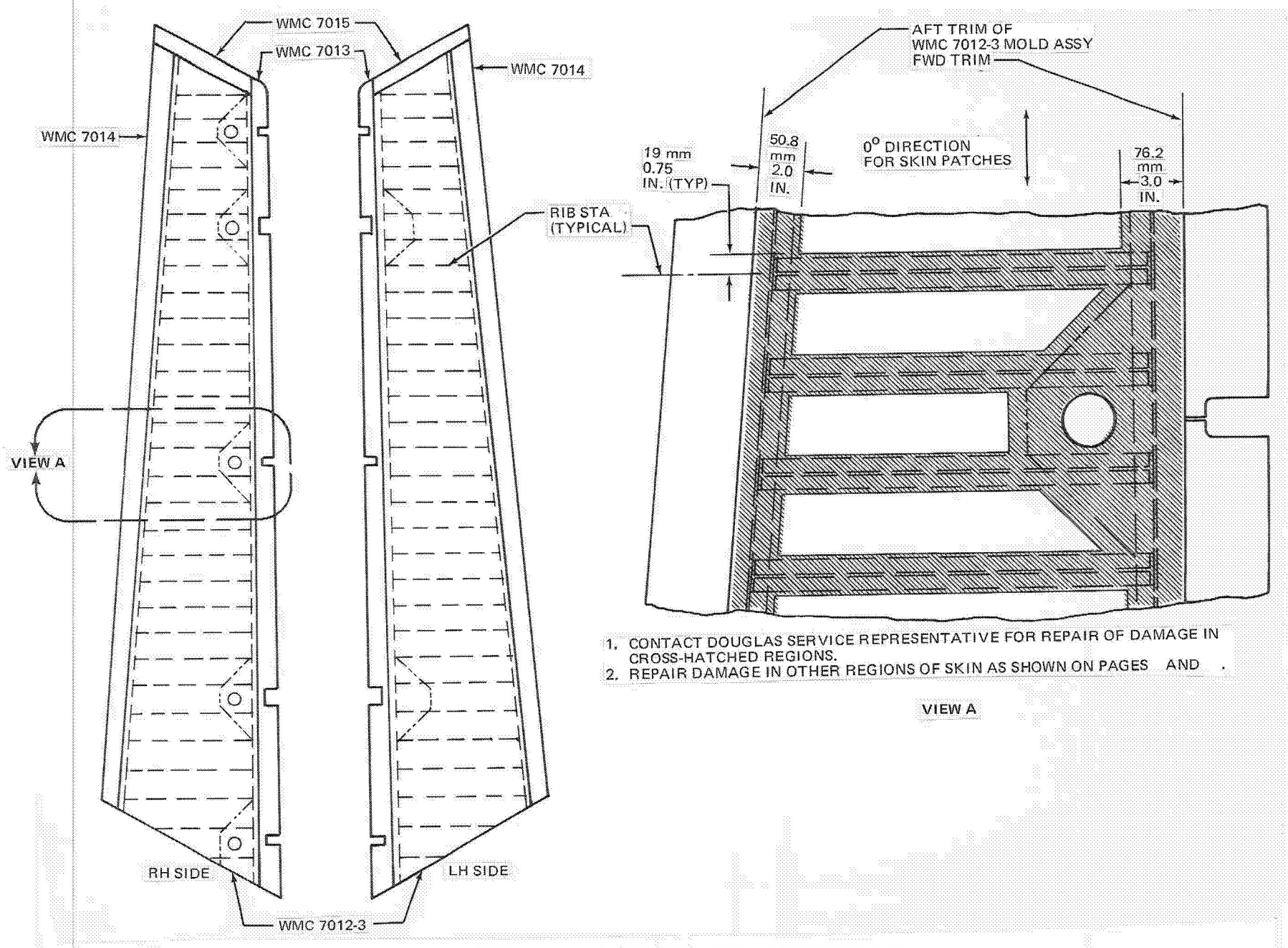

FIGURE C4. GRAPHITE SKIN PANEL REPAIR REGIONS

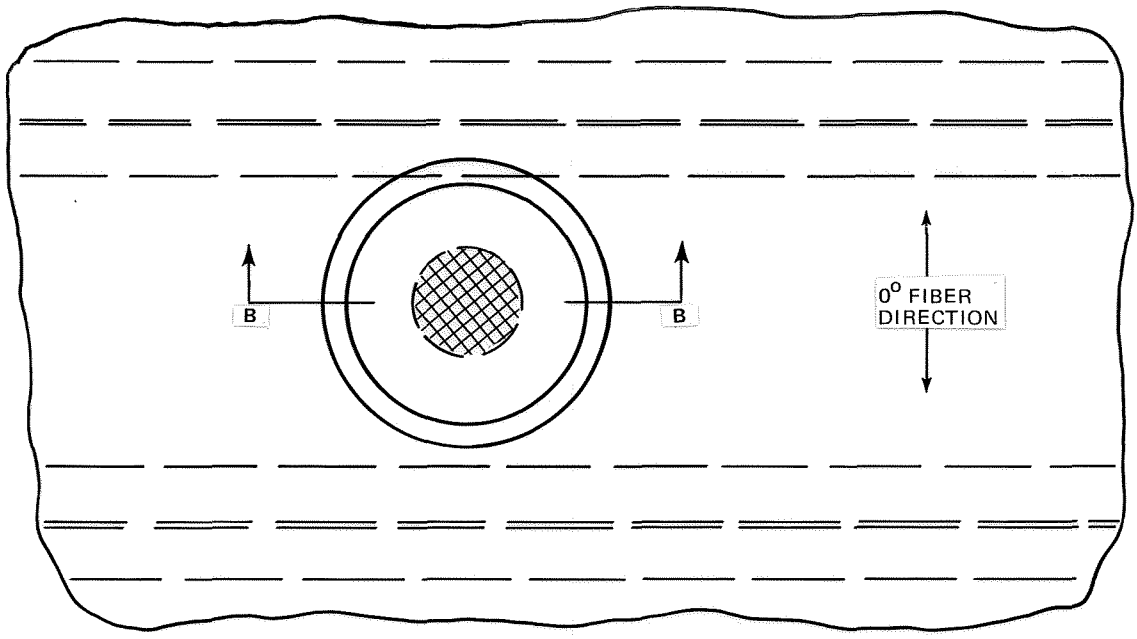

(1) INTERIM (FIELD) REPAIR
REPLACE IN 6 MONTHS

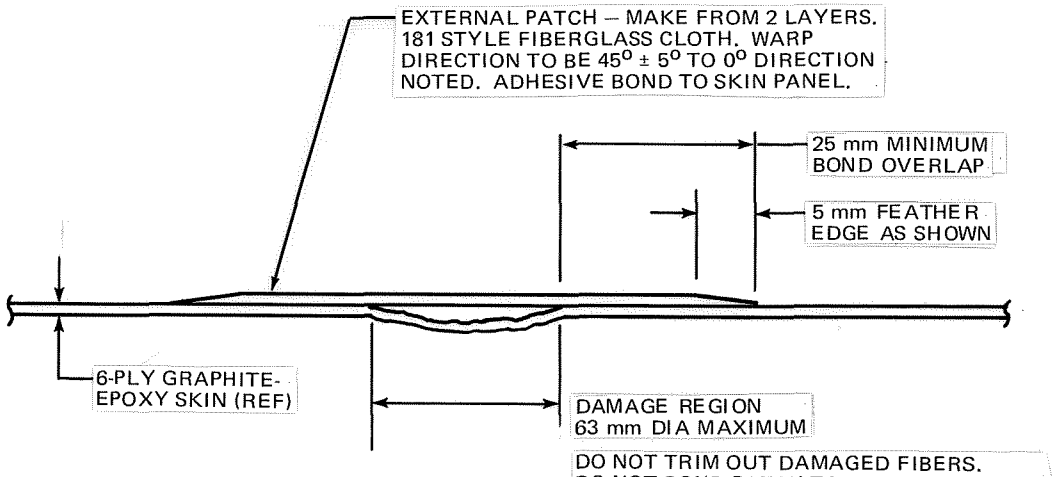

SECTION B-B

FIGURE C5. GRAPHITE SKIN PANEL INTERIM REPAIRS

c. Smooth damaged fibers and fill with resin (adhesive). Do not trim out damaged fibers.

d. Bond graphite-epoxy discs to repair area as shown in Figure C6. Apply pressure to repair and cure as described previously. Remove leading edge structure and fiberglass covers from front spar for internal access. Reseal fiberglass covers and reinstall leading edge after repair is complete.

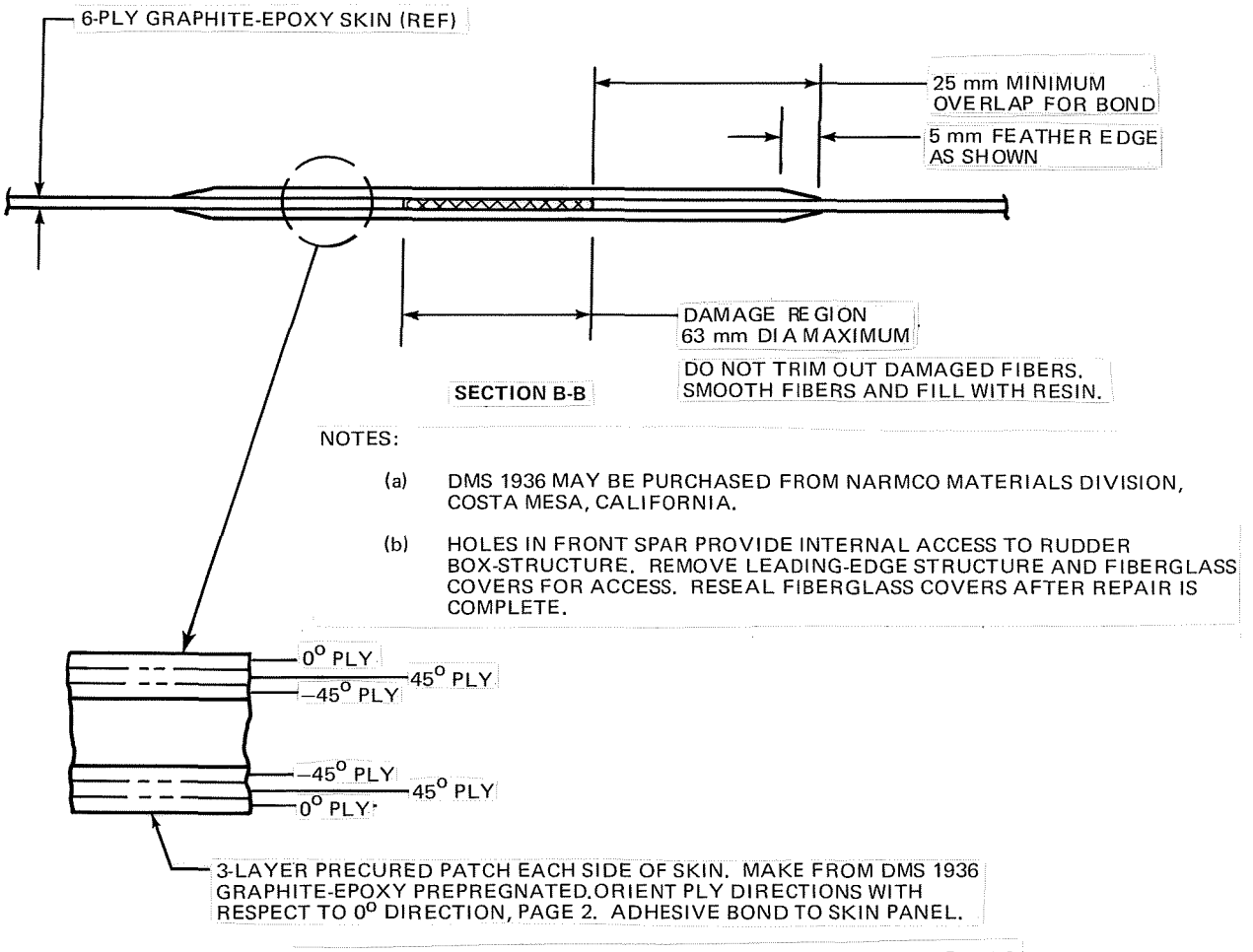

FIGURE C6. GRAPHITE SKIN PANEL PERMANENT REPAIRS